A DFT STUDY OF CHLORINE BASED COPPER CORROSION AND ITS INHIBITION

by
Ezgi USLU

Submitted to Graduate School of Natural and Applied Sciences
in Partial Fulfillment of the Requirements
for the Degree of Master of Science in
Chemical Engineering

Yeditepe University
2022

A DFT STUDY OF CHLORINE BASED COPPER CORROSION AND ITS INHIBITION

APPROVED BY:

Prof. Dr. Tuğba Davran Candan ……
(Thesis Supervisor)
(Yeditepe University)

Assist. Prof. Dr. Murat Oluş Özbek ……
(Thesis Co-Supervisor)
(Gebze Technical Univeristy)

Assist. Prof. Dr. Cem Levent Altan ……
(Yeditepe University)

Prof. Dr. Mehmet Ferdi Fellah ……
(Bursa Technical University)

Assist. Prof. Dr. Levent Organ ……
(Yeditepe University)

DATE OF APPROVAL: …./…./20….

I hereby declare that this thesis is my own work and that all information in this thesis has been obtained and presented in accordance with academic rules and ethical conduct. I have fully cited and referenced all material and results as required by these rules and conduct, and this thesis study does not contain any plagiarism. If any material used in the thesis requires copyright, the necessary permissions have been obtained. No material from this thesis has been used for the award of another degree.

I accept all kinds of legal liability that may arise in case contrary to these situations.

Name, Last name ……..…. Ezgi Uslu…..……

Signature …..…….……..

ACKNOWLEDGEMENTS

First and foremost, I would like to thank Assist. Prof. Dr. Murat Oluş Özbek, for his immense knowledge, patience, motivation, enthusiasm, and guidance throughout my bachelor's and master's education, especially during the thesis stage. I am always grateful to him for helping me become the person I am today. I was very proud to work with him at each step of my academic life. I was able to stand privileged and confident on this path because he answered my every question, held my hand every time I fell, never took his hand off my shoulder, and always made me feel that he was behind me in all circumstances. I would also like to thank him for being a family, listening to all my problems, and giving me advice as well as being an advisor.

Furthermore, I would like to express my great appreciation to Prof. Dr. Tuğba Davran Candan, for being an excellent guide throughout my education. I am also highly indebted and thankful to her because she is always in contact with me and for standing behind me in every issue. I am grateful to her for always being more than a mentor and professor to me. I don't know if anyone else is better able to listen, understand and calm me down.

I wish to thank all my professors in the Chemical Engineering Department at Yeditepe University who have taken a significant part during my education. Among all, I would like to express my sincere gratitude to Assist. Prof. Dr. Cem Levent Altan has always supported me and made me believe in myself. He was always by my side with his possessive approach. Words cannot express my gratitude to him for allowing me to do projects together, for always trusting me, for giving me a place in his research group, and for opening my horizons. Moreover, I would like to thank Dr. Melis Çağdaş who has always been there with her incredible personality and poise. I feel extremely lucky that she changed my perspective, reminded me of whom I was meant to be, and talked about the beauty of staying out of line. Having a strong supporter like her motivated me a lot especially during the thesis period. Also, it was such a relief to know that her door was always open to me.

Special thanks to late Dr. Ali Türkyılmaz who encouraged me to start my master's journey. Our memories will be unforgettable for me. I hope he's proud of me. I also wish to thank Nur Pehlivan Akalın, Serpil Türkyılmaz, Selda Sarı, Gizem Karaca and Aydan Özden. Their moral support and experiences will always be invaluable in my entire life.

I would also like to extend my deepest gratitude to Beyza Abişoğlu, Katia Haviters, Kemal Düzkar, and Berk Alarcin for their unwavering support. They were always there when I was in trouble, when I was depressed or when I needed any help. This accomplishment would not have been possible without them. I would thank all of them, again and again, to make my whole life enjoyable. You've always been so much more than a friend to me, and I am glad to have you.

I cannot be to express my thanks to Mustafa Kılıç, who has always been there for me since the first day I met him. I am grateful to him for his unconditional support, trust, and endless patience. I am so lucky and happy to have someone like him in every moment of my life. Knowing that he is always behind me allows me to take more confident steps. I would also like thank to Nazlı Dilara Bakan for her sisterhood and support. She is the best gift that Yeditepe gave me.

Last but not the least, I would express my very profound gratitude to my parents, brother, and my grandparents for their unfailing support and unceasing encouragement throughout my education and through the research and writing of this thesis. In addition, I would like to thank them for their patience, self-sacrifice, and efforts for me. I know very well that I will not be able to repay their effort for the rest of my life. I hope I can make them proud and happy throughout my life. That's my only purpose. I am very lucky that they have made me a strong and independent person who can stand on my own feet. I am always honored to be their child.

ABSTRACT

A DFT STUDY OF CHLORINE BASED COPPER CORROSION AND ITS INHIBITION

Corrosion is the destructive attack of a metal by a chemical or electrochemical reaction with its environment. Due to its good mechanical properties and electrical and thermal conductivity, copper is one of the most useful metals. Likewise, the chemistry of chlorine on metal surfaces is involved in many technological processes, such as corrosion. Corrosion and its inhibition gain interest both on the experimental and theoretical sides. This work investigates the Cl adsorption on the metallic Cu (100), Cu (110), and Cu (111) surface and inhibitor effect of organic and inorganic inhibitor candidates on Cu (100) surface. Cl adsorption was studied at varying coverage from 1 ML to 1/16 ML and at different adsorption positions (4-fold, 3-fold (fcc, hcp), 2-fold (brg, l-brg, s-brg) and 1-fold (on top)). Inhibition effect of azole derivatives such as pyrazole and imidazole, relatively small atomic and molecular species such as O, H, OH, CO and HCO_3, and ammonia and chromic acid were studied on clean Cu (100) surface. Moreover, Cl adsorption energies in the presence of inhibitor atoms/molecules were also calculated. The results show that adsorption energies on different clean copper surfaces are coverage dependent. On average, Cl adsorption energy changes between +19 kJ/mol to -204 kJ/mol, -19 kJ/mol to -193 kJ/mol and +66 kJ/mol to -196 kJ/mol for Cu (100), Cu (110) and Cu (111), respectively. The preferable adsorption sites are 4-fold, 2-fold s-brg and 3-fold fcc, respectively. Among the tested inhibitor molecules azole derivatives, surface ions, chromic acid and ammonia were found to be stable on the surface. However, inhibition effect of these molecules could not be observed due to the high electron affinity of chlorine. Along with the copper surface, any co-adsorbed molecule becomes an electron donor for the chlorine, only making its adsorption stronger.

ÖZET

KLOR BAZLI BAKIR KOROZYONU VE İNHİBİSYONU ÜZERİNE DFT ÇALIŞMASI

Korozyon, bir metalin çevresiyle kimyasal veya elektrokimyasal reaksiyon sonucu yıkıcı saldırısıdır. İyi mekanik özellikleri, elektriksel ve termal iletkenliği nedeniyle bakır en kullanışlı metallerden biridir. Aynı şekilde, metal yüzeylerdeki klor kimyası, korozyon gibi birçok teknolojik süreçte yer alır. Korozyon ve inhibisyonu hem deneysel hem de teorik yönden ilgi görmektedir. Bu çalışma, metalik bakır (100), (110) ve (111) yüzeyindeki Cl adsorpsiyonunu ve organic/ inorganik inhibitör adaylarının Cu (100) yüzeyindeki inhibisyon etkisini araştırmaktadır. Cl adsorpsiyonu, 1 ML ila 1/16 ML arasında değişen kaplama düzeylerinde ve farklı adsorpsiyon pozisyonlarında (4-fold, 3-fold (fcc, hcp), 2-fold (brg, l-brg, s-brg) ve 1-kat (üstte)) çalışılmıştır. Pirazol ve imidazol gibi inhibisyon etkisi olan azol türevleri, O, H, OH, CO ve HCO3 gibi göreceli küçük atomik ve moleküler türler ile amonyak ve kromik asit temiz Cu (100) yüzeyinde incelenmiştir. Ayrıca inhibitör atomların/moleküllerin varlığında Cl adsorpsiyon enerjileri de hesaplanmıştır. Sonuçlar, farklı temiz bakır yüzeylerdeki adsorpsiyon enerjilerinin kaplama düzeylerine bağlı olduğunu göstermektedir. Cu (100), Cu (110), Cu (111) için sırasıyla +19 kJ/mol ila -204 kJ/mol, -19 kJ/mol ila -193 kJ/mol ve +66 kJ/mol ila -196 kJ/mol arasında ortalama bir Cl adsorpsiyon enerjisi değişimi gözlemlenmiştir. Tercih edilen adsorpsiyon bölgeleri 4-fold, 2-fold s-brg ve 3-fold fcc'dir. Test edilen inhibitör molekülleri arasında azol türevleri, yüzey iyonları, kromik asit ve amonyak yüzeyde kararlı bulunmuştur. Ancak klorun yüksek elektron afinitesi nedeniyle bu moleküllerin inhibisyon etkisi gözlenememiştir. Bakır yüzeyi ile birlikte, adsorbe edilen herhangi bir molekül, klor için bir elektron donörü olur ve yalnızca adsorpsiyonunu daha güçlü hale getirmektedir.

TABLE OF CONTENTS

LIST OF FIGURES

LIST OF TABLES

LIST OF SYMBOLS/ABBREVIATIONS

ads	Adsorption
AES	Auger electron spectroscopy
brg	Bridge
CF	Kinetic energy of a uniform gas
Clads	Chlorine adsorption
DFT	Density functional theory
DFT-GGA	Generalized gradient approximation
e-	Electron
E	Total energy
EF	Fermi energy
EIS	Electrochemical impedance spectroscopy
FCC	Face-centered cubic
GGA	Generalized gradient approximation
H	Hamiltonian
HEX	Heat Exchanger
HOMO	High occupied molecular orbital
ICCP	Impressed current cathodic protection
IE	Inhibition efficiency
Inh	Inhibitor
J[ρ]	Hartre mean field
l-brg	Long bridge
LDA	Local density approximation
LEED	Low-energy electron diffraction
LT-STM	Low-temperature scanning tunneling microscopy
LUMO	Lowest unoccupied molecular orbital
m	Mass
ML	Monolayer
NaN	Not a Number
NIXSW	Normal incident X-ray standing wave
Oxi	Oxidation

PAW	Projector augmented wave
PBE	Perdew–Burke–Ernzerhof
PES	Potential energy surface
QE	Quantum Espresso
Red	Reduction
rxn	Reaction
sbrg	Short bridge
scf	Self-consistent field
SEXAFS	Surface expanded X-ray absorption fine structure
SIMS	Secondary ion mass spectrometry
STM	Scanning tunneling microscope
T	Temperature
T	Kinetic energy
TF	Thomas-Fermi
U	Interaction energy
V	Potential energy
4-f	4-fold
3-f	3-fold
2-f	2-fold
1-f	1-fold
ΔG	Gibbs free energy
ΔH	Enthalpy
ΔH_{Cl}^{ads}	Adsorption energy of chlorine
ΔS	Entropy
$\delta E_{XC}[\rho(\vec{r})]$.	exchange correlation energy
εi	Kohn-Sham eigenvalue
$\bar{h}$	Reduced Planck constant
$h\rho(\vec{r})$	Particle density
θ	Monolayer
ν	Frequency
$\rho_0(r)$	Ground state density
$\rho(\vec{r})$	Charge density

σ	Bader charge
ϕ	Work function
Ψ	Wave function
ψ_i	Ground state of the system
ψ	Electrostatic potential
Å	Armstrong
K	Kelvin
Ry	Rydberg

1. INTRODUCTION

This section gives the necessary background information for better understanding the effect of chlorine-based copper corrosion and its inhibition. General information about copper, corrosion types and corrosion chemistry, chlorine-induced corrosion and corrosion inhibitors are presented below.

1.1. METALLIC COPPER

Copper has been an essential metal and had a significant impact on human civilization [1]. It is one of the most used materials due to its good mechanical properties as well as excellent thermal and electrical conductivity [2]. Table 1.1 gives the chemical properties of elemental copper. Nowadays copper, which has a wide range of uses and can be found almost all over the world, frequently takes place in industry in the form of heating and cooling pipes, heat transfer equipment, electrical appliances, architectural components, catalysis, power transmission equipment, industrial machinery, and military equipment [1,2]. In addition, copper and its alloys are preferred in heat exchangers, reactors operating with carbon monoxide and experimental systems due to copper's inability to dissociate the C-O bond. Copper can be classified as an environmentally friendly metal through its superior electrical and thermal conductivity that helps in protecting the environment by increasing energy efficiency, thereby reducing harmful emissions [3]. Moreover, copper is one of the rare metals that can be recycled 100 percent with no loss during recycling. Recycled copper and mined copper can be used interchangeably in the industry since there exists no quality differences [4]. Although copper has many different uses and advantages, corrosion of copper in the presence of oxygen, strong acidic medium and/or conditions containing chloride ions should be kept in mind.

Table 1.1. Chemical properties of elemental copper (Cu) [5]

Group	11	**Melting point**	1084.62°C
Period	4	**Boiling point**	2560°C
Block	d	**Density (gcm^{-3})**	8.96
Atomic number	29	**Relative atomic mass (g)**	63.546
State at 20°C	Solid	**Key isotopes**	^{63}Cu
Electron configuration	[Ar] $3d^{10}4s^{1}$	**CAS number**	7440-50-8

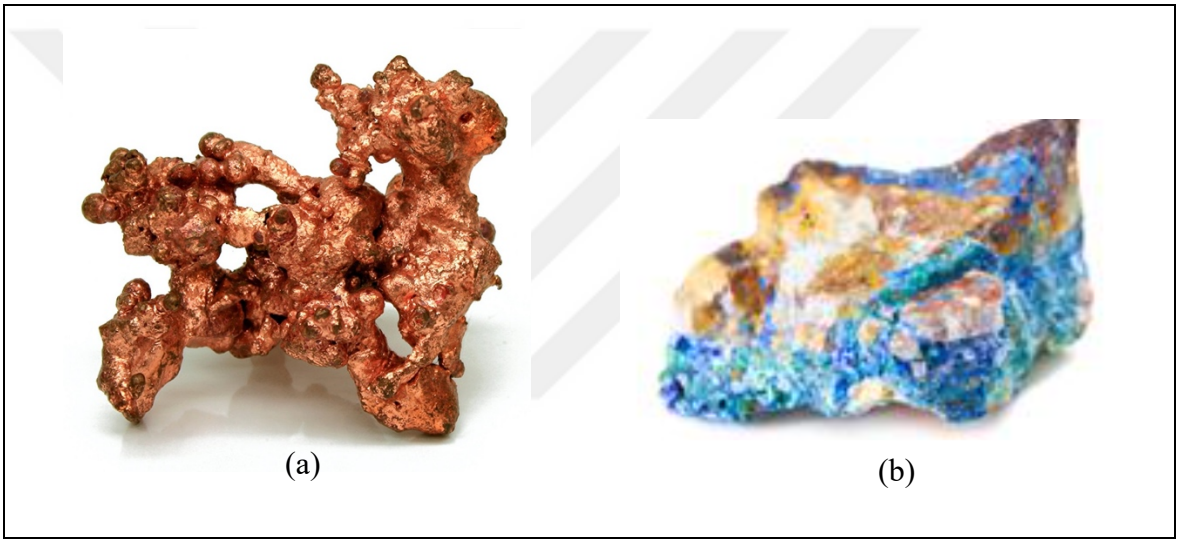

(a) (b)

Figure 1.1. (a) Metallic copper [6] and (b) Mineral copper (Rosasite) [7]

1.2. CORROSION

Corrosion is as an electrochemical process, which involves the deterioration of any material (metal, ceramic, polymer) by reaction with its environment [8]. Corrosion often causes detrimental effects on the usage of the material; physical or mechanical processes such as melting, evaporation, abrasion or mechanical fracture are also included in the term "corrosion" [9]. In addition to material loss, capital, labor and energy losses as well as adverse effects on human health and the environment are observed in case of corrosion [10]. As an example, although copper kitchen utensils have been used commonly for centuries copper oxide is harmful to human health, thus those items are tinned prior to use. In addition,

atmospheric and water pollution are among the main damages caused by corrosion [11]. Mining and metallurgical operations to replace lost material also fuel environmental damage.

1.2.1. Corrosion Types

Corrosion can be categorized according to the mechanism, the type of exposed material, type of the corrosive environment and the appearance of the corrosion-exposed material. General corrosion (uniform corrosion) is characterized by corrosive attack that spreads evenly over the entire surface area or a large part of the total area. As a result, general thinning occurs on the surface and damages the material. Uniform corrosion is relatively easy to measure and predict, making failures rarer. In the case of copper corrosion, for example the high ion concentration of seawater causes damage to the surface due to the attack of chloride ions [12].

Pitting corrosion, which is a second type of corrosion, is a localized type of corrosion by which cavities or “holes” are produced in the material. It is harder to detect, predict and design against so pitting is considered to be more dangerous than uniform corrosion. Corrosion products often cover the pits and a small, narrow pit with minimal overall metal loss can lead to the failure of an entire engineering system. Chloride is the most frequently encountered aggressive agent, which causes pitting of many metals [13].

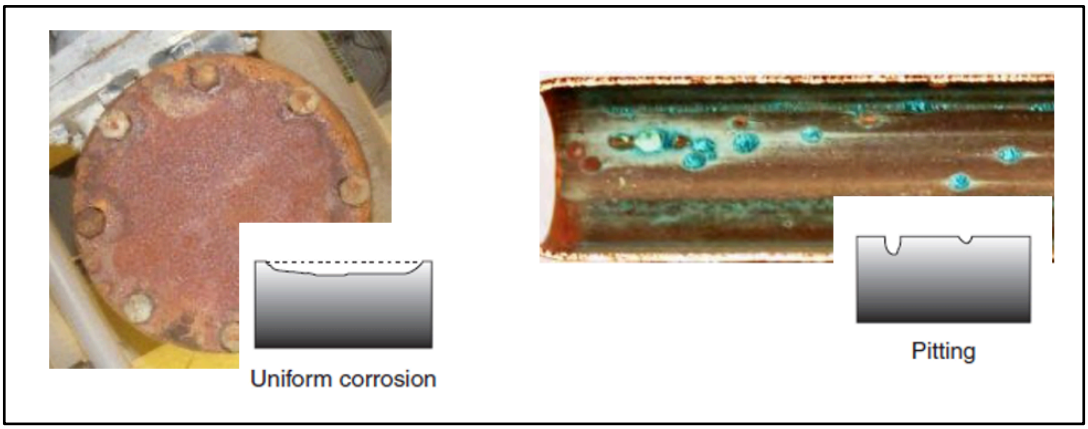

Figure 1.2. Schematic representation [14] and surface figure of (a) General (uniform) corrosion [15], (b) Pitting corrosion [16]

1.2.2. Chemistry of Corrosion

Corrosion of a metal is a redox reaction. When a metal contacts with an aqueous environment, both oxidation and reduction reactions occur simultaneously on the surface until some equilibrium is reached. Anodic half-reaction, (Equation 1.1), involves a metal oxidation process while cathodic half-reaction (Equation 1.2) is the reduction of an electrochemically active oxidant. Thus, general overall corrosion reaction (Equation 1.3) can be thought of as a combination of these two half-reactions.

$$\text{Anodic half-reaction: } M \rightleftarrows M^{n+} + ne^{-} \tag{1.1}$$

$$\text{Cathodic half-reaction: } Oxi + ne^{-} \rightleftarrows Red \tag{1.2}$$

$$\text{Overall reaction: } M + Oxi \rightarrow M^{n+} + Red \tag{1.3}$$

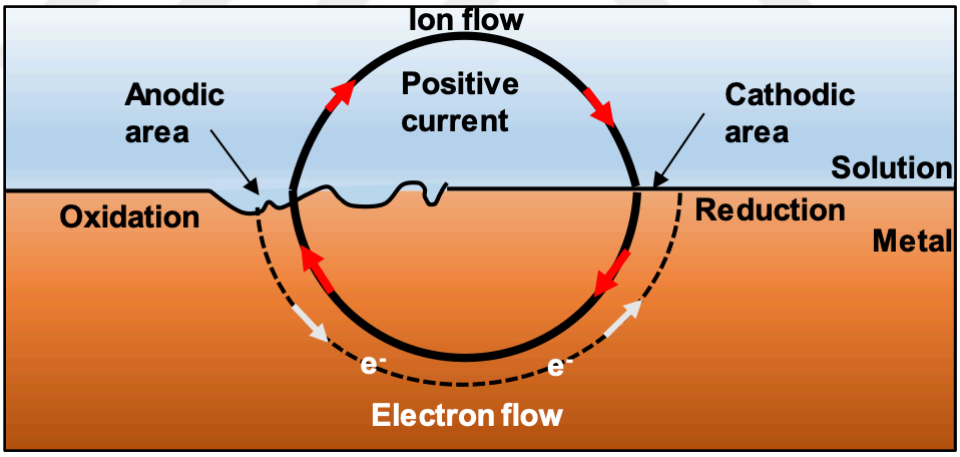

Figure 1.3. A diagram showing a corrosion process [17]

A corrosion system can be considered as a short-circuited electrochemical cell where the driving force is the potential difference between the anodic and cathodic half-cell reactions that leads to a current flow (electron transfer) within this corrosion cell.

To prevent corrosion, one of the half reactions must be inhibited. Inhibition of the anodic area was investigated when a chlorine-based copper corrosion studied.

1.2.3. Chlorine as the Corrosive Agent

The seas cover more than seventy percent of the Earth and seawater is considered to be the most ample and natural electrolyte [18]. Metal structures exposed to seawater or marine environment are damaged due to corrosion. According to Farro et al.[19], the main cause of corrosion occurring at the marine environment is the erosion of the material by sea water. Presence of dissolved gases (O_2, CO_2), free ions (due to decreasing order: Cl^-, Na^+, SO_4^{2-}, Mg^{2+}, Ca^{2+}, K^+, HCO^{3-}, Br^-, Sr^{2+}, B^{3+}, F^-, Mo^{2+}), living organic matters, other substances in the state of decomposition and abundant dissolved ionic salt in the water increase the corrosiveness. Sea water is an aggressive environment for metals and in the short term it can cause serious corrosion damage to metallic structures and the resulting corrosion products can pollute the environment [19].

The interaction of chlorine with copper surfaces is an important issue for understanding the electrodesorption and catalytic mechanisms as well as for the basic surface science associated with corrosion. Due to the widespread use of copper and its alloys, corrosion of copper, especially in environments containing chloride ions, has been investigated in many studies [20–23]. Chloride ions are highly corrosive and aggressive to copper and its alloys owing to the chloride ion tendency to form an unstable film (CuCl) and soluble chloride complex like $CuCl_2$ and $CuCl_3^{2-}$ [24]. Accordingly, even traces of chloride ions can cause corrosion problems in copper. Therefore, copper has attracted the attention of the researchers in a wide variety of environments, especially when they contain chloride ions [25–27].

When Cl^- is present, active dissolution of Cu proceeds through a series of electrochemical and chemical reactions where equations are given in (Equation 1.4- Equation 1.7).

$$Cl^- \rightarrow Cl^-_{ads} \quad (1.4)$$

$$Cu + Cl^- \rightarrow CuCl_{ads} + e^- \quad (1.5)$$

$$CuCl_{ads} + Cl^- \rightarrow CuCl_2^-(surface) \quad (1.6)$$

$$CuCl_2^-(surface) \rightarrow CuCl_2^- \quad (1.7)$$

Where the solution at the copper surface and solution remote from the copper surface were shown as “surface” and “bulk”, respectively [28].

Chlorine interaction with copper surfaces and the basis of this interaction is the key issue for understanding corrosion, electrodeposition and catalysis.

1.3. CORROSION INHIBITORS

Although there are many different ways to prevent corrosion such as Impressed Current Cathodic Protection (ICCP) [29], where an electric current is applied to prevent the cathodic half redox reaction, this work is limited to chemical aspects. This study [29], deals with chemical processes and chemical inhibitors. Choosing the appropriate prevention method depends on the cost of material, application difficulty, safety conditions and technical evaluations such as high mechanical and corrosive resistance. Among these methods to prevent the destruction of the metal surface and to prevent surface deterioration, inhibitors are the best known and widely used corrosion protection methods in the industry.

Corrosion inhibitors are chemicals that reduce, slow down or prevent corrosion of a metal when placed in an corrosive environment [30]. Inhibitors block the corrosion zones thus inhibit the adsorption process of the corrosive material to the surface, thus prolonging the life of metal [31]. Using corrosion inhibitors is very important to prevent metal dissolution and to prevent the raw materials' waste. Although inhibitors have been widely accepted in industry because of their excellent anti-corrosive properties, some of them were observed to be environmentally hazardous. Thus, scientists have begun to look for environmental-friendly inhibitors, such as organic inhibitors [32,33].

Corrosion inhibitors can either be synthetic or natural chemicals and can be classified in three as follows;

i. As organic or inorganic according to their chemical structure;
ii. as anodic, cathodic or anodic-cathodic mixture depending on the mechanism of action;
iii. as oxidant or non-oxidant

Generally, inorganic inhibitors are either cathodic or anodic in their nature, while organic inhibitors can be both cathodic and anodic simultaneously and act with a protective film adsorption [33]. Figure 1.4. shows classification of the inhibitors.

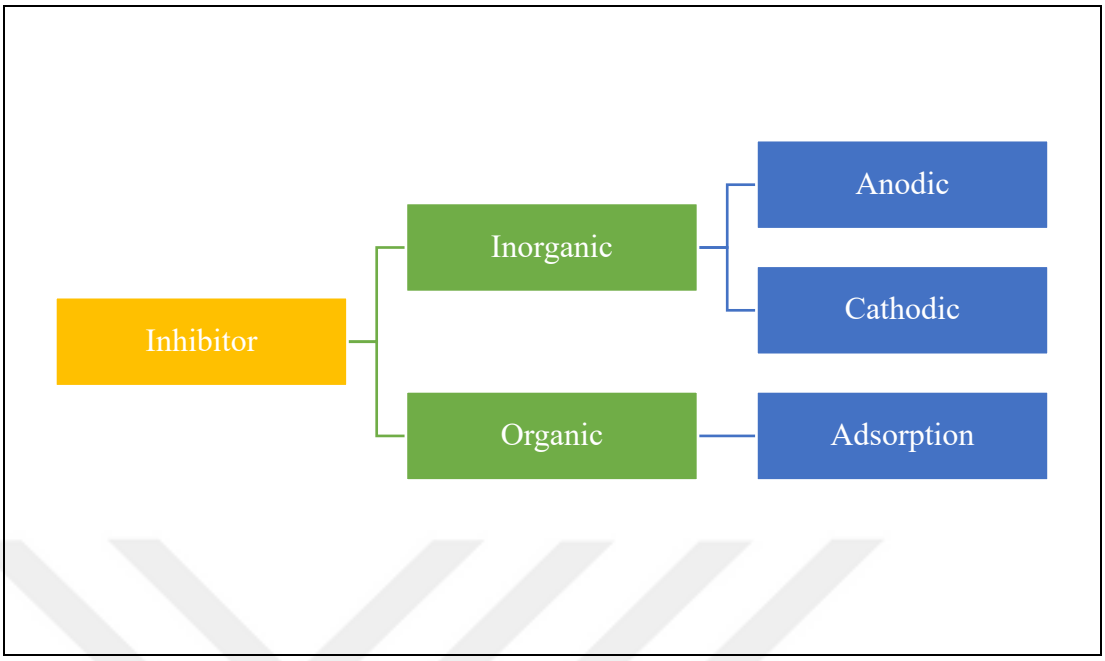

Figure 1.4. Classification of corrosion inhibitors as adapted from [33]

The working principles of inorganic inhibitors can be examined under two mechanisms. These are anodic and cathodic protection as mentioned above. Anodic inhibitors (also called passivation inhibitors) act through a reductive anodic reaction. They block the anodic reaction and support the natural reaction of the metal surface passivation through forming an adsorbate layer on the protected metal. Generally, the inhibitors react with the initial corrosion product forming a cohesive and insoluble film on the metal surface. Nitrates, molybdates, phosphates and chromates are major examples of anodic inorganic inhibitors. On the other hand, during corrosion, cathodic inhibitors prevent the cathodic reaction of the metal. These inhibitors have metal ions that can produce a cathodic reaction due to alkalinity, thus selectively precipitating at the cathodic sites and producing insoluble compounds. A compact and adhesive film is placed over the metal that restricts the diffusion of reducible species in these areas. In this way, the inhibitors provide cathodic protection. Antimony accumulating in the cathode area in acid solutions, oxides and salts of arsenic and bismuth can be listed as examples of cathodic inhibitors [33,34].

Although many inorganic inhibitors are effective, they are usually not safe nor economical. Attempts to find environmental-friendly alternatives with less adverse effects have recently intensified. Therefore, environmentally sensitive materials have begun to replace toxic inhibitors.

The well-known inhibitors for acidic medium are organic compounds that contain oxygen, nitrogen and sulfur atoms. Organic compounds with heteroatoms (O, N, S) can donate electron pairs to inhibit metal corrosion in many different aggressive electrolytes. The use of organic inhibitors is an environmental-friendly alternative for preventing corrosion. The inhibition action of organic compounds on the metallic surface can be described with adsorption interaction between the inhibitor molecule and metal surface as shown in the Figure 1.5. These inhibitors are adsorbed on the metal surface by a covalent bond or electrostatic interaction between the inhibitor and the metal. This adsorption forms a protective hydrophobic film layer on the metal surface, which cut or reduce contact with the acidic, corrosive medium and provides barrier. The efficiency of these inhibitor molecules depends on their ability to generate complexes with metal surface atoms since adsorption behavior of organic inhibitors on the metal surface [35,36].

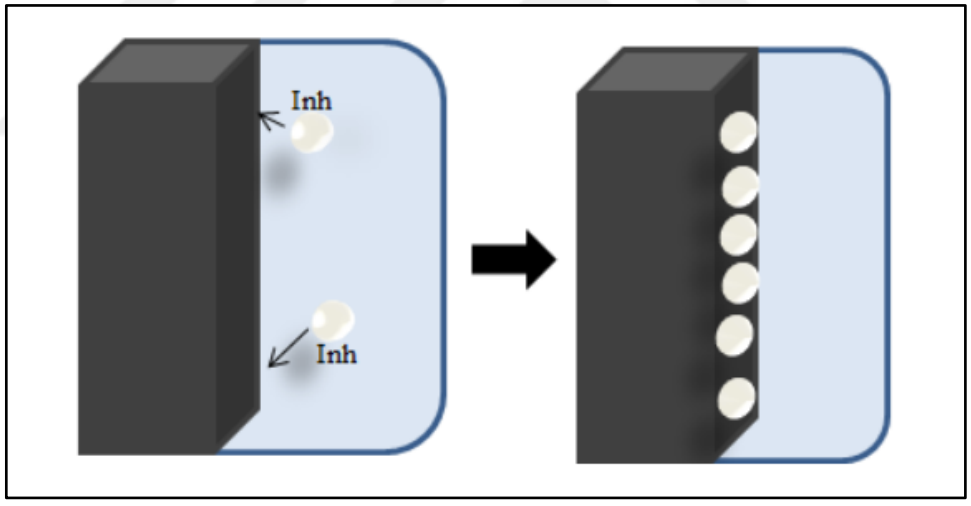

Figure 1.5. Adsorption of the organic inhibitor molecule on the metal surface [33]

1.4. BACKGROUND ON TERMINOLOGY

1.4.1. Adsorption

Adsorption can be examined under two subheadings depending on the interaction strength between adsorbate and adsorbent.

i. “physisorption” with weak interactions
ii. “chemisorption” with strong interactions

Physisorption describes the weakest interaction between adsorbent and adsorbate due to weak Van der Waals forces between atoms. Binding energies relatively low, being in the order of 10-100 meV. Because the interaction is weak, the physisorbed atom or molecule does not significantly disrupt the structural environment near the adsorption site. It can be detected under conditions where there is no stronger chemisorption in the vicinity and the adsorption temperature is low [37].

Chemisorption refers to the situation where strong chemical bonds form between the adsorbate and adsorbent. These bonds might be covalent or ionic. Binding energy is in the range of 1-10 eV. As a result of this reaction, new chemical bonds are formed between the adsorbate and the adsorbent. Strong interaction can change the structure of the adsorbate or adsorbent [37].

1.4.2. Coverage of Adsorbate

The adsorbate coverage, θ, is used to describe the surface concentration of the adsorbed material (as the number of adsorbates per surface atom/site) in terms of monolayer (ML) unit. By using Equation (1.8.) surface coverage can be determined. Figure 1.6 illustrates the varying adsorption coverage.

$$\theta = \frac{\text{number of adsorbed atom/molecule}}{\text{number of surface atoms}} \qquad (1.8.)$$

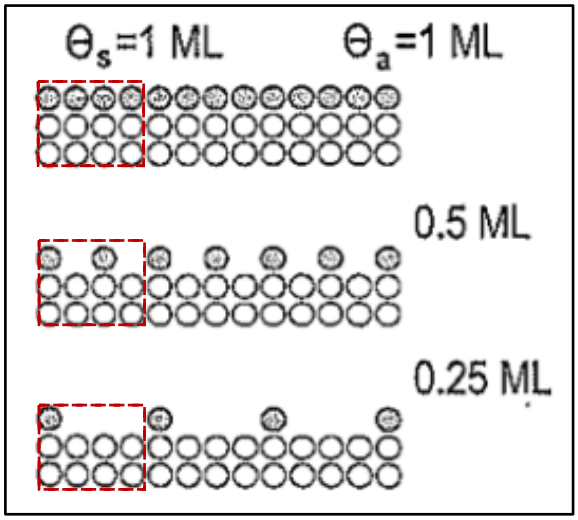

Figure 1.6. Illustration of varying surface coverage in terms of ML [37]

1.4.3. Work Function

The minimum thermodynamic energy/work required to remove an electron from the metal surface and move it to a point in the vacuum region outside the surface interactions gives the work function (ϕ). Based on this definition, the low work function means that electrons can be removed from the surface more easily. In other words, it indicates that the adsorption is weaker. The drawing showing the energies related to the work function as a result of the electrostatic potential applied near the metal surface is presented in Figure 1.7. Blue circles represent atoms in the same plane with a distance d between them. The vertical dashed line indicates the geometric metal surface location, and the shaded gray area indicates the filled energy levels [38].

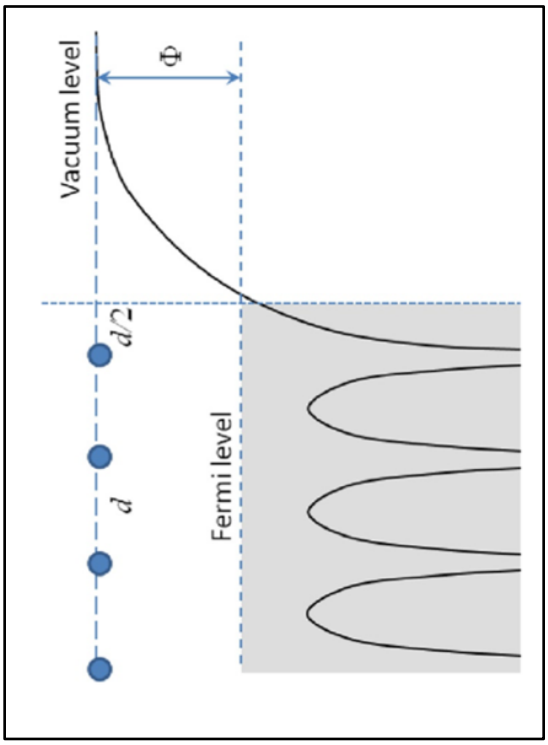

Figure 1.7. Illustration of electron on a metal surface transfer fermi to vacuum level [38]

1.5. OBJECTIVE

The main objective of this study is to investigate the interaction of chlorine with copper surfaces for a better understanding of chlorine caused copper corrosion; and to test and propose a possible/suitable corrosion inhibitor. For this purpose, Cu (100), Cu (110) and Cu (111) were studied at p(1x1), p(2x2), p(3x3), p(4x4) surface slab models with chlorine coverage values of θ = 1 ML, 0.75 ML, 0.50 ML, 0.33 ML,0.25 ML, 0.22 ML, 0.11 ML and 0.0625 ML. Although Cu (111) surface is the most stable and dominant surface due to low surface energy [39], other low index copper surfaces were also included. Selection of multiple surfaces stem from the fact that any copper material used would exhibit different surfaces due to the existing grains. Having the minimum surface energies, thus being the most stable ones (100), (110) and (111) surfaces of copper were selected. In the second part of the study, on the other hand, metal-inhibitor and metal-chlorine-inhibitor interactions are examined by using organic and inorganic inhibitors that will prevent or reduce copper corrosion.

“Literature Survey” chapter contains information about the previous experimental and computational studies on corrosion and its inhibition. Subsequently, “Theory and Methodology” presents detailed information about Density Functional Theory (DFT), software utilized, and computational details applied in this work, “Results and Discussion” includes all the results with discussions. Finally, "Conclusions and Future work" summarizes the major conclusions from the results along with the suggestions for future studies.

2. LITERATURE SURVEY

A summary of previous experimental and computational studies is given in this section in the order of experimental metal-halogen studies, computational metal-halogen studies and corrosion inhibitor studies.

2.1. METAL-HALOGEN ADSORPTION STUDIES

Corrosion of any metal is a very suitable research topic for theoretical chemistry and electrochemistry. In theoretical chemistry structures are electronically modeled, and electronic properties are studied. Electrochemistry is also ideal for investigating halogen-metal interactions at the electronic-atomic level and the effect of inhibitors on these processes.

Chlorine-copper interaction and its inhibition has been investigated since 70's [40–47]. In 1977, Goddard et. al compiled results from low-energy electron diffraction (LEED), Auger electron spectroscopy (AES), work function measurements, and desorption experiments [40]. Surface expanded X-ray absorption fine structure (SEXAFS) and photoelectron diffraction [41], normal incident X-ray standing wave field absorption (NIXSW) [42,43], secondary ion mass spectrometry (SIMS) [44] scanning tunneling microscope (STM) [45] method show strong interaction between Cu-Cl. More studies have been carried out in the following years using different analysis methods such as LEED, AES, thermal and electron stimulated desorption [46]. Much recent studies reported results obtained under monolayer chlorine coverage (<0.33 ML) on Cu (111). Measurements with low-temperature scanning tunneling microscopy (LT-STM) showed that chlorine tended to form chain-like structures in the single-layer sub-stage of adsorption. In the case of single atomic chains, chlorine atoms can occupy the 3-fold fcc-hcp positions alternately. It was found that indirect electronic interaction is caused by the abnormally short Cl-Cl interatomic distances in the chains [47].

With the development of technology, having the necessary software and hardware, computer simulations (modeling) have become a powerful tool for investigating complex processes. Inhibition mechanisms can be investigated in depth by examining molecular structures,

electron distributions and surface adsorption processes. In the early 70's, Vosta [48] introduced quantum chemical methods to investigate corrosion and its inhibition and established the field of quantum corrosion electrochemistry. After this development, the focus of quantum chemistry methods was mainly on the discovery and establishment of relationships between molecular structure and inhibition efficiency. In the 1990s interest was directed to describing the interaction between inhibitor molecules and metal surfaces using quantum chemical techniques.

Compared to the long-standing experimental studies, theoretical research on corrosion is rather recent and limited in number. Furthermore, most of the studies limit themselves to the investigation of frontier orbitals, HOMO (high occupied molecular orbital), LUMO (lowest unoccupied molecular orbital) of the gas phase molecules [49–51]. However, later studies included the interactions of the candidate molecule with the metal atoms or surfaces [52–59]. Nevertheless, analysis of the properties of the molecule alone, cannot reveal the details of molecule-surface interactions. Self-assembly properties of the molecules and atoms must be taken into account to explain the interaction between molecules and metal surface. Theoretical studies covering the complete picture where metal surface, adsorbed corrosive element and the inhibitor molecules are included within the model do not exist in the literature to our best knowledge.

2.2. CHLORINE ADSORPTION STUDIES

Computational studies for the Cl/Cu (111) system based on DFT calculations has been published by different groups [2,60–62]. Peljhan and Kokalj [2] deal with adsorption of chlorine on Cu (111) surface by using DFT-GGA (generalized gradient approximation) calculation. Total chemisorption energy as a function of chlorine coverage is shown in Figure 2.1 [2]. Figure 2.2 shows the work function change due to chlorine coverage.

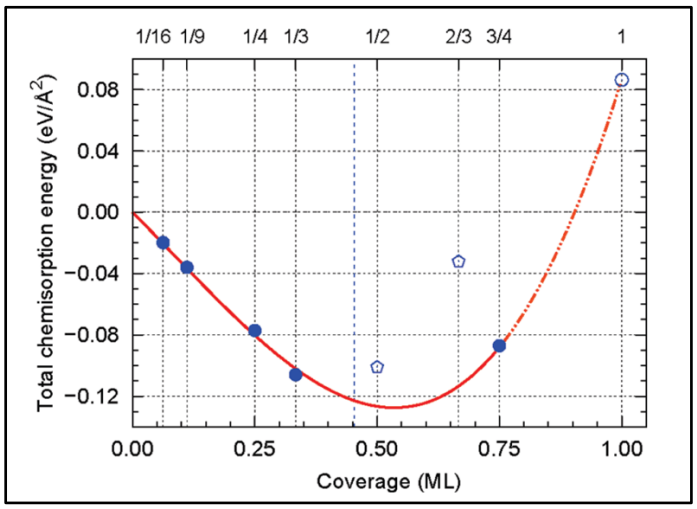

Figure 2.1. Theoretical measured of the total chemisorption energy per surface unit area of on-surface chlorine due to chlorine coverage [2]

Migani and Illas [62] presented a systematic study of halogens on various metal surfaces. For the Cl/Cu (111) system, the authors considered two supercells ((√3 × √3)R30° and (3 × 3) and confirmed the main findings of Doll and Harrison [60]. Chlorine adsorption on Cu (111) has been studied by Roman and Gross [63]. In their recent study, experimentally observed monotonic increase of chlorine coverage [40] and work function are supported by density-functional theory (DFT) calculations. As may be observed in Figure 2.3, the work function increased with increasing coverage (adsorbed chlorine amount), while the polarization effect of chlorine was insignificant in the adsorption of chlorine on Cu (111).

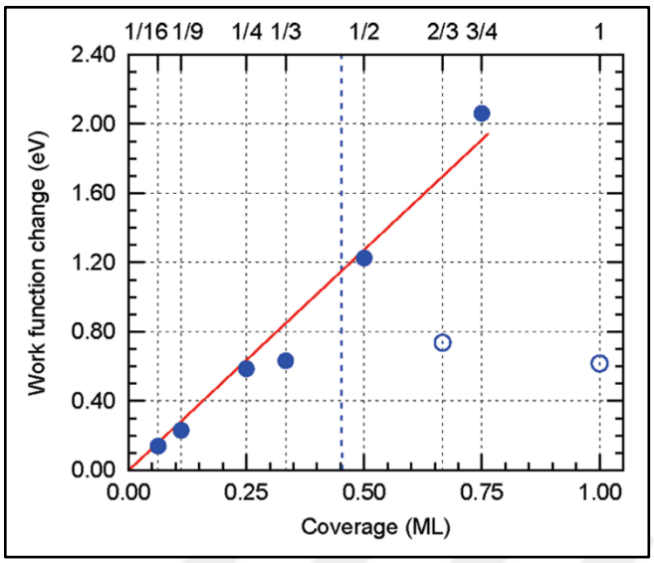

Figure 2.2. Work function change due to chlorine coverage [2]

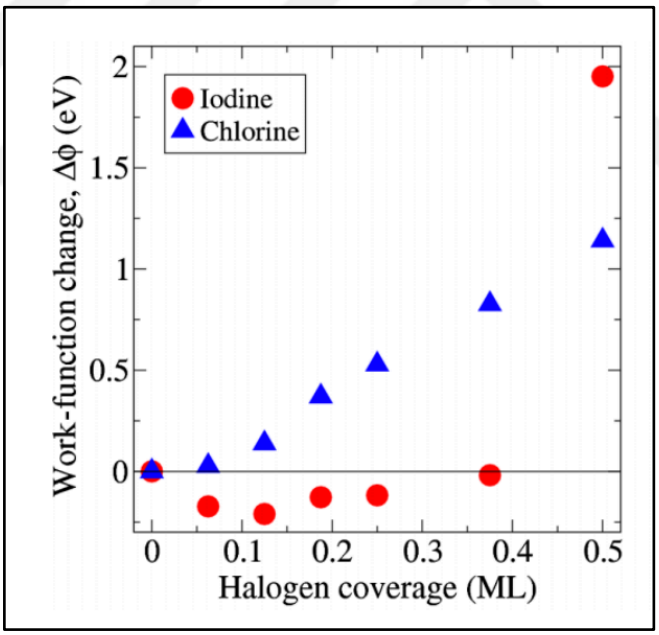

Figure 2.3. Chlorine (blue) coverage dependence of the change in the work function [63]

Pavlova et al. [64], carried out a systematic computational study of molecular chlorine adsorption on the Cu (111) surface. All the chlorine structures detected by STM experiments were identified theoretically, various defect structures were examined and their stabilities were tested. In addition to all these, first-principle calculations were performed for all stages of Cu (111) chlorination, i.e. dissociation of Cl molecule, adsorption of chlorine atoms, diffusion of copper and chlorine atoms along the surface, coupling and desorption of reaction

products. In the work reported by Suleiman et. al. [65] , findings of the ab-initio atomistic calculations performed to determine the thermodynamic stability of Cl-induced Cu (110) surface under various Cl exposure (pressure and temperature) conditions were given. According to the study, under ultra-high vacuum conditions, the p(2x 2)-Cl configuration was found to be the most stable one for inclusions up to (including) 1/2 ML and it was concluded that the 1 ML geometries, which were the most stable (thermodynamically) structures under high chlorine exposure were only kinetically accessible.

2.3. INHIBITOR STUDIES

Due to the complexity and multiple-step nature of corrosion inhibition, good inhibitors have been determined purely empirically from large clusters of organic compounds, where experimental tests provide information as to whether a particular compound is effective in a particular medium for a particular substrate. The current state of the art in this field is represented by high-throughput experimental work [66–70].

Traditionally, the inhibitory effect is studied by experimental methods such as weight loss determination, electrochemical potentiodynamic polarization, and electrochemical impedance spectroscopy (EIS). However, these methods are expensive, time consuming, and often inadequate to elucidate inhibition mechanisms and interaction between inhibitor molecules and metallic surface.

Contrary to such trial-and-error approaches, rational designs of potential corrosion inhibitors with superior corrosion inhibition ability represent a major breakthrough in this field [71,72]. For this purpose, the popularity of molecular modeling studies has increased [73,74]. Even if the experiment takes place under well-designed conditions, the interpretation of the results on the inhibitor-metal interaction is usually subject to a few assumptions. In this respect, computer simulation studies based on density functional theory (DFT) have gained importance. Especially in the last decade, they have become widely used in surface science to aid in the interpretation of experimental results. From this point of view, it is quite surprising that the bonding of organic corrosion inhibitors to metal surfaces, in particular, has rarely been investigated through explicit DFT calculations [55,56,75,76].

The basis of molecular modeling studies is the proposal of new and effective inhibitors. Among the various approaches, machine learning techniques currently have the potential to establish reasonably robust and predictive models for screening for novel inhibitors, but such studies are not plentiful [50,77–83]. Instead, the vast majority of molecular modeling studies of corrosion inhibitors rely on calculating many molecular electronic properties and correlating them with empirically determined corrosion inhibition efficiency (IE) through some correlation analysis, which in most cases is a simple linear correlation between a given molecule.

Most of the experimental studies supported that azole and their derivatives are effective corrosion inhibitors for copper corrosion [84–88]. Recently, molecular-level approaches to corrosion prevention, namely understanding the adsorption modes of inhibitors on metal surfaces, have gained importance. While Grillo et al. [89] conducted a study on the adsorption of benzotriazole on the Cu (111) surface, Kokalj and Peljhan [55] examined 3-amino 1,2,4-triazole and 1-hydroxybenzotriazole adsorption on the Cu (111) surface in their study. Awad et al. [90] applied molecular to study the adsorption of some triazole derivatives on the copper surface. Obot et al. [91] investigated the adsorption of 2-mercaptobenzimidazole using density functional theory (DFT) and molecular dynamics simulations. However, although the results obtained by computer simulations of the electronic properties of inhibitor molecules appear similar to the experimental findings, this cannot be considered a rule in a study presented by Kokalj [92].

3. THEORY AND METHODOLOGY

All of the results reported in this study have been achieved by modeling the adsorption system and reactions with quantum chemical methods. The theory behind, the software used, models and methodology are explained in this section.

3.1. DENSITY FUNCTIONAL THEORY

Density functional theory (DFT) is used as a research tool in all disciplines that deal with atoms and molecules such as chemistry, chemical engineering, physics, biology, and materials science [93].

DFT is a highly successful approach to find solutions to the fundamental equation that describes the quantum behavior of atoms and molecules, namely the Schrödinger equation. This approach quickly evolved from being a special art applied by a small number of physicists and chemists at the cutting edge of quantum mechanical theory to a tool used by the disciplines which are mentioned above [94]. Nowadays, DFT has a unique role to understand many-body systems.

In most of the solid-state and quantum chemistry approaches, the goal is to solve the time-independent, non-relative Schrödinger equation. In 1925, Erwin Schrödinger formulated the Schrödinger equation, describing how the quantum state of a physical system changes over time. The time-independent Schrödinger equation for any N-electron system in a stationary time or steady state is,

$$H\Psi=[T+V_{ext}+U]\Psi \tag{3.1}$$

$$-\frac{\bar{h}^2}{2m}\frac{\partial^2\Psi}{\partial x^2}+U\Psi=E\Psi \tag{3.2}$$

$$\hat{H}\Psi=E\Psi \tag{3.3}$$

Where, H is the Hamiltonian, T is the kinetic energy, V is the potential energy due to the nuclei and U represent the interaction energy between two electrons, m is the mass, Ψ is the wavefunction, $\bar{h}$ is the reduced Planck constant and E is the total energy.

The exact solution of such equation is not possible for non-hydrogenoid species. Therefore, some approximations are made such as Born-Oppenheimer approximation or separating nucleus and electrons [95]. Hartree-Fock method, or post-Hartree-Fock methods are not suitable for computation in larger and more complex systems, at this point DFT offers an attractive alternative that is much more versatile.

In the DFT the key variable is the particle density, $\rho(\vec{r})$ which is given by,

$$\rho(\vec{r})=N\int d^3r_2 \int d^3r_3 \ldots \int d^3r_N\, \Psi^*(\vec{r},\vec{r}_2,\ldots,\vec{r}_N)\Psi(\vec{r},\vec{r}_2,\ldots,\vec{r}_N) \tag{3.4}$$

As a first step to understanding DFT, one should take a look at the Thomas-Fermi (TF) theorem proposed by Enrico Fermi and L.H. Thomas for solving many electron problems [96,97]. Thomas-Fermi energy functional for an atom with N electrons and with an atomic number Z expressed as,

$$E[\rho]= C_F\int \rho^{\frac{5}{3}}(r)dr - Z\int \frac{\rho(r)}{r}dr + J[\rho] \tag{3.5}$$

The Thomas-Fermi kinetic energy functional is insufficient. A good approximation is possible by directly applying the Euler-Lagrange equations to find ρ and E[ρ]. An approach that uses only electron density in the Euler-Lagrange equations is desired [98].

Hohenberg and Kohn (1964) [99] states that by minimizing the functional of the electron density, the ground state properties of the multi-electron system can be obtained. Hohenberg and Kohn basically mentioned two key theorems of DFT [100]:

Any observable quantity of a stationary quantum mechanical system can only be determined from the ground state density. The exact ground state density of a system at external potential can be found by minimizing the energy functional. If the ground state of the system is not degenerate, there is a single charge density that corresponds to the given external potential and gives the ground state energy by minimizing the energy.

The relationship between electron density and multi-electron wave function according to the Hohenberg-Kohn theorem is as follows:

$$\rho(\vec{r})=N\int |\,\Psi_0(\vec{r},\vec{r}_2,\ldots,\vec{r}_N)|^2\, d\vec{r}_2 \ldots d\vec{r}_N) \tag{3.6}$$

After then, in 1965, Kohn and Sham proposed that the electron density of the interacting system can be written in terms of single electron wave functions of the non-interacting system.

$$\rho(\vec{r})= \sum_{i=1}^{N} \left|\psi_i(\vec{r})\right|^2 \tag{3.7}$$

According to the Kohn-Sham theorem, the ground state of the system and hence the ground state density and energy can be obtained from the minimization of the total energy functional. For this, self-consistent solutions of the set of equations are made.

Kohn-Sham equation for a single electron is as follows:

$$\left[-\frac{h^2}{2m}\nabla^2+V_d(\vec{r})+V_H(\vec{r})+V_{XC}(\vec{r})\right]\psi_i(\vec{r})=\varepsilon_i\psi_i \tag{3.8}$$

Where ε_i is the Kohn-Sham eigenvalue.

Each term in the Hamiltonian is expressed as a function of density. Hartree potential is,

$$V_H(\vec{r})= e^2 \int d\vec{r}\frac{\rho(\vec{r})}{\left|\vec{r}-\vec{r}'\right|} \tag{3.9}$$

and exchange correlation potential,

$$V_{XC}(\vec{r})= \frac{\delta E_{XC}[\rho(\vec{r})]}{\delta\rho(\vec{r})} \tag{3.10}$$

It is not possible to precisely calculate the exchange correlation energy.

Since the form of this term is unknown, it is difficult to write it as a functional of density. However, its value can be calculated approximately with some developed approaches. These approaches are; local density approach (Local Density Approximation, LDA) [101], generalized gradient approach (Generalized Gradient Approximation, GGA) [102] and Hybrid Approximations. LDA is a model developed by assuming that the exchange correlation energy of each electron at all points in space is equal to the exchange energy of each electron in a homogeneous electron gas. The GGA is based on the idea that, in addition to LDA, the spatial variation of this density should be taken into account as well as the

electronic charge density at each point. There is no general selection rule regarding the use of LDA or GGA. LDA gives good results in electronic structure calculations of some materials and GGA in others. Beyond LDA and GGA, Axel Becke [103] introduced a new mixing of LDA and Hartree-Fock theories as Hybrid. Hartee-Fock overestimates gaps and magnetic moments, while LDA underestimates such things. It has been concluded that a hybrid model can be made from these two methods. Hybrid functions are popular and used in quantum chemistry. Although both theories individually have almost equivalent simplicity and computational efficiency, hybrid functions have higher accuracy [103]. Figure 3.1 shows the self-consistent field (scf) calculation procedure.

Step 1: Assume random charge density to start. It is generally convenient to choose atomic densities. (The densities to be obtained as a result of self-matching calculations starting from different densities must be exactly the same. This result gives the Kohn-Sham equations: The charge density that gives a certain crystal potential is unique.)

Step 2: Calculate $V_H(\vec{r})$ and $V_{XC}(\vec{r})$ potentials using density found in step 1.

Step 3: The matrix representation of the Hamiltonian is created and this matrix is diagonalized. Kohn-Sham equation is solved for the whole system.

Step 4: The new density is calculated from the obtained wavefunction solution.

$$\rho_{new}(\vec{r}) = \int \psi^{*}(\vec{r})\,\psi(\vec{r})\,d\tau$$

Step 5: If the difference between $\rho_{new}(\vec{r})$ and $\rho(\vec{r})$ is greater than the sensitivity of the calculation that was determined at the beginning, step 4 is used by using $\rho_{new}(\vec{r})$ and the processes are repeated. When the difference of $\rho^{+1}(\vec{r}) - \rho(\vec{r})$ is smaller than the specified sensitivity, the calculation is cut and the solution sought is obtained and the self-consistent calculation is completed.

Step 6: The total energy of the system, forces and etc. is calculated.

Figure 3.1. The Self-Consistent Field (SCF) calculation procedure

3.2. SOFTWARE UTILIZED

Quantum Espresso [104] is utilized to compute electronic structures. Molecules, copper surfaces, their interactions, and geometries are visualized by XCrySDen [105] software. In this chapter, these softwares are explained in detail.

3.2.1. Quantum Espresso

All periodic DFT computation in this study were performed by using the QUANTUM ESPRESSO (QE), which is an integrated package of computer codes for electronic structure calculations and material modeling based on DFT, plane-wave fundamental sets and pseudo-potentials representing electron-ion interactions. QUANTUM ESPRESSO is a free, open-source software. It implements various methods and algorithms that aimed chemically realistic material modeling at the nano scale based on the solution of density-functional theory (DFT) problems [104].

3.2.2. XCrySDen

In computer graphics, simulating material at atomic scale has become more important in recent times. Computer graphics are very useful for identifying and studying chemical structures, as it is now possible to study complex systems with density functional theory and a few hundred equivalent atoms. In addition, computer graphics are an indispensable tool in the analysis of computed data and facilitate interpretation of results. XCrySDen is a general solid-state visualization program. The name of the program stands for Crystalline Structures and Density and X because it works in the X-Window. The crystal structure facilitates the visualization of overlaid and interactively rotated and manipulated isosurfaces and contours. It also has some tools for the analysis of mutual space properties, such as the interactive selection of k-paths in the Brillouin region for band structure graphics and the visualization of Fermi surfaces [105].

3.3. COMPUTATION TYPES AND CALCULATIONS

The presented results were obtained through different types of computations and post-process calculations. These are briefly explained below. Figure 3.2 shows the computation and calculation procedure as a scheme.

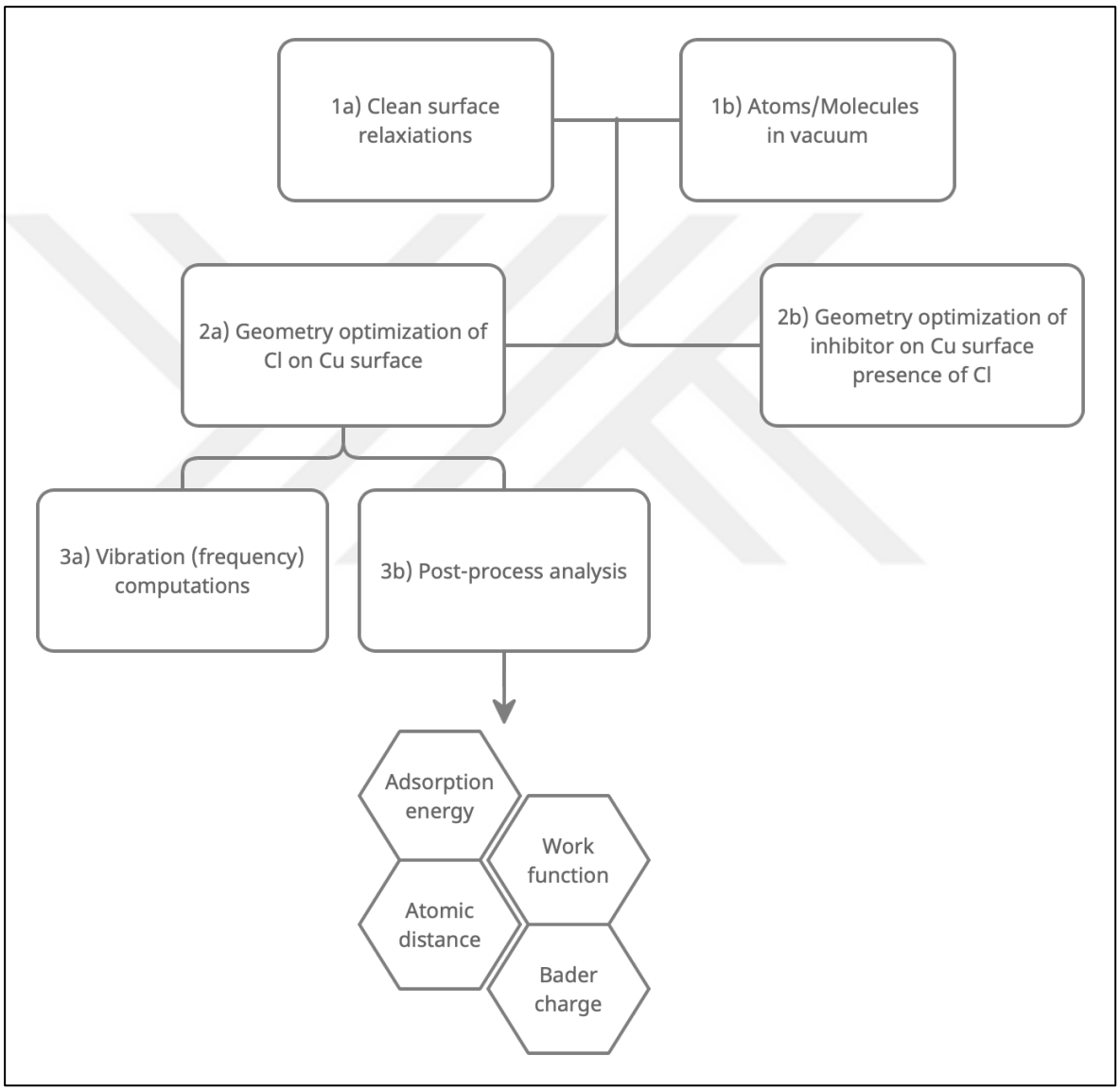

Figure 3.2. Procedure scheme

3.3.1. Geometry Relaxation Computations

Advances in computer science and the development of density functional theory (DFT) methods have made possible reliable theoretical investigations and calculations of much larger molecules [106].

In computational chemistry, geometry optimization corresponds to energy minimization. It is the process of finding the organization of the system's atoms that minimizes the force and thus the energy of the system. For the geometry optimization that reaches to the 'ground state' the system lies in the bottom of the potential energy surface's (PES) well. A collection of atoms (i.e. the system) can be a single molecule, an ion, a condensed phase, a transition state, or even the sum of some of these. Optimized structures usually correspond to a substance as it occurs in nature [107].

By using PWSCF (pw.x) code on Quantum Espresso geometry relaxations were done. Everything that needs to be defined in the pw.x input file with explanations can be found in Quantum Espresso web page, under "pw.x: input description" title [108]. Input and output files for the case where 1 Cl was adsorbed on the Cu (100) p(2x2) surface are given in Appendix A.1. and A.2 as an example.

3.3.2. Frequency (Vibration) Computations

During the vibrational frequency calculations on the ground and transition states, selected atoms are moved in Cartesian coordinates and the resulting force difference is calculated. Computations of the vibrational energy in the "Quasi Harmonic Approximation" [109] were performed using Quantum Espresso. The primary use of vibration calculations is to verify the accuracy of optimized geometries. It is also very suitable for comparison of the simulation-based results with experimentally measured frequencies via IR or Raman techniques.

Cl_2 vibration frequency calculated as 536.8 cm^{-1} which is also in agreement with the experimental findings [110].

During the frequency computations symmetry was excluded explicitly. The frequencies of the surface ions were excluded basing on the frozen phonon approximation. In Espresso, "phonon" works with the code “ph.x”. As a result, vibrational energies (frequencies) of atoms / molecules were obtained. With the data obtained from frequency calculations, surface potentials can be calculated, and work function calculations can be performed. Appendix A.3. and A.4. shows the example input and output file of “ph.x” respectively.

3.3.3. Work Function Calculation

In solid state physics, the work function is the minimum energy required to move an electron from a solid to a point outside the solid surface in a vacuum. The potential energy of the electron is approximately at the Fermi level and this is defined as the energy for which there is a probability of finding electrons for the system in thermal equilibrium. The work function (ϕ) is calculated (3.15) as the difference between the Fermi energy (E_F) of the structure and the electrostatic potential (ψ) of the vacuum,

$$\phi=\psi-E_F \tag{3.15}$$

3.3.4. Adsorption Energy Calculation

Adsorption energy is simply defined as the change in energy when an atom, ion or molecule (adsorbate) is attached to a solid surface (adsorbent).

For the reaction below

$$A + B \rightarrow C$$

The adsorption energy is calculated by using the following equation:

$$\Delta G = \Delta H + T\Delta S \tag{3.11}$$

Since DFT energies computed at 0 K,

$$\Delta G_{rxn} = \Delta H_{rxn} \tag{3.12}$$

$$\Delta H_{rxn} = E_C - (E_A + E_B) \quad (3.13)$$

As a result, the adsorption energy can be calculated by calculating the enthalpy of reaction. Each energy is result of a geometry relaxation and take from "pw.x" out file.

$$E_{adsorption} = E_{adsorbate/adsorbent(adsorption\ system)} - E_{adsorbent} - E_{adsorbate} \quad (3.14)$$

Figure 3.3 visualized the Equation 3.14 respectively.

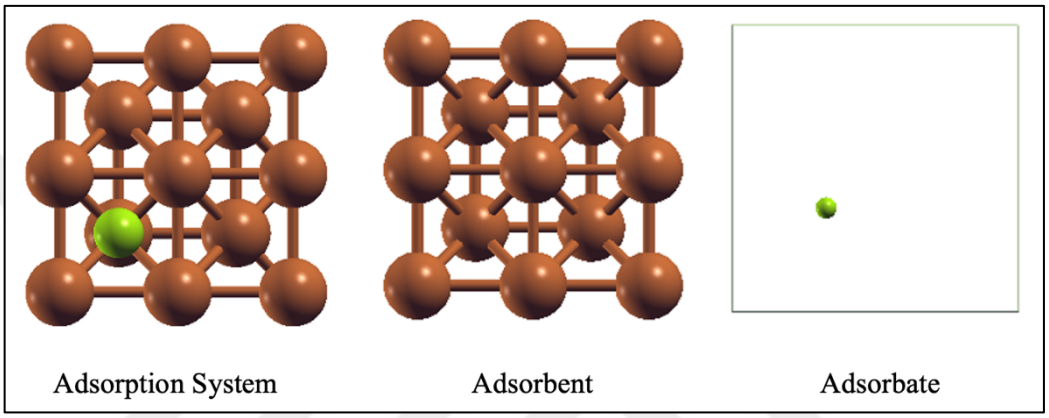

Figure 3.3. XCrySDen representation of adsorbent-adsorbate couple (Cu: orange, Cl: green)

3.3.5. Bader Charge Analysis

Richard Bader intuitively developed a way to divide molecules into atoms. Bader's definition of atom is entirely based on the electronic charge density. He used what are called zero flux surfaces to split atoms. A zero-flux surface is a 2-dimensional surface where the charge density is minimum and that is perpendicular to the surface. In molecular systems, the charge density reaches a minimum between atoms and this is the ideal place to separate atoms from each other. Besides being an intuitive diagram for visualizing atoms in molecules, Bader's definition is useful for charge analysis. The charge distribution is used to determine the multipolar moments of interacting atoms or molecules [111]

As a result of the Bader analysis, basically two files (ACF.dat and BCF.dat) are produced. Table A.5 and Table A.6 include example of those output files. ACF.dat contains the coordinates of each atom, its charge associated with it according to the Bader partitioning method, the percentage of the whole according to the Bader partitioning method, and the

minimum distance to the surface. The output of BCF.dat contains the coordinates of each Bader maximum, the charge in that volume, the neighboring atom and the distance to that atom. Table C.1, Table C.2 and Table C.3 shows the Bader charges of Cl atom(s) at varying coverage and adsorption positions on Cu(111), Cu(110) and Cu(100), respectively.

3.4. COMPUTATIONAL DETAILS

The results presented in this study were obtained with the periodic DFT simulations that were performed with Quantum Espresso [104] software package. Perdew–Burke–Ernzerhof (PBE) functional is used for the exchange-correlation energy. All results presented are obtained by optimizing the structures until the net force acting on the ions is "Fnet <0.001 Ry / Bohr". Necessary dipole corrections due to the asymmetric use of slabs were included. In the frequency computations the symmetry operator was turned off explicitly and the frequencies of the surface ions were excluded by freezing the surface metal atoms.

For the computation of the atoms and molecules in vacuum, they were placed in a supercell where the periodic atoms/molecules were separated with a minimum distance of 10 Å vacuum in all Cartesian directions. For these computations a (1x1x1) k-points mesh (i.e. gamma point) were used.

3.4.1. Crystal Optimization and Surface Preparation

First, copper crystal structure was optimized to obtain the computationally optimum lattice parameter. As Figure 3.4 shows, metallic Cu crystal have face-centered cubic (FCC) structure [112] with a Fm-3m symmetry [113]. Transition state metal Cu (3d element) was studied in its metallic phase.

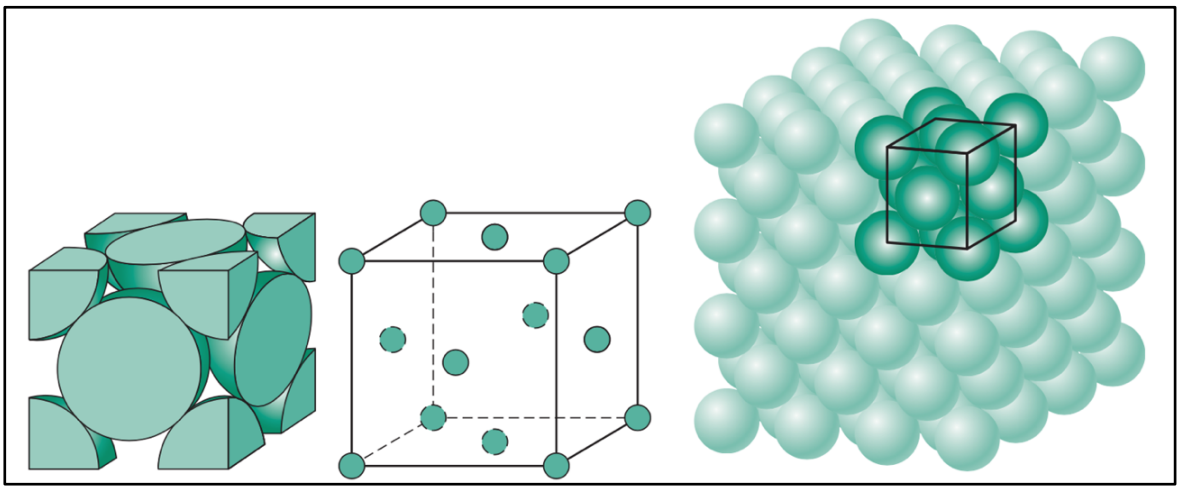

Figure 3.4. Schematic representations for FCC crystal structure [114]

Once the optimum lattice parameter for the crystal was determined, construction and optimization of the surface models (slab) were carried out.

The studied surface models are,

- p(1x1) Cu (100), Cu (110) and Cu (111) metallic surfaces
- p(2x2) Cu (100), Cu (110) and Cu (111) metallic surfaces
- p(3x3) Cu (100), Cu (110) and Cu (111) metallic surfaces
- p(4x4) Cu (100), Cu (110) and Cu (111) metallic surfaces

Periodic super cells were prepared by placing 5 copper layers and a vacuum region over the surface. The minimum height of the vacuum region used was 15 Å. During the simulations top 3 layers were relaxed whereas bottom 2 layers were kept frozen to represent the bulk behavior. In the computations, automatic generated Monkhorst k-points 2x2x1, 3x3x1, 4x4x1 and 8x8x1 meshes were used for p(1x1), p(2x2), p(3x3) and p(4x4) slabs, respectively. Each surface model (supercell) was relaxed to observe surface relaxation. Table 3.1 shows the slabs' parameters. Figure 3.5 shows the schematic representation of the slab models.

Later on, adsorption of chlorine and inhibitors were studied on these surfaces.

Table 3.1. Supercell thicknesses of copper surfaces

Surface	Slab Thickness (Å)	Slab Thickness (Atomic Layer)	Vacuum Thickness (Å)
Cu (100)	7.20	5	15
Cu (110)	5.02	5	15
Cu (111)	8.31	5	15

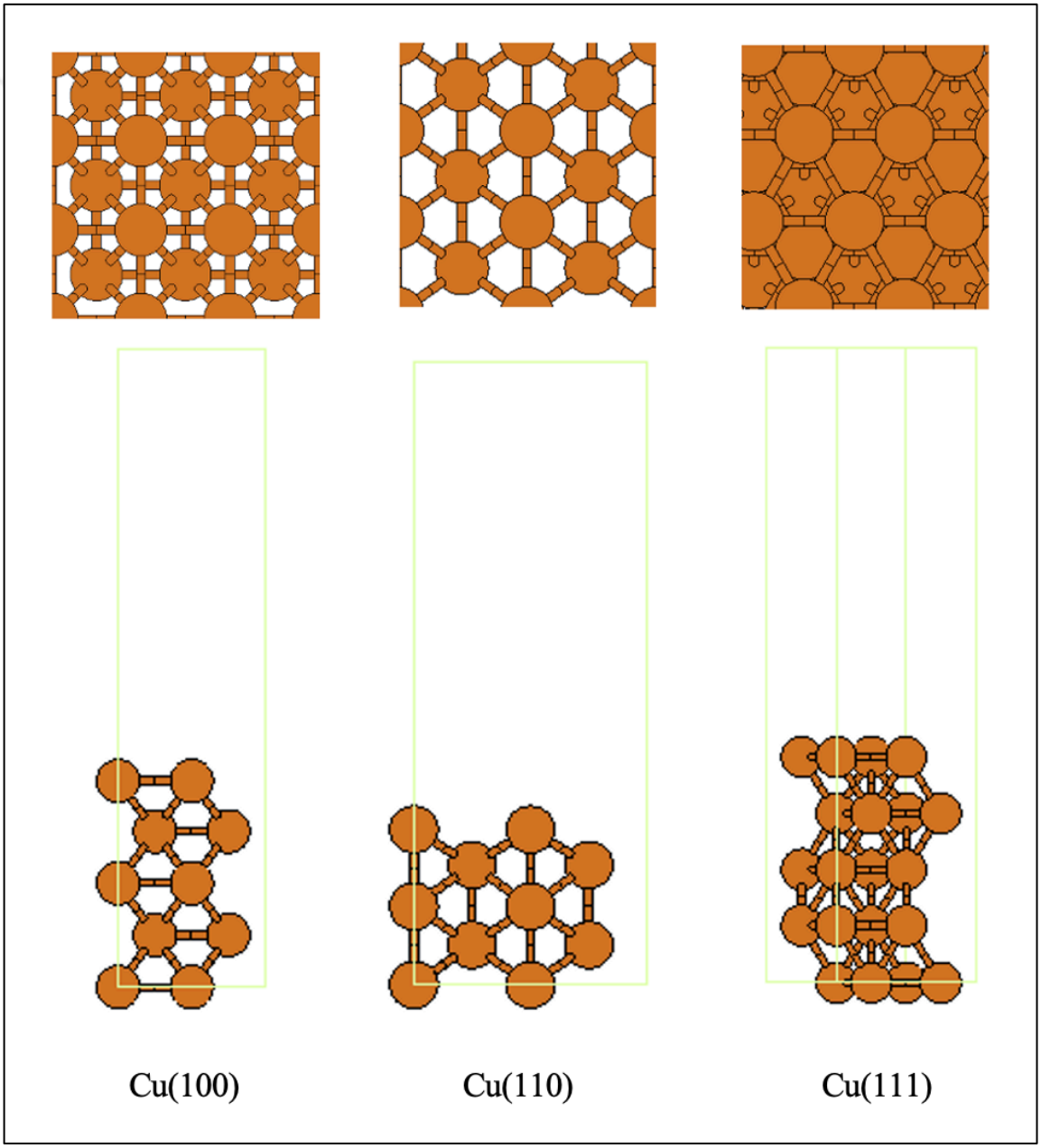

Figure 3.5. Schematic representation of studied metallic surfaces (Cu: orange)

3.4.2. Chlorine Adsorption on Copper Surface

For geometry relaxations of chlorine on copper surfaces, chlorine atoms were placed on the clean copper surface in different adsorption positions (symmetry points) at varying coverage. Figure 3.6 and Table 3.2 shows the studied adsorption sites.

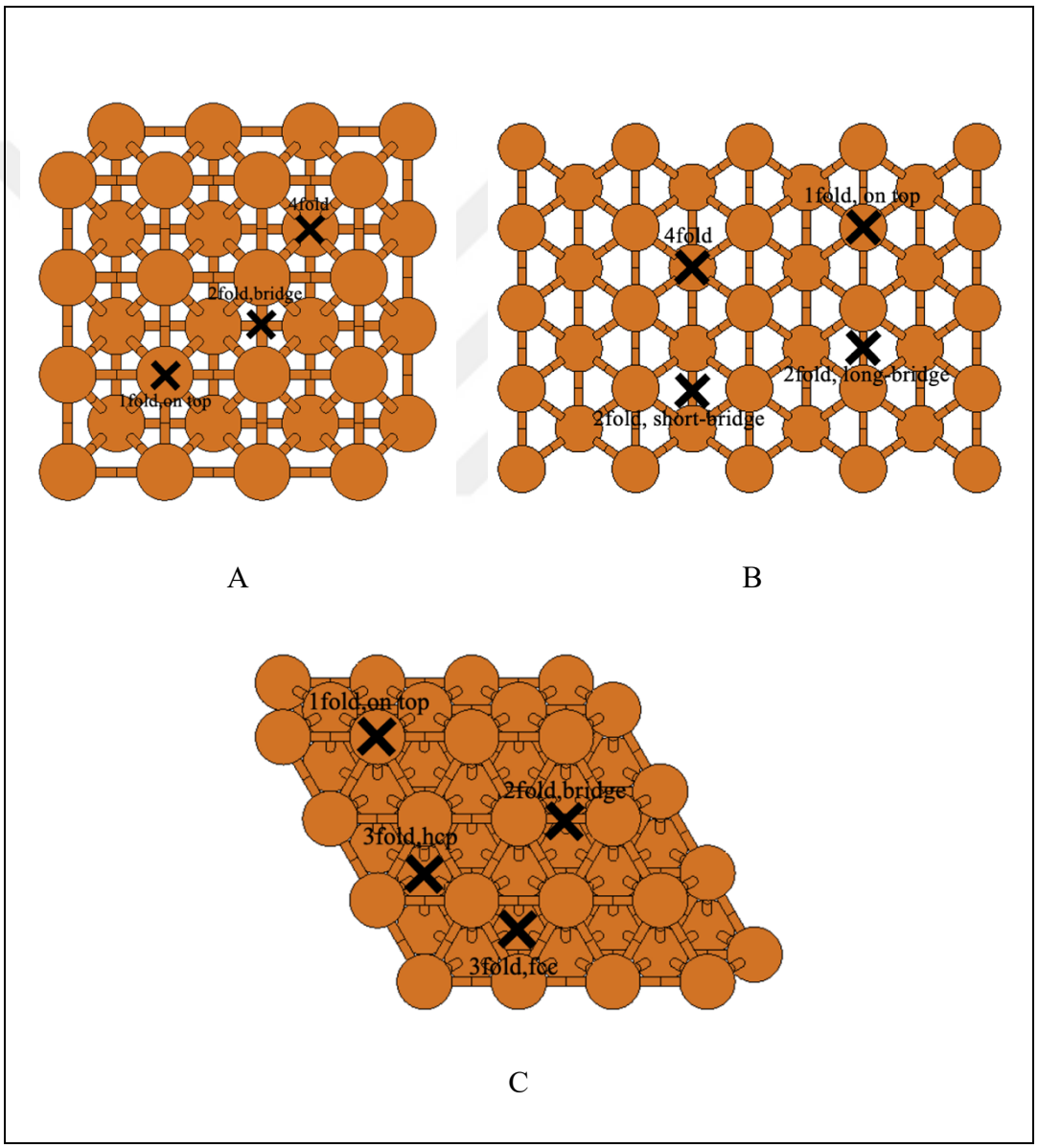

Figure 3.6. Studied adsorption sites A) Cu (100), B) Cu (110) and C) Cu (111) (Cu: orange)

Table 3.2. Studied adsorption sites with respect to surfaces

Metal Surface / Adsorption Site	**Cu (100)**	**Cu (110)**	**Cu (111)**
4-fold (4f)	X	X	NaN
3-fold fcc site	NaN	NaN	X
3-fold hcp site	NAN	NaN	X
Bridge (2f)	X	NaN	X
Short bridge (2f)	NaN	X	NaN
Long bridge (2f)	NaN	X	NaN
Top (1f)	X	X	X

When producing the data, both homogenous (for ex. 4-fold + 4-fold) and non-homogenous (for ex. 4-fold + bridge) adsorption position combinations were studied. However, it was noticed that non-homogeneous distribution did not have a major effect on site-specific adsorption data [115]. Therefore, only homogeneous combinations of adsorption positions were chosen.

To study the corrosion effect of chlorine on different copper surfaces the adsorption energies of $Cl_2(g)$ were calculated by placing them on empty (clean) copper surfaces. Then, total energy computations were carried out with the same input parameters.

The adsorption energies of the chlorine molecule were calculated as the difference between the DFT energies of the products (Cl_2 adsorbed structure) and the sum of the reactants (clean Cu (hkl) + $Cl_2(g)$).

$$\Delta E_{ads} = E_{Cl/Cu\ (hkl)} - (E_{Cl_{2(g)}} + E_{Cu(hkl)}) \tag{3.14}$$

As an example, Equation 3.14 derived for Cu (100), 0.25 ML, 4fold position and sample calculation shown below,

$$\Delta E_{ads} = E_{Cl/Cu\ (100)} - \left(\frac{1}{2} E_{Cl_{2(g)}} + E_{Cu(100)}\right)$$

$$\Delta E_{ads} = -4341.0 - \left(\frac{1}{2}\ (-158.6) + (-4261.5)\right)$$

$$\Delta E_{ads} = -\ 0.138\ Ry = -181\ kJ/mol$$

3.4.3. Selection of Inhibitor Candidates

Appropriate inhibitor selection is very important and it depends on the corrosive surface and the chemical causing surface corrosion. It was already mentioned that many organic and inorganic inhibitors exist. The major points to be considered in the search for inhibitors suitable for computational study are as follows.

i. To be of suitable size for the surface and unbranched
ii. Having less computational and purchasing cost
iii. Having less number of conformations
iv. Having a good fit onto surface model

A search in literature with these criteria showed that, azole derivatives are the well-known organic and environmentally friendly copper corrosion inhibitors as mentioned in the "2. LITERATURE SURVEY". In this direction imidazole and pyrazole molecules were selected as azole derivative inhibitor candidates. In addition, the inhibition effects of

- pyridine, anisidine, toluidine and thiophene as organic inhibitors,
- ammonia and chromic acid as inorganic inhibitors, as well as
- possible surface ions $-O^+$, $-OH^-$, $-CO$, $-OCH_3$, $-H^+$

were investigated to increase the scale of the research. Figure 3.7 shows molecular structures of inhibitor candidates.

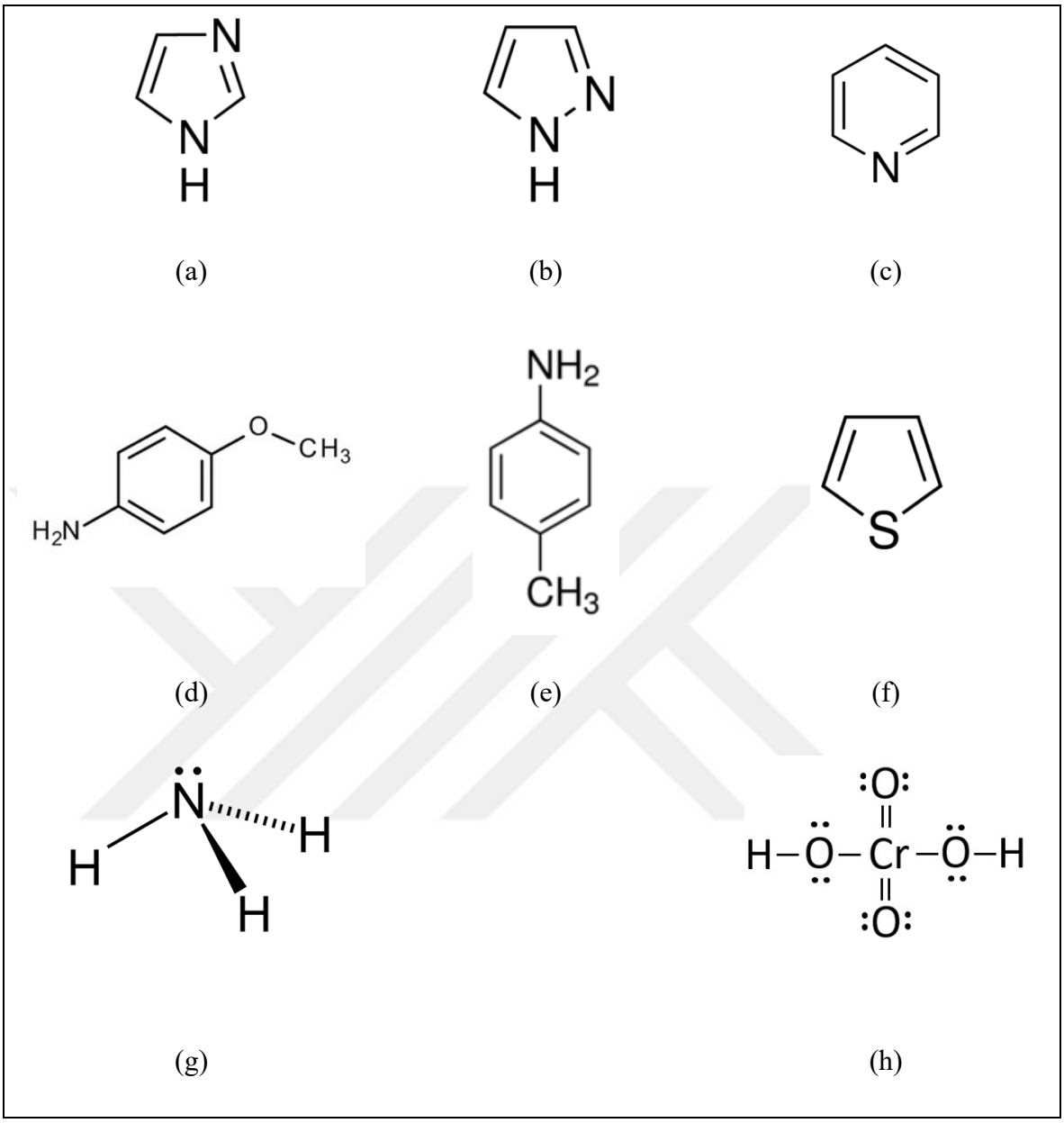

Figure 3.7. Structures of (a) imidazole, (b) pyrazole, (c) pyridine, (d) anisidine, (e) toluidine, (f) thiophene, (g) ammonia and (h) chromic acid

All these inhibitor candidates were relaxed on the copper surfaces as the following step.

3.4.4. Inhibitor Adsorption on Copper Surface

For the adsorption of all selected inhibitors on copper surface, several possible adsorption geometries were tested on p(3x3) Cu (100) surface. The selection of the Cu (100) surface

was based on the higher activity of this surface, although Cu (111) is more stable with a higher surface energy [39].

The adsorption energies of the inhibitor molecules were calculated as the difference between the DFT energies of the products (Inh/Cu (hkl)-inhibitor adsorbed surface) and the sum of the reactants (clean Cu (hkl) + inhibitor).

$$\Delta E_{ads} = E_{inh/Cu\ (hkl)} - (E_{inh} + E_{Cu(hkl)}) \tag{3.16}$$

As an example, Equation 3.16 derived for p(3x3) oxygen adsorption on Cu (100), sample calculation shown as,

$$\Delta E_{ads} = E_{O/Cu\ (100)} - (E_{O_{2(g)}} + E_{Cu(100)})$$

$$\Delta E_{ads} = -9630.2 - \left(\frac{1}{2}(-82.9) + (-9588.5)\right)$$

$$\Delta E_{ads} = -0.25\ Ry = -322\ kJ/mol$$

By means of these calculations, the adsorption energies of the selected inhibitors on the copper surface models were calculated.

3.4.5. Study of Inhibitor Effect

For investigating the inhibition effects, chloride ion is added in the presence of pre-adsorbed inhibitor molecule, and the adsorption energies were calculated. Chlorine adsorption energies are expected to decrease in the presence of inhibitor on the surface.

The adsorption energies of the chlorine in the presence of pre-adsorbed inhibitor molecule

on the surface model were calculated as the difference between the DFT energies of the products (inhibitor + $Cl_2(g)$ adsorbed structure on copper surface) and the sum of the reactants (Inh/Cu (hkl) + Cl(g)).

$$\Delta E_{ads} = E_{(Cl+inh)/Cu\ (hkl)} - \left(E_{inh/Cu\ (hkl)} + \frac{1}{2} E_{Cl_2(g)}\right) \tag{3.17}$$

As an example, Equation 3.17 derived for p(3x3) chlorine adsorption on Cu (100) presence of oxygen, sample calculation shown as,

$$\Delta E_{ads} = E_{(Cl+O)/Cu\ (100)} - (E_{O/Cu\ (100)} + \frac{1}{2} E_{Cl_{2(g)}})$$

$$\Delta E_{ads} = -9709.7 - (-9630.2 + \frac{1}{2}(-158.7))$$

$$\Delta E_{ads} = -0.14\ Ry = -184\ kJ/mol$$

Results of the computations are given in the next chapter with discussion.

4. RESULTS AND DISCUSSION

The effect of chlorine coverage on surface corrosion was investigated using various surface coverage values (1 ML to 1/16 ML) on Cu (100), Cu (110) and Cu (111). Adsorption of selected inhibitors on the clean copper surfaces as well as chlorine-adsorbed surfaces were studied. This section presents the obtained results with discussions.

4.1. LATTICE (CRYSTAL) OPTIMIZATION

The first step in the simulations was to optimize the lattice parameters. In order to estimate the lattice parameters, scf calculations were made at the lower and upper values of an experimental value. A curve was plotted with the obtained scf energies and a quadratic polynomial equation was fitted as shown in Figure 4. The minimum point of this graph (where the derivative of the equation is equal to 0) gives the optimum lattice parameter.

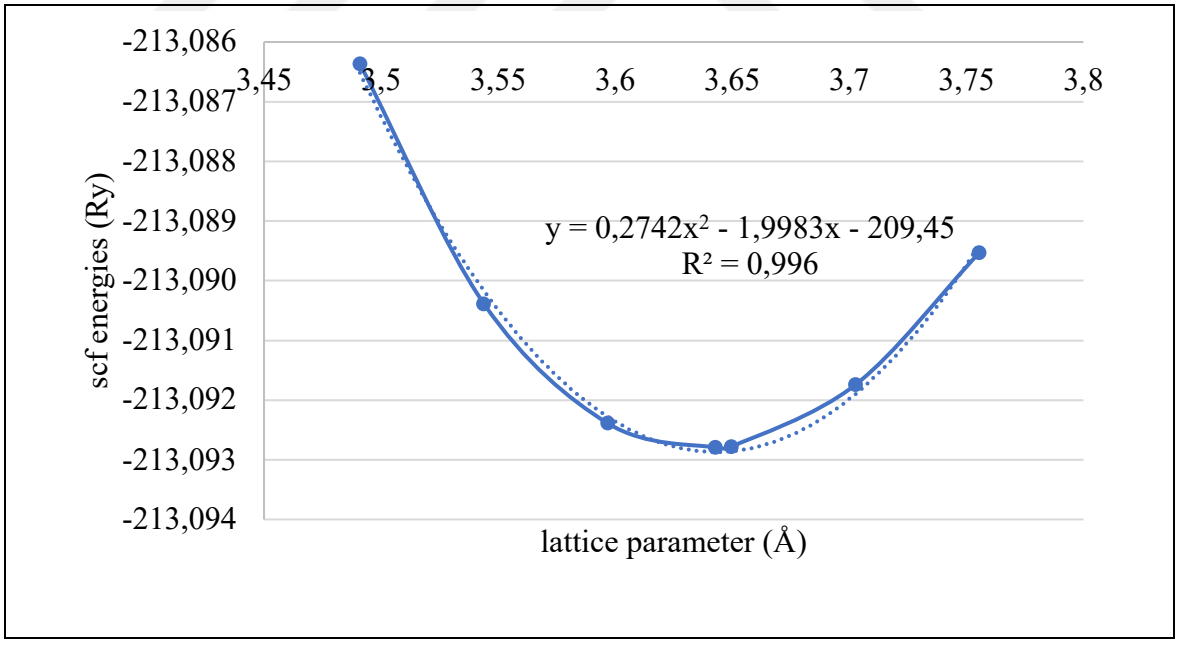

Figure 4.1. Lattice parameter estimation

In order to estimate the k points used for the p(1x1) slab, scf calculations were performed at different k-points and the graph given in Figure 4.2 was drawn. 8x8x1 k-points were selected for p(1x1) and the k-points for other slabs were accordingly determined as 4x4x1, 3x3x1 and 2x2x1 for p(2x2), p(3x3) and p(4x4), respectively.

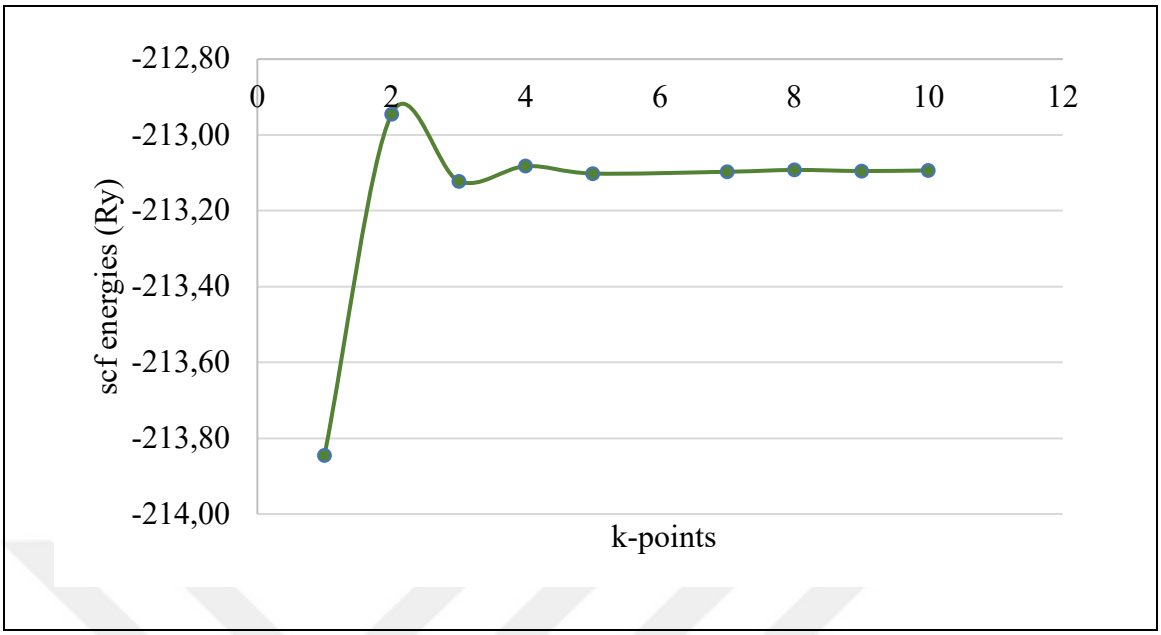

Figure 4.2. k-point estimation

Using the parameters given "Computational Details", Cu (100), Cu (110) and Cu (111) surface slabs were relaxed. Figure 4.3 shows clean copper surface, top and side view.

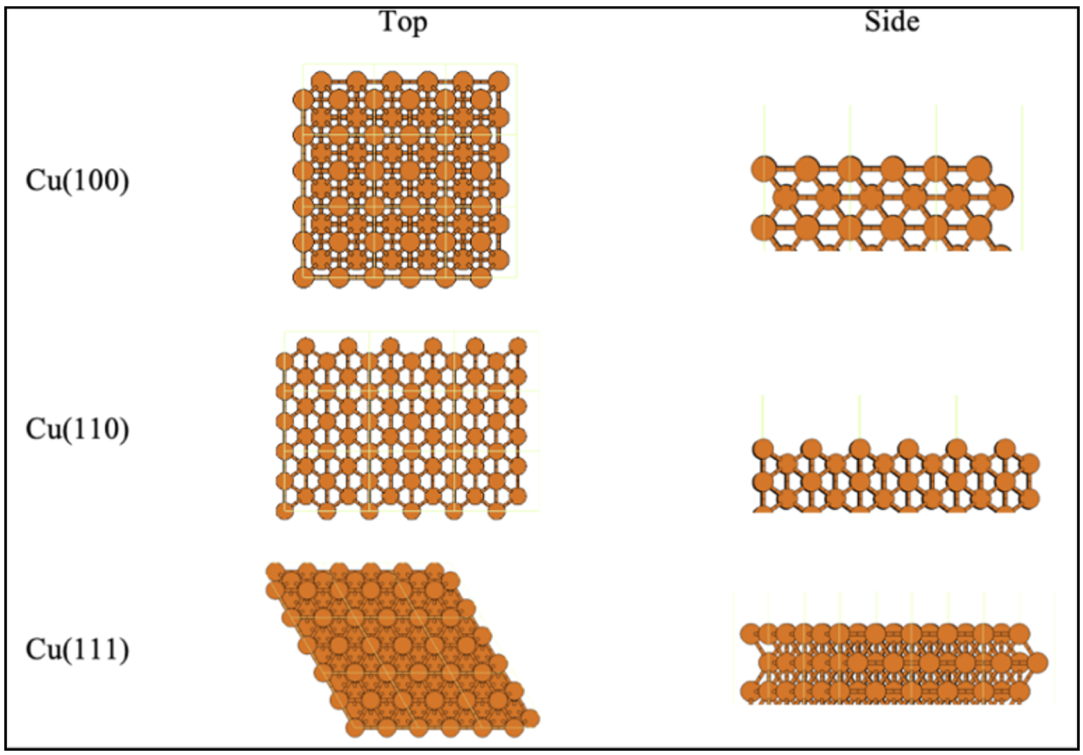

Figure 4.3. Optimized clean copper surface geometries (Cu:orange)

4.2. SURFACE RELAXATION

The multilayer relaxation of Cu (100), Cu (110) and Cu (111) surfaces obtained by DFT are listed in Table 4.1.

Table 4.1. Comparison of surface structure

Surface	Δd_{12}	Δd_{23}	Δd_{34}	Δd_{45}	Reference No.
Cu (100)	-1.88 %	-0.25 %	-0.34 %	0.00 %	Present study
	-1.06 %	-0.65 %	1.28 %	-0.58 %	[116][a]
	-3.79 %	-0.54 %	0.02 %	0.00 %	[117][b]
Cu (110)	-2.60 %	1.00 %	-0.74 %	0.00 %	Present study
	-7.76 %	4.17 %	3.70 %	-0.47 %	[116][a]
	-8.73 %	1.56 %	-1.20 %	0.43 %	[117][b]
Cu (111)	-1.06 %	-1.20 %	-1.08 %	0.00 %	Present study
	0.56 %	-0.07 %	0.55 %	0.20 %	[116][a]
	-2.48 %	-0.04 %	0.00 %	0.00 %	[117][b]

[a] Method: Ab-initio pseudopotential

[b] Method: Embedded atom method (EAM)

Results of this study and theoretical data (shown in Table 4.1) show that the surface relaxation of Cu (100) is slightly inward. Δd shows change in the distance between the copper layers before and after relaxation done. Figure B.1. shows layers and distance between the layers. Our calculations show that top layer relaxation results in a reduction with a magnitude of 1.88 percent, which agrees with the literature values. For Cu (110) surface

inward relaxation magnitude, especially for the top layer, is larger than that of the Cu (100) surface, in agreement with other theoretical results. The second layer has an expansion behavior in contrast to top layer with a magnitude 1.00 percent, which is compatible with the previously obtained results. Cu (111) surface, on the other hand, has inward relaxation and magnitude of the relaxation of the top layer is quite smaller compared to those of Cu (100) and Cu (111).

4.3. COPPER (111) SURFACE

After relaxing the Cu (111) surface, optimum geometries and adsorption energies were obtained for Cl adsorption.

4.3.1. Chlorine Adsorption

Effect of chlorine coverage on copper metal was investigated on the Cu (111) surfaces for the 1/16 ML, 1/9 ML, 2/9 ML, 1/4 ML, 3/9 ML, 2/4 ML ,3/4 ML, 1 ML chlorine coverage.

Table 4.2 shows the adsorption energies, frequencies, bond distances and work function for Cl adsorption on Cu (111) surface at given positions for 1 ML. Figure 4.4 presents the top views of these studied Cl adsorptions.

Table 4.2. Adsorption energy, Cl stretching frequency, Cl-Cu bond distances and work function for Cl adsorbed on Cu (111) surface at given positions for 1/1 ML (1 ML)

Coverage	Position	E_{ads} (kJ/mol)	ν_{Cl} (cm^{-1})	|Cl-Cu| (Å)[a]	ϕ (eV)
1 ML	2-fold	64	138	2.588	5.796
	3-fold (fcc)	66 48 [2]	130	2.691	5.794
	3-fold (hcp)	66	127	2.690	5.790
	1-fold	52	210	2.309	5.881

[a] Linear average of the Cu-Cl distances for 2-fold and 3-fold positions were reported.

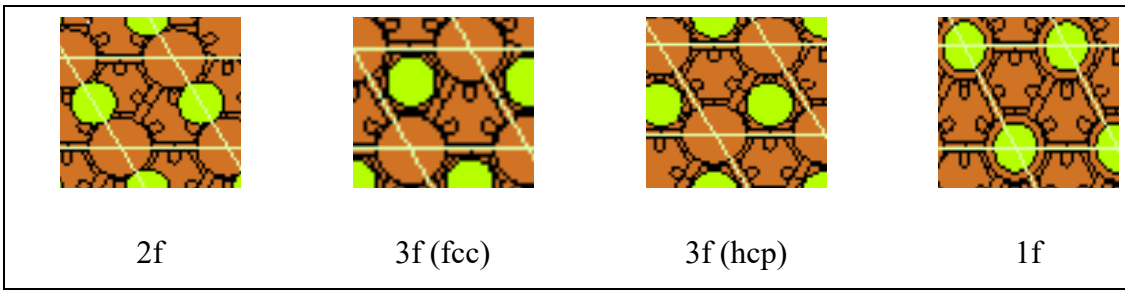

Figure 4.4. Optimized geometries of Cl/Cu (111) at 1 ML coverage (Cu: orange, Cl: green)

Table 4.3 shows the adsorption energies, frequencies, bond distances and work function for Cl adsorption on Cu (111) surface at given positions for 0.75 ML. Figure 4.5 presents the top views of these studied Cl adsorptions.

Table 4.3. Adsorption energy, Cl stretching frequency, Cl-Cu bond distances and work function for Cl adsorbed on Cu (111) surface at given positions for 3/4 ML (0.75 ML)

Coverage	Position	E_{ads} (kJ/mol)	ν_{Cl} (cm^{-1})	|Cl-Cu| (Å)[a]	|Cl-Cu| (Å)[a]	|Cl-Cu| (Å)[a]	ϕ (eV)
0.75 ML	2-fold	NaN	NaN	NaN	NaN	NaN	NaN
	3-fold (fcc)	30	449	2.574	2.573	2.572	5.206
	3-fold (hcp)	28	502	2.574	2.574	2.574	5.206
	1-fold	11	472	2.281	2.281	2.281	5.471

[a] Linear average of the Cu-Cl distances for 2-fold and 3-fold positions were reported.

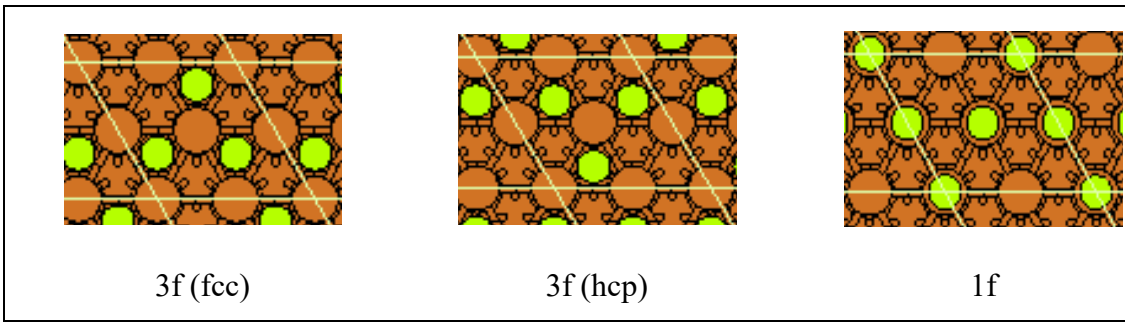

Figure 4.5. Optimized geometries of Cl/Cu (111) at 0.75 ML coverage (Cu: orange, Cl: green)

Table 4.4 shows the adsorption energies, frequencies, bond distances and work function for Cl adsorption on Cu (111) surface at given positions for 0.50 ML. Figure 4.6 presents the top views of these studied Cl adsorptions.

Table 4.4. Adsorption energy, Cl stretching frequency, Cl-Cu bond distances and work function for Cl adsorbed on Cu (111) surface at given positions for 2/4 ML (0.50 ML)

Coverage	Position	E_{ads} (kJ/mol)	ν_{Cl} (cm^{-1})	|Cl-Cu| (Å)[a]	|Cl-Cu| (Å)[a]	ϕ (eV)
0.50 ML	2-fold	-147	426	2.375	2.375	5.317
	3-fold (fcc)	-148	433	2.470	2.468	5.142
	3-fold (hcp)	-148	433	2.475	2.475	5.149
	1-fold	-126	358	2.241	2.241	5.750

[a] Linear average of the Cu-Cl distances for 2-fold and 3-fold positions were reported.

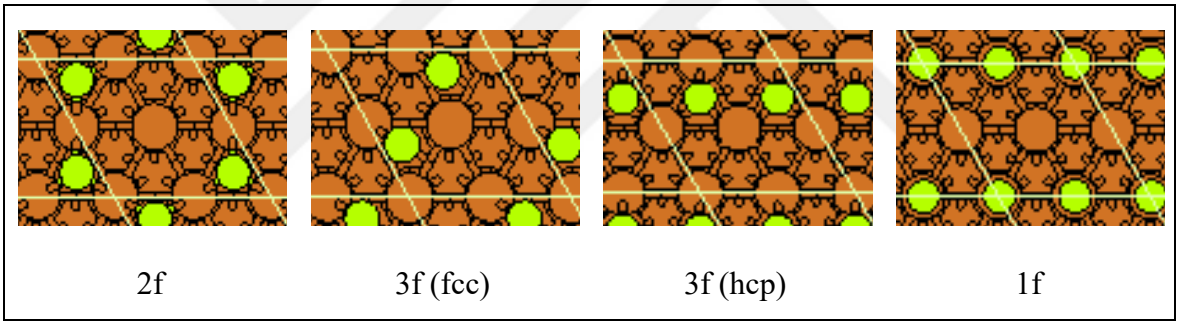

Figure 4.6. Optimized geometries of Cl/Cu (111) at 0.50 ML coverage (Cu: orange, Cl: green)

Table 4.5 shows the adsorption energies, frequencies, bond distances and work function for Cl adsorption on Cu (111) surface at given positions for 0.33 ML. Figure 4.7 presents the top views of these studied Cl adsorptions.

Table 4.5. Adsorption energy, Cl stretching frequency, Cl-Cu bond distances and work function for Cl adsorbed on Cu (111) surface at given positions for 3/9 ML (0.33 ML)

Coverage	Position	E_{ads} (kJ/mol)	ν_{Cl} (cm^{-1})	|Cl-Cu| (Å)[a]	|Cl-Cu| (Å)[a]	|Cl-Cu| (Å)[a]	ϕ (eV)
0.33 ML	2-fold	-222	354	2.352	2.352	2.356	4.762
	3-fold (fcc) (conv. to 2f)	-483 -179 [2]	NaN	NaN	NaN	NaN	NaN
	3-fold (hcp) (conv. to 2f)	-489	NaN	NaN	NaN	NaN	NaN
	1-fold	-178	270	2.242	2.241	2.241	5.007

[a] Linear average of the Cu-Cl distances for 2-fold and 3-fold positions were reported.

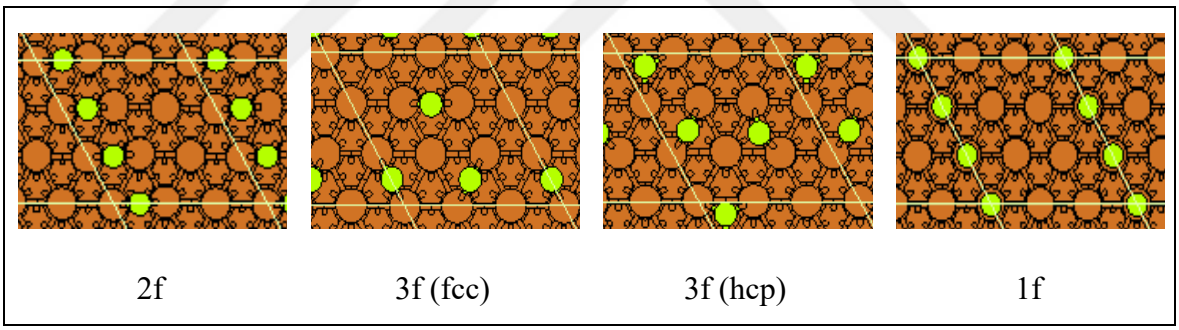

Figure 4.7. Optimized geometries of Cl/Cu (111) at 0.33 ML coverage (Cu: orange, Cl: green)

Table 4.6 shows the adsorption energies, frequencies, bond distances and work function for Cl adsorption on Cu (111) surface at given positions for 0.25 ML. Figure 4.8 presents the top views of these studied Cl adsorptions.

Table 4.6. Adsorption energy, Cl stretching frequency, Cl-Cu bond distances and work function for Cl adsorbed on Cu (111) surface at given positions for 1/4 ML (0.25 ML)

Coverage	Position	E_{ads} (kJ/mol)	ν_{Cl} (cm^{-1})	|Cl-Cu| (Å)[a]	ϕ (eV)
0.25 ML	2-fold (conv. to fcc)	-169	NaN	NaN	NaN
	3-fold (fcc)	-169 -174 [2]	245	2.397	4.855
	3-fold (hcp)	-168	246	2.404	4.863
	1-fold	-132	310	2.172	5.257

[a] Linear average of the Cu-Cl distances for 2-fold and 3-fold positions were reported.

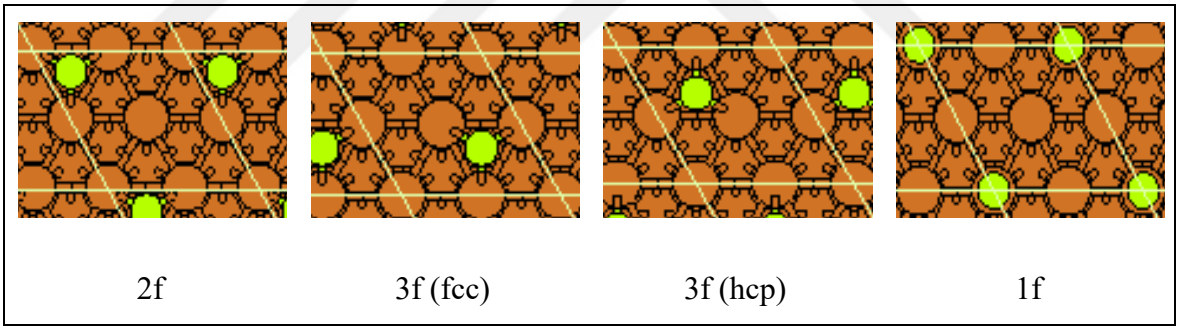

Figure 4.8. Optimized geometries of Cl/Cu (111) at 0.25 ML coverage (Cu: orange, Cl: green)

Table 4.7 shows the adsorption energies, frequencies, bond distances and work function for Cl adsorption on Cu (111) surface at given positions for 0.22 ML. Figure 4.9 presents the top views of these studied Cl adsorptions.

Table 4.7. Adsorption energy, Cl stretching frequency, Cl-Cu bond distances and work function for Cl adsorbed on Cu (111) surface at given positions for 2/9 ML (0.22 ML)

Coverage	Position	E_{ads} (kJ/mol)	ν_{Cl} (cm^{-1})	|Cl-Cu| (Å)[a]	|Cl-Cu| (Å)[a]	ϕ (eV)
0.22 ML	2-fold (conv. to fcc)	-163	NaN	NaN	NaN	NaN
	3-fold (fcc) (conv. to 2f)	-308	NaN	NaN	NaN	NaN
	3-fold (hcp) (conv. to 2f)	-322	NaN	NaN	NaN	NaN
	1-fold	-276	271	2.226	2.226	4,936

[a] Linear average of the Cu-Cl distances for 2-fold and 3-fold positions were reported.

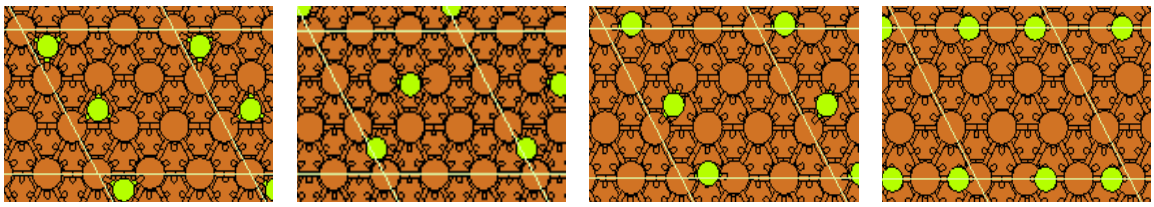

Figure 4.9. Optimized geometries of Cl/Cu (111) at 0.22 ML coverage (Cu: orange, Cl: green)

Table 4.8 shows the adsorption energies, frequencies, bond distances and work function for Cl adsorption on Cu (111) surface at given positions for 0.11 ML. Figure 4.10 presents the top views of these studied Cl adsorptions.

Table 4.8. Adsorption energy, Cl stretching frequency, Cl-Cu bond distances and work function for Cl adsorbed on Cu (111) surface at given positions for 1/9 ML (0.11 ML)

Coverage	Position	E_{ads} (kJ/mol)	ν_{Cl} (cm^{-1})	|Cl-Cu| (Å)[a]	ϕ (eV)
0.11 ML	2-fold (conv. to hcp)	-139	NaN	NaN	NaN
	3-fold (fcc)	-141 -182 [2]	258	2.378	4.865
	3-fold (hcp)	-139	258	2.385	4.871
	1-fold	-98	288	2.179	5.147

[a] Linear average of the Cu-Cl distances for 2-fold and 3-fold positions were reported.

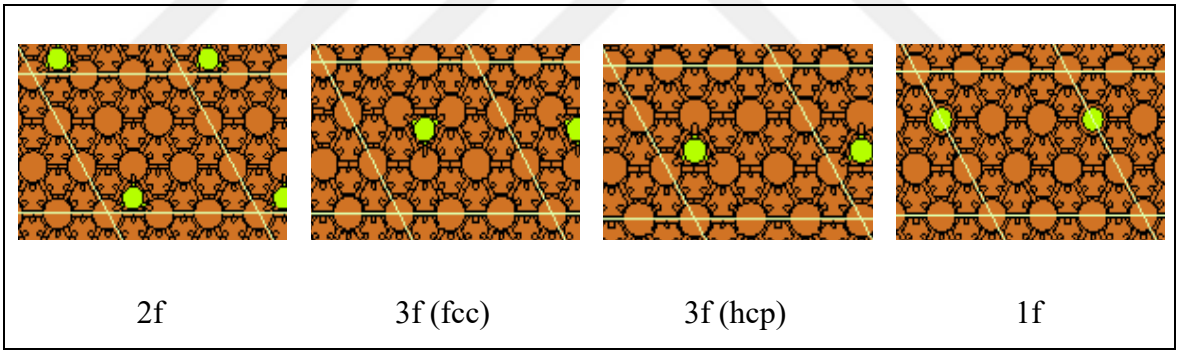

Figure 4.10. Optimized geometries of Cl/Cu (111) at 0.11 ML coverage (Cu: orange, Cl: green)

Table 4.9 shows the adsorption energies, frequencies, bond distances and work function for Cl adsorption on Cu (111) surface at given positions for 0.0625 ML. Figure 4.11 presents the top views of these studied Cl adsorptions.

Table 4.9. Adsorption energy, Cl stretching frequency, Cl-Cu bond distances and work function for Cl adsorbed on Cu (111) surface at given positions for 1/16 ML (0.0625 ML)

Coverage	Position	E_{ads} (kJ/mol)	ν_{Cl} (cm^{-1})	|Cl-Cu| (Å)[a]	ϕ (eV)
0.0625 ML	2-fold (conv. to fcc)	-196	NaN	NaN	NaN
	3-fold (fcc)	-196 -179 [2]	200	2.385	4.779
	3-fold (hcp)	-195	228	2.396	4.784
	1-fold	-158	277	2.186	5.012

[a] Linear average of the Cu-Cl distances for 2-fold and 3-fold positions were reported.

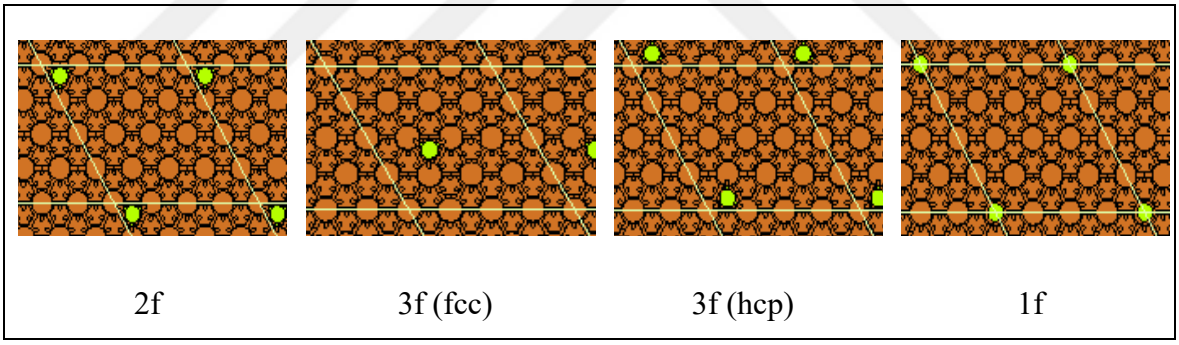

Figure 4.11. Optimized geometries of Cl/Cu (111) at 0.0625 ML coverage (Cu: orange, Cl: green)

4.4. COPPER (110) SURFACE

After relaxing the Cu (110) surface, optimum geometries and adsorption energies were obtained for Cl by using DFT.

4.4.1. Chlorine Adsorption

Effect of chlorine coverage on copper metal was investigated on the Cu (110) surfaces for the 1/16 ML, 1/9 ML, 2/9 ML, 1/4 ML, 3/9 ML, 2/4 ML ,3/4 ML, 1 ML chlorine coverage.

Table 4.10 shows the adsorption energies, frequencies, bond distances and work function for Cl adsorption on Cu (110) surface at given positions for 1 ML. Figure 4.12 presents the top views of these studied Cl adsorptions.

Table 4.10. Adsorption energy, Cl stretching frequency, Cl-Cu bond distances and work function for Cl adsorbed on Cu (110) surface at given positions for 1/1 ML (1 ML)

Coverage	Position	E_{ads} (kJ/mol)	ν_{Cl} (cm^{-1})	|Cl-Cu| (Å)[a]	ϕ (eV)
1 ML	4-fold	-55	165	2.666	4.288
	2-fold (l-brg)	-71 -109 [65]	173	2.389	4.328
	2-fold (s-brg)	-69 -103 [65]	223	2.346	4.407
	1-fold	-66 -102 [65]	255	2.212	4.468

[a] Linear average of the Cu-Cl distances for 2-fold and 4-fold positions were reported.

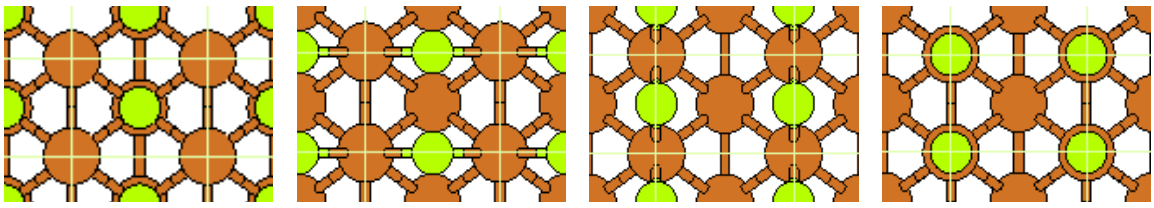

4f 2f (l-brg) 2f (s-brg) 1f

Figure 4.12. Optimized geometries of Cl/Cu (110) at 1 ML coverage (Cu: orange, Cl: green)

Table 4.11 shows the adsorption energies, frequencies, bond distances and work function for Cl adsorption on Cu (110) surface at given positions for 0.75 ML. Figure 4.13 presents the top views of these studied Cl adsorptions.

Table 4.11. Adsorption energy, Cl stretching frequency, Cl-Cu bond distances and work function for Cl adsorbed on Cu (110) surface at given positions for 3/4 ML (0.75 ML)

Coverage	Position	E_{ads} (kJ/mol)	ν_{Cl} (cm^{-1})	|Cl-Cu| (Å)[a]	|Cl-Cu| (Å)[a]	|Cl-Cu| (Å)[a]	ϕ (eV)
0.75 ML	4f + 4f + 4f	-465	305	2.696	2.755	2.645	4.070
	2f + 2f + 2f (l-brg)	-334	422	2.349	2.400	2.340	4.057
	2f + 2f + 2f (s-brg)	-350	388	2.226	2.340	2.338	4.257
	1f + 1f + 1f	-294	342	2.214	2.212	2.576	4.248

[a] Linear average of the Cu-Cl distances for 2-fold and 4-fold positions were reported.

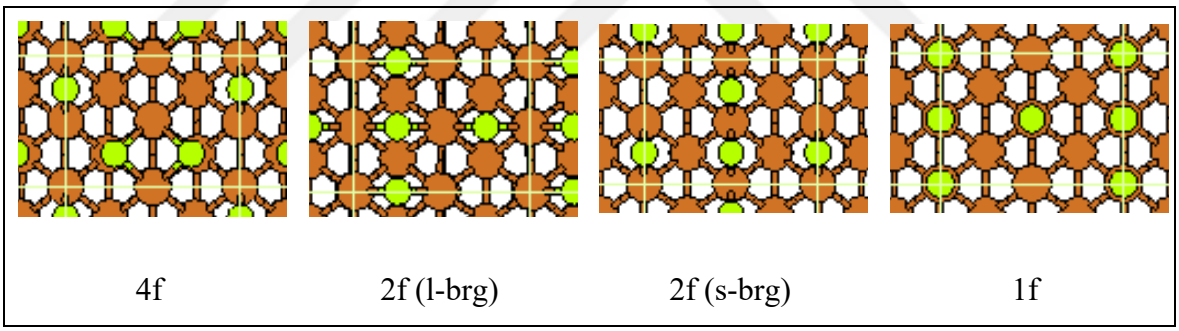

Figure 4.13. Optimized geometries of Cl/Cu (110) at 0.75 ML coverage (Cu: orange, Cl: green)

Table 4.12 shows the adsorption energies, frequencies, bond distances and work function for Cl adsorption energies, frequencies, bond distances, work function and Bader charges for Cl adsorption on Cu (110) surface at given positions for 0.50 ML. Figure 4.14 presents the top views of these studied Cl adsorptions.

Table 4.12. Adsorption energy, Cl stretching frequency, Cl-Cu bond distances and work function for Cl adsorbed on Cu (110) surface at given positions for 2/4 ML (0.50 ML)

Position	Position	E_{ads} (kJ/mol)	ν_{Cl} (cm^{-1})	|Cl-Cu| (Å)[a]	|Cl-Cu| (Å)[a]	ϕ (eV)
0.50 ML	4f + 4f (conv. to l-brg)	-306	NaN	NaN	NaN	NaN
	2f + 2f (l-brg)	-347 -204 [65]	213	2.322	2.321	5.714
	2f + 2f (s-brg)	-385 -216 [65]	312	2.233	2.233	5.578
	1f + 1f	-274	358	2.110	2.110	5.442

[a] Linear average of the Cu-Cl distances for 2-fold and 4-fold positions were reported.

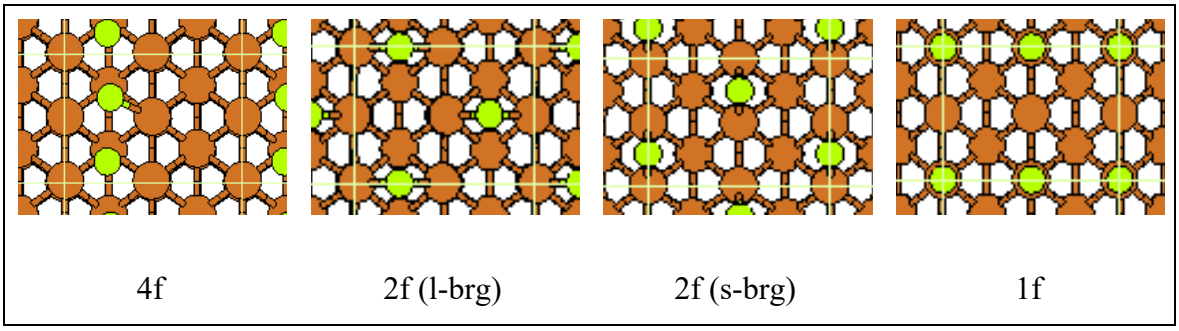

Figure 4.14. Optimized geometries of Cl/Cu (110) at 0.50 ML coverage (Cu: orange, Cl: green)

Table 4.13 shows the adsorption energies, frequencies, bond distances and work function for Cl adsorption on Cu (110) surface at given positions for 0.33 ML. Figure 4.15 presents the top views of these studied Cl adsorptions.

Table 4.13. Adsorption energy, Cl stretching frequency, Cl-Cu bond distances and work function for Cl adsorbed on Cu (110) surface at given positions for 3/9 ML (0.33 ML)

Coverage	Position	E_{ads} (kJ/mol)	ν_{Cl} (cm^{-1})	|Cl-Cu| (Å)[a]	|Cl-Cu| (Å)[a]	|Cl-Cu| (Å)[a]	ϕ (eV)
0.33 ML	4f + 4f + 4f (conv. to l-brg+ l-brg+ s-brg)	-526	NaN	NaN	NaN	NaN	NaN
	2f + 2f + 2f (l-brg) (conv. to l-brg+ l-brg+ s-brg)	-533	NaN	NaN	NaN	NaN	NaN
	2f + 2f + 2f (s-brg)	-530	291	2.243	2.293	2.279	4.390
	1f + 1f + 1f (conv. to s-brg)	-530	NaN	NaN	NaN	NaN	NaN

[a] Linear average of the Cu-Cl distances for 2-fold and 4-fold positions were reported.

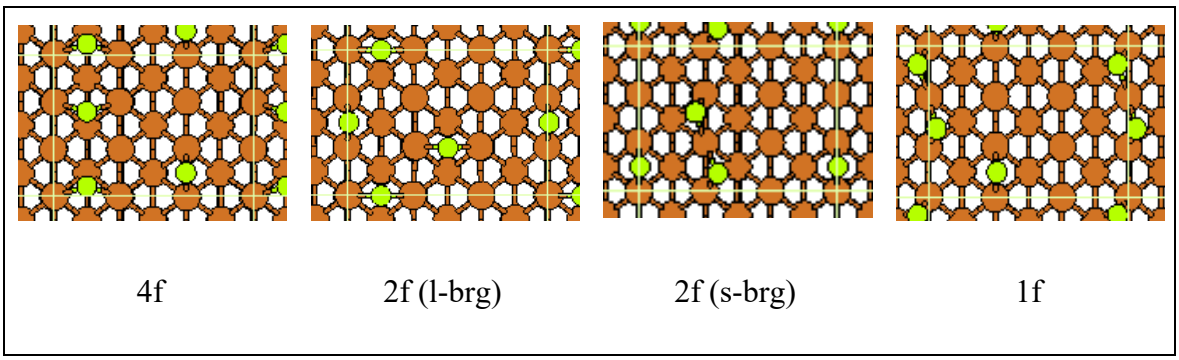

Figure 4.15. Optimized geometries of Cl/Cu (110) at 0.33 ML coverage (Cu: orange, Cl: green)

Table 4.14 shows the adsorption energies, frequencies, bond distances and work function for Cl adsorption on Cu (110) surface at given positions for 0.25 ML. Figure 4.16 presents the top views of these studied Cl adsorptions.

Table 4.14. Adsorption energy, Cl stretching frequency, Cl-Cu bond distances and work function for Cl adsorbed for Cl adsorbed on Cu (110) surface at given positions for 1/4 ML (0.25 ML)

Coverage	Position	E_{ads} (kJ/mol)	ν_{Cl} (cm^{-1})	|Cl-Cu| (Å)[a]	ϕ (eV)
0.25 ML	4-fold	-163	164	2.634	4.403
	2-fold (l-brg)	-173 -206 [65]	202	2.337	4.335
	2-fold (s-brg)	-193 -220 [65]	274	2.253	4.397
	1-fold	-150 -179 [65]	339	2.136	5.257

[a] Linear average of the Cu-Cl distances for 2-fold and 4-fold positions were reported.

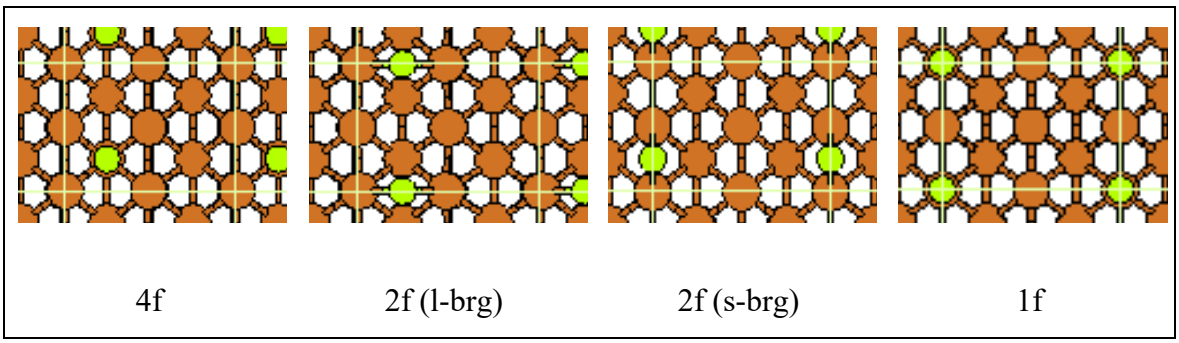

Figure 4.16. Optimized geometries of Cl/Cu (110) at 0.25 ML coverage (Cu: orange, Cl: green)

Table 4.15 shows the adsorption energies, frequencies, bond distances and work function for Cl adsorption on Cu (110) surface at given positions for 0.22 ML. Figure 4.17 presents the top views of these studied Cl adsorptions.

Table 4.15. Adsorption energy, Cl stretching frequency, Cl-Cu bond distances and work function for Cl adsorbed on Cu (110) surface at given positions for 2/9 ML (0.22 ML)

Coverage	Position	E_{ads} (kJ/mol)	ν_{Cl} (cm^{-1})	|Cl-Cu| (Å)[a]	|Cl-Cu| (Å)[a]	ϕ (eV)
0.22 ML	4f + 4f (conv. to s-brg)	-284	NaN	NaN	NaN	NaN
	2f + 2f 1 (l-brg)	-292	206	2.337	2.337	4.491
	2f + 2f 2 (l-brg)	-292	211	2.337	2.337	4.491
	2f + 2f 1 (s-brg)	-332	266	2.250	2.250	4.555
	2f + 2f 2 (s-brg)	-332	332	2.245	2.250	4.555
	1f + 1f	-243	264	2.132	2.131	4.550

[a] Linear average of the Cu-Cl distances for 2-fold and 4-fold positions were reported.

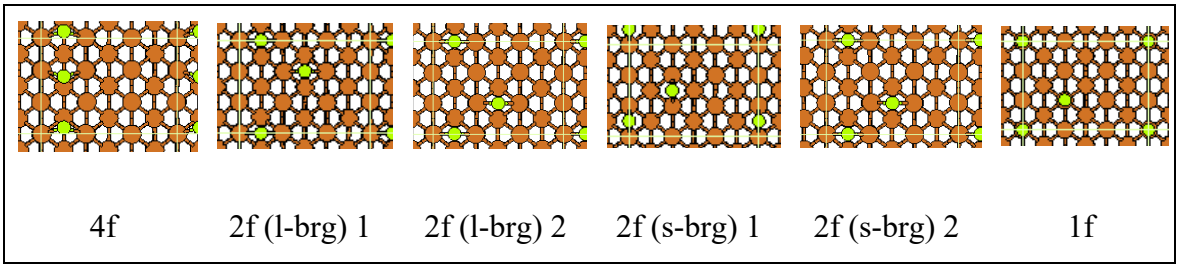

Figure 4.17. Optimized geometries of Cl/Cu (110) at 0.22 ML coverage (Cu: orange, Cl: green)

Table 4.16 shows the adsorption energies, frequencies, bond distances and work function for Cl adsorption on Cu (110) surface at given positions for 0.11 ML. Figure 4.18 presents the top views of these studied Cl adsorptions.

Table 4.16. Adsorption energy, Cl stretching frequency, Cl-Cu bond distances and work function for Cl adsorbed Cu (110) surface at given positions for 1/9 ML (0.11 ML)

Coverage	Position	E_{ads} (kJ/mol)	ν_{Cl} (cm^{-1})	|Cl-Cu| (Å)[a]	ϕ (eV)	σ_{Cl}
0.11 ML	4-fold	-108	176	2.660	4.053	0.693
	2-fold (l-brg)	-120 -208 [65]	193	2.345	4.276	-1.327
	2-fold (s-brg)	-142 -223 [65]	261	2.264	4.317	0.330
	1-fold	-101	321	2.146	6.440	-5.541

[a] Linear average of the Cu-Cl distances for 2-fold and 4-fold positions were reported.

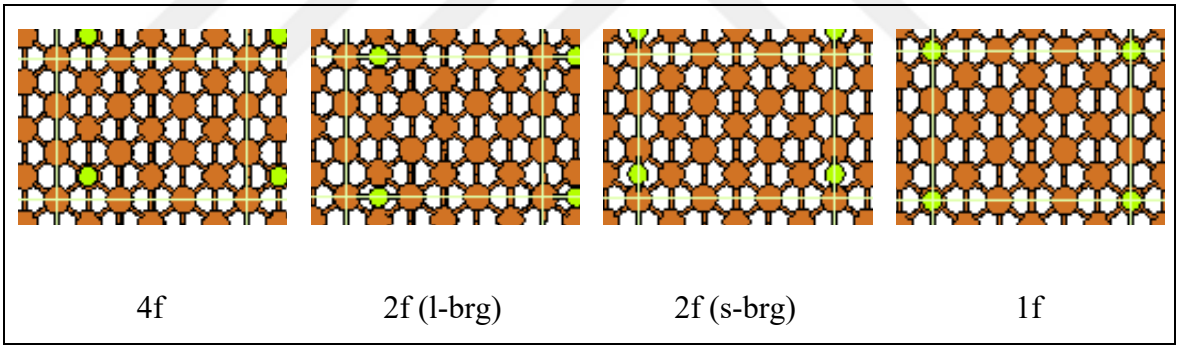

Figure 4.18. Optimized geometries of Cl/Cu (110) at 0.11 ML coverage (Cu: orange, Cl: green)

Table 4.17 shows the adsorption energies, frequencies, bond distances and work function for Cl adsorption on Cu (110) surface at given positions for 0.0625 ML. Figure 4.19 presents the top views of these studied Cl adsorptions.

Table 4.17. Adsorption energy, Cl stretching frequency, Cl-Cu bond distances and work function for Cl adsorbed on Cu (110) surface at given positions for 1/16 ML (0.0625 ML)

Coverage	Position	E_{ads} (kJ/mol)	ν_{Cl} (cm^{-1})	|Cl-Cu| (Å)[a]	ϕ (eV)
0.0625 ML	4-fold	-26	226	2.648	4.267
	2-fold (l-brg)	-38	220	2.345	4.288
	2-fold (s-brg)	-58	235	2.265	4.309
	1-fold	-19	294	2.541	4.358

[a] Linear average of the Cu-Cl distances for 2-fold and 4-fold positions were reported.

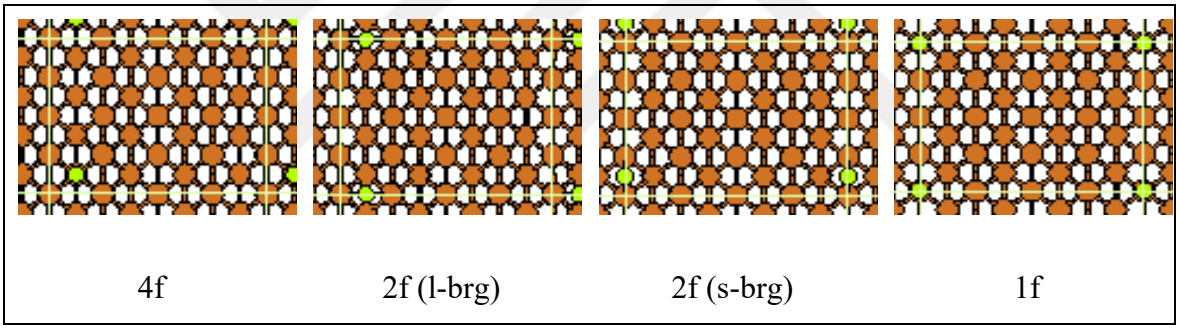

Figure 4.19. Optimized geometries of Cl/Cu (110) at 0.0625 ML coverage (Cu: orange, Cl: green)

4.5. COPPER (100) SURFACE

After relaxing the Cu (100) surface, optimum geometries and adsorption energies were obtained for Cl adsorption.

4.5.1. Chlorine Adsorption

Effect of chlorine coverage on copper metal was investigated on the Cu (100) surfaces for the 1/16 ML, 1/9 ML, 2/9 ML, 1/4 ML, 3/9 ML, 2/4 ML ,3/4 ML, 1 ML chlorine coverage.

Table 4.18 shows the adsorption energies, frequencies, bond distances and work function for Cl adsorption on Cu (100) surface at given positions for 1 ML. Figure 4.20 presents the top views of these studied Cl adsorptions.

Table 4.18. Adsorption energy, Cl stretching frequency, Cl-Cu bond distances and work function for Cl adsorbed on Cu (100) surface at given positions for 1/1 ML (1 ML)

Coverage	Position	E_{ads} (kJ/mol)	ν_{Cl} (cm^{-1})	|Cl-Cu| (Å)[a]	ϕ (eV)
1 ML	4-fold	19	72	2.836	5.281
	2-fold	4	137	2.512	4.887
	1-fold	-4	181	2.316	4.978

[a] Linear average of the Cu-Cl distances for 2-fold and 4-fold positions were reported.

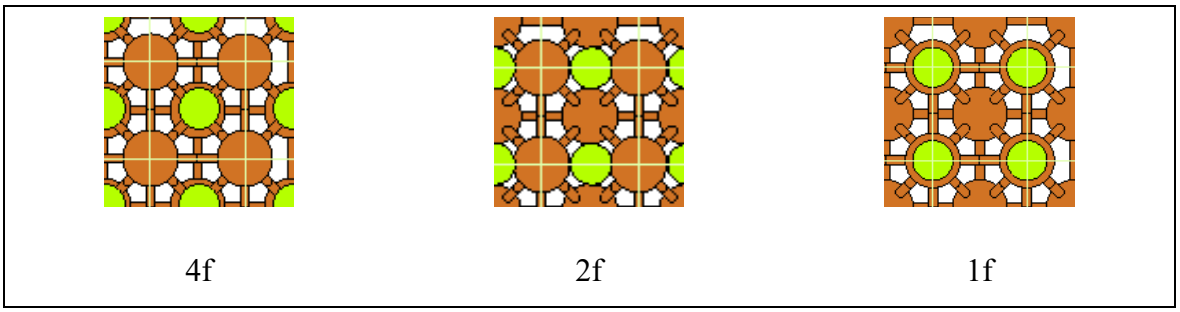

Figure 4.20. Optimized geometries of Cl/Cu (100) at 1ML coverage (Cu: orange, Cl: green)

Table 4.19 shows the adsorption energies, frequencies, bond distances and work function for Cl adsorption on Cu (100) surface at given positions for 0.75 ML. Figure 4.21 presents the top views of these studied Cl adsorptions.

Table 4.19. Adsorption energy, Cl stretching frequency, Cl-Cu bond distances and work function for Cl adsorbed on Cu (100) surface at given positions for 3/4 ML (0.75 ML)

Coverage	Position	E_{ads} (kJ/mol)	ν_{Cl} (cm^{-1})	|Cl-Cu| (Å)[a]	|Cl-Cu| (Å)[a]	|Cl-Cu| (Å)[a]	ϕ (eV)
0.75 ML	4f + 4f + 4f	-260	268	3.599	2.375	2.375	5.923
	2f + 2f + 2f	-202	305	3.327	2.214	2.207	5.913
	1f + 1f + 1f	-149	379	2.317	2.219	2.219	5.090

[a] Linear average of the Cu-Cl distances for 2-fold and 4-fold positions were reported.

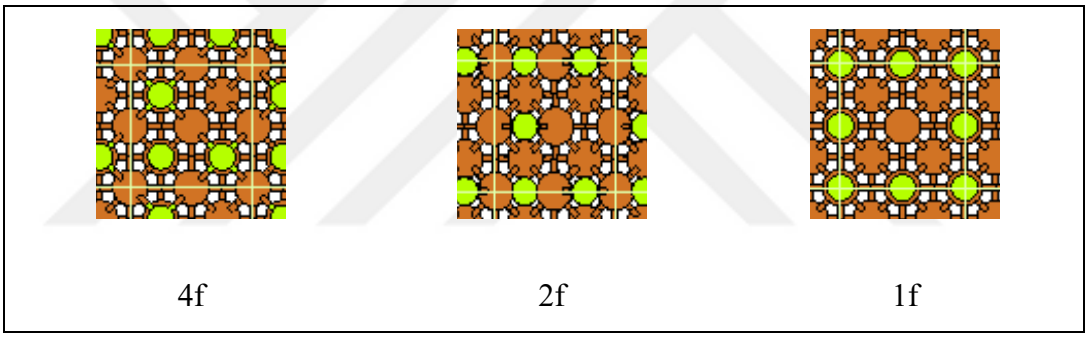

Figure 4.21. Optimized geometries of Cl/Cu (100) at 0.75ML coverage (Cu: orange, Cl: green)

Table 4.20 shows the adsorption energies, frequencies, bond distances and work function for Cl adsorption on Cu (100) surface at given positions for 0.50 ML. Figure 4.22 presents the top views of these studied Cl adsorptions.

Table 4.20. Adsorption energy, Cl stretching frequency, Cl-Cu bond distances and work function for Cl adsorbed on Cu (100) surface at given positions for 2/4 ML (0.50 ML)

Coverage	Position	E_{ads} (kJ/mol)	ν_{Cl} (cm^{-1})	|Cl-Cu| (Å)[a]	|Cl-Cu| (Å)[a]	|Cl-Cl| (Å)[a]	ϕ (eV)
0.50 ML	4f + 4f	-349	234	2.461	2.424	3.644	4.295
	2f + 2f	-324	311	2.259	2.259	3.641	4.432
	1f + 1f	-256	355	2.124	2.125	3.675	4.570

[a] Linear average of the Cu-Cl distances for 2-fold and 4-fold positions were reported

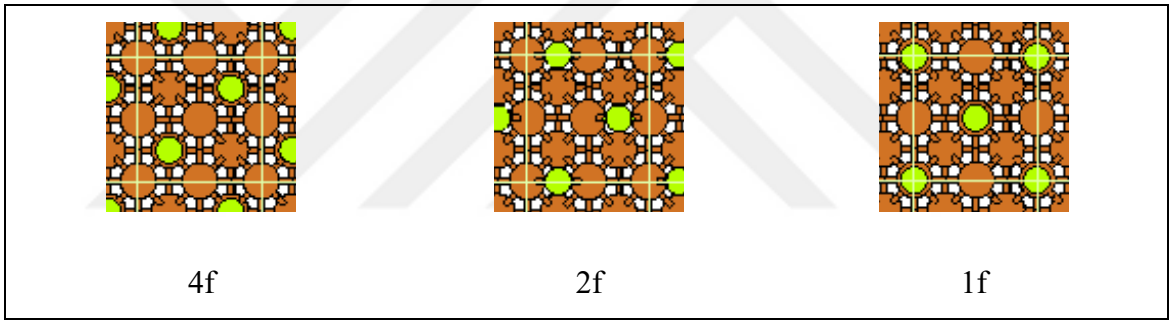

Figure 4.22. Optimized geometries of Cl/Cu (100) at 0.50ML coverage (Cu: orange, Cl: green)

Table 4.21 shows the adsorption energies, frequencies, bond distances and work function for Cl adsorption on Cu (100) surface at given positions for 0.33 ML. Figure 4.23 presents the top views of these studied Cl adsorptions.

Table 4.21. Adsorption energy, Cl stretching frequency, Cl-Cu bond distances and work function for Cl adsorbed on Cu (100) surface at given positions for 3/9 ML (0.33 ML)

Coverage	Position	E_{ads} (kJ/mol)	ν_{Cl} (cm^{-1})	|Cl-Cu| (Å)[a]	|Cl-Cu| (Å)[a]	|Cl-Cu| (Å)[a]	ϕ (eV)
0.33 ML	4f + 4f + 4f	-180	226	2.484	2.484	2.483	4.274
	2f + 2f + 2f	-165	289	2.283	2.272	2.299	4.416
	1f + 1f + 1f	-124	372	2.137	2.136	2.136	4.565

[a] Linear average of the Cu-Cl distances for 2-fold and 4-fold positions were reported.

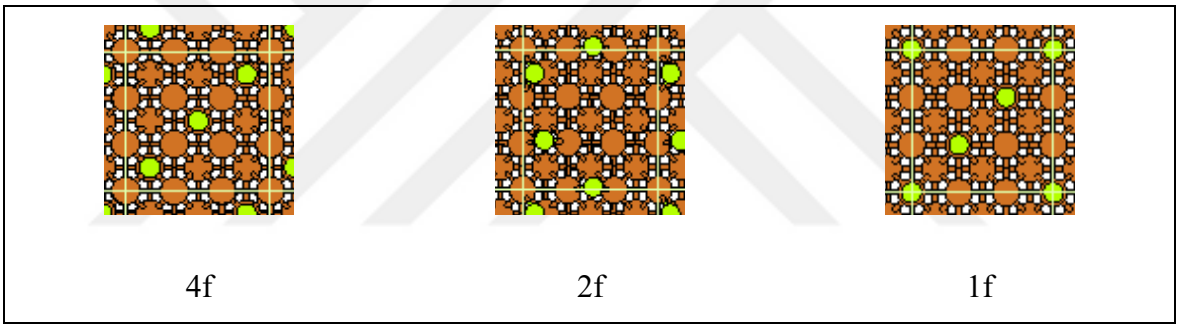

Figure 4.23. Optimized geometries of Cl/Cu (100) at 0.33ML coverage (Cu: orange, Cl: green)

Table 4.22 shows the adsorption energies, frequencies, bond distances and work function for Cl adsorption on Cu (100) surface at given positions for 0.25 ML. Figure 4.24 presents the top views of these studied Cl adsorptions.

Table 4.22. Adsorption energy, Cl stretching frequency, Cl-Cu bond distances and work function for Cl adsorbed on Cu (100) surface at given positions for 1/4 ML (0.25 ML)

Coverage	Position	E_{ads} (kJ/mol)	ν_{Cl} (cm^{-1})	|Cl-Cu| (Å)[a]	ϕ (eV)
0.25 ML	4-fold	-181 -328 [118]	219	2.487	4.542
	2-fold	-173 -318 [118]	288	2.283	4.646
	1-fold (conv. to 4-fold)	-179	NaN	NaN	NaN

[a] Linear average of the Cu-Cl distances for 2-fold and 4-fold positions were reported.

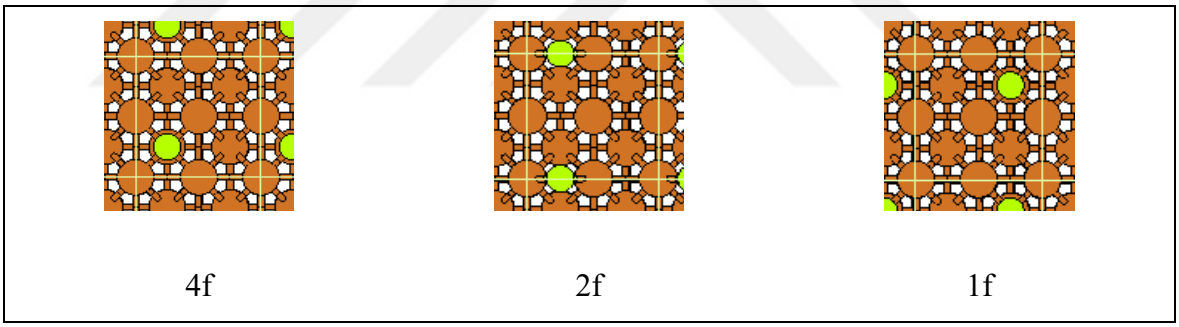

Figure 4.24. Optimized geometries of Cl/Cu (100) at 0.25ML coverage (Cu: orange, Cl: green)

Table 4.23 shows the adsorption energies, frequencies, bond distances and work function for Cl adsorption on Cu (100) surface at given positions for 0.22 ML. Figure 4.25 presents the top views of these studied Cl adsorptions.

Table 4.23. Adsorption energy, Cl stretching frequency, Cl-Cu bond distances and work function for Cl adsorbed on Cu (100) surface at given positions for 2/9 ML (0.22 ML)

Coverage	Position	E_{ads} (kJ/mol)	ν_{Cl} (cm^{-1})	|Cl-Cu| (Å)[a]	|Cl-Cu| (Å)[a]	ϕ (eV)
0.22 ML	4f + 4f 1	-333	218	2.496	2.496	4.436
	4f + 4f 2	-334	225	2.496	2.496	4.437
	2f + 2f	-328	267	2.327	2.316	4.480
	1f + 1f (conv. to 4f)	-334	NaN	NaN	NaN	NaN

[a] Linear average of the Cu-Cl distances for 2-fold and 4-fold positions were reported.

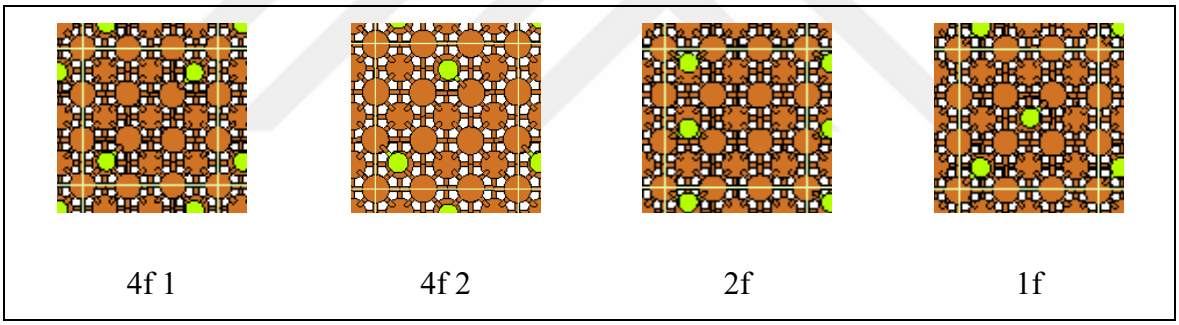

Figure 4.25. Optimized geometries of Cl/Cu (100) at 0.22ML coverage (Cu: orange, Cl: green)

Table 4.24 shows the adsorption energies, frequencies, bond distances and work function for Cl adsorption on Cu (100) surface at given positions for 0.11 ML. Figure 4.26 presents the top views of these studied Cl adsorptions.

Table 4.24. Adsorption energy, Cl stretching frequency, Cl-Cu bond distances and work function for Cl adsorbed on Cu (100) surface at given positions for 1/9 ML (0.11 ML)

Coverage	Position	E_{ads} (kJ/mol)	ν_{Cl} (cm^{-1})	|Cl-Cu| (Å)[a]	ϕ (eV)
0.11 ML	4-fold	-147	229	2.492	4.572
	2-fold	-142	278	2.285	4.628
	1-fold	-107	319	2.164	4.564

[a] Linear average of the Cu-Cl distances for 2-fold and 4-fold positions were reported.

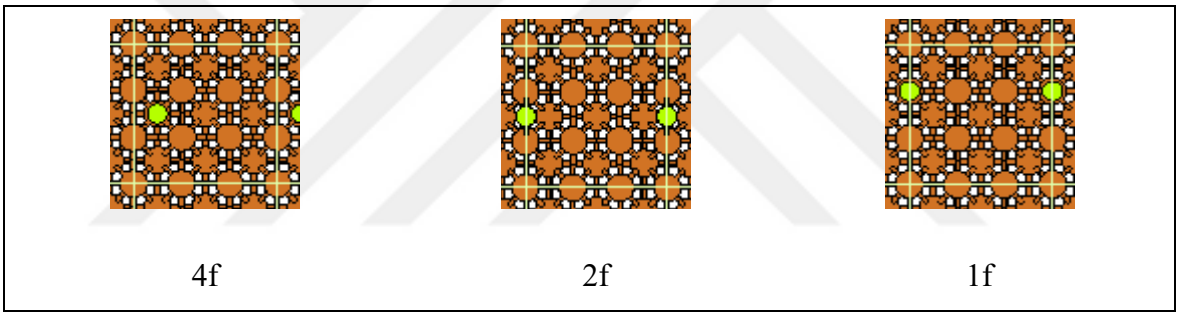

Figure 4.26. Optimized geometries of Cl/Cu (100) at 0.11ML coverage (Cu: orange, Cl: green)

Table 4.25 shows the adsorption energies, frequencies, bond distances and work function for Cl adsorption Cu (100) surface at given positions for 0.0625 ML. Figure 4.27 presents the top views of these studied Cl adsorptions.

Table 4.25. Adsorption energy, Cl stretching frequency, Cl-Cu bond distances and work function for Cl adsorbed on Cu (100) surface at given positions for 1/16 ML (0.0625 ML)

Coverage	Position	E_{ads} (kJ/mol)	ν_{Cl} (cm^{-1})	|Cl-Cu| (Å)[a]	ϕ (eV)
0.0625 ML	4-fold	-204	198	2.497	4.475
	2-fold	-198	221	2.290	4.505
	1-fold	-165	250	2.173	4.552

[a] Linear average of the Cu-Cl distances for 2-fold and 4-fold positions were reported.

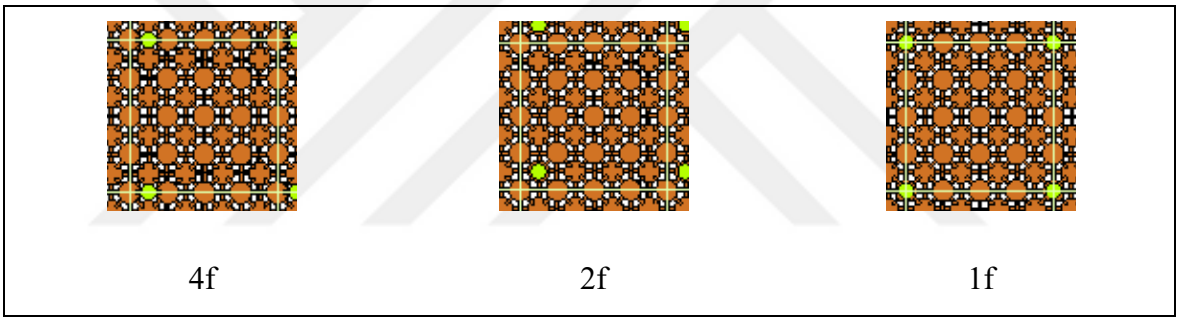

Figure 4.27. Optimized geometries of Cl/Cu (100) at 0.0625ML coverage (Cu: orange, Cl: green)

4.5.2. Inhibitor Adsorption

This section presents the results of the inhibitor studies. First the adsorption of the inhibitor molecules on the clean Cu (100) surface are presented. Then, the adsorption of the inhibitors are studied in the presence of Cl atom(s) over Cu (100) surface to observe the effect of the inhibitor molecule(s) on the Cl adsorption.

Firstly, the geometry optimizations were achieved by performing the adsorption of the selected inhibitor candidates. The p(3x3) Cu (100) surface was selected for the inhibitor adsorptions since it presents a large enough area. For the heterocyclic molecules (inhibitors), all possible adsorption geometries were tested, including the H-stripped geometries, in order to identify the most stable configurations. Among the tested configurations, most stable geometries with highest adsorption energies were selected. The results are presented below starting with azole derivatives, followed by thiophane, pyridine, aniline derivatives, surface ions and finally inorganic molecules.

Different configurations were obtained/tested for the inhibitor molecules through rotating each molecule along its molecular plane in clockwise direction. For the cases where the hydrogen atoms meet the surface adsorption, calculations were performed with both H-containing and H-stripped molecule.

Azole Derivatives

Table 4.26 gives the adsorption energies of pyrazole on p(3x3) Cu (100) surface and Figure 4.28 represents the optimized geometries of pyrazole with varying configurations on Cu (100) surface.

Table 4.26. Adsorption energies of pyrazole at different configuration

Inhibitor Candidates	E_{ads} (kJ/mol)
Configuration 1	-6
Configuration 2	86
Configuration 3	89
Configuration 4	92
Configuration 5	129

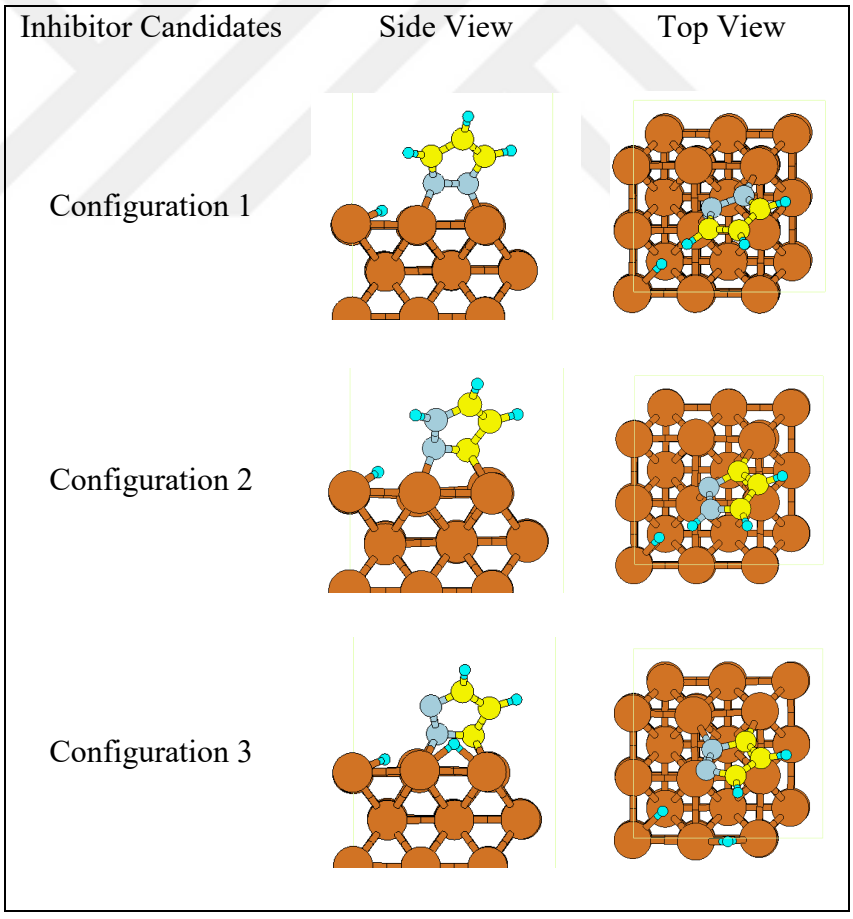

Figure 4.28. Optimized geometries of pyrazole on p(3x3) Cu (100) surface (Cu: orange, H: cyan, C: yellow, N: light blue)

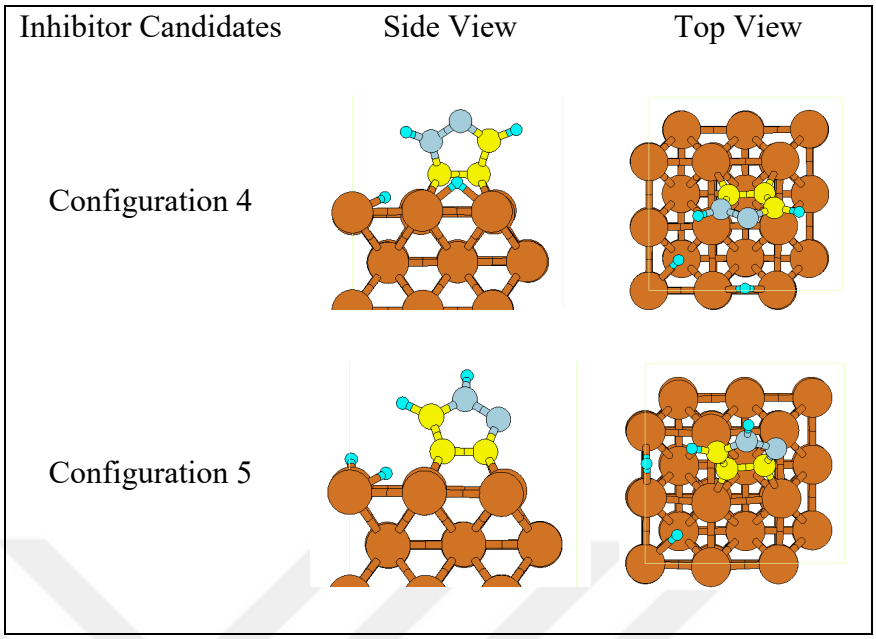

Figure 4.28. Optimized geometries of pyrazole on p(3x3) Cu (100) surface (Cu: orange, H: cyan, C: yellow, N: light blue) (Continued)

Table 4.27 gives the adsorption energies of imidazole on p(3x3) Cu (100) surface. Numbers indicate the different configurations of imidazole. Figure 4.29 represents optimized geometries of imidazole due to varying configurations on Cu (100) surface.

Table 4.27. Adsorption energies of imidazole at different configuration

Inhibitor Candidates	E_{ads} (kJ/mol)
Configuration 1	34
Configuration 2	40
Configuration 3	47
Configuration 4	66
Configuration 5	79

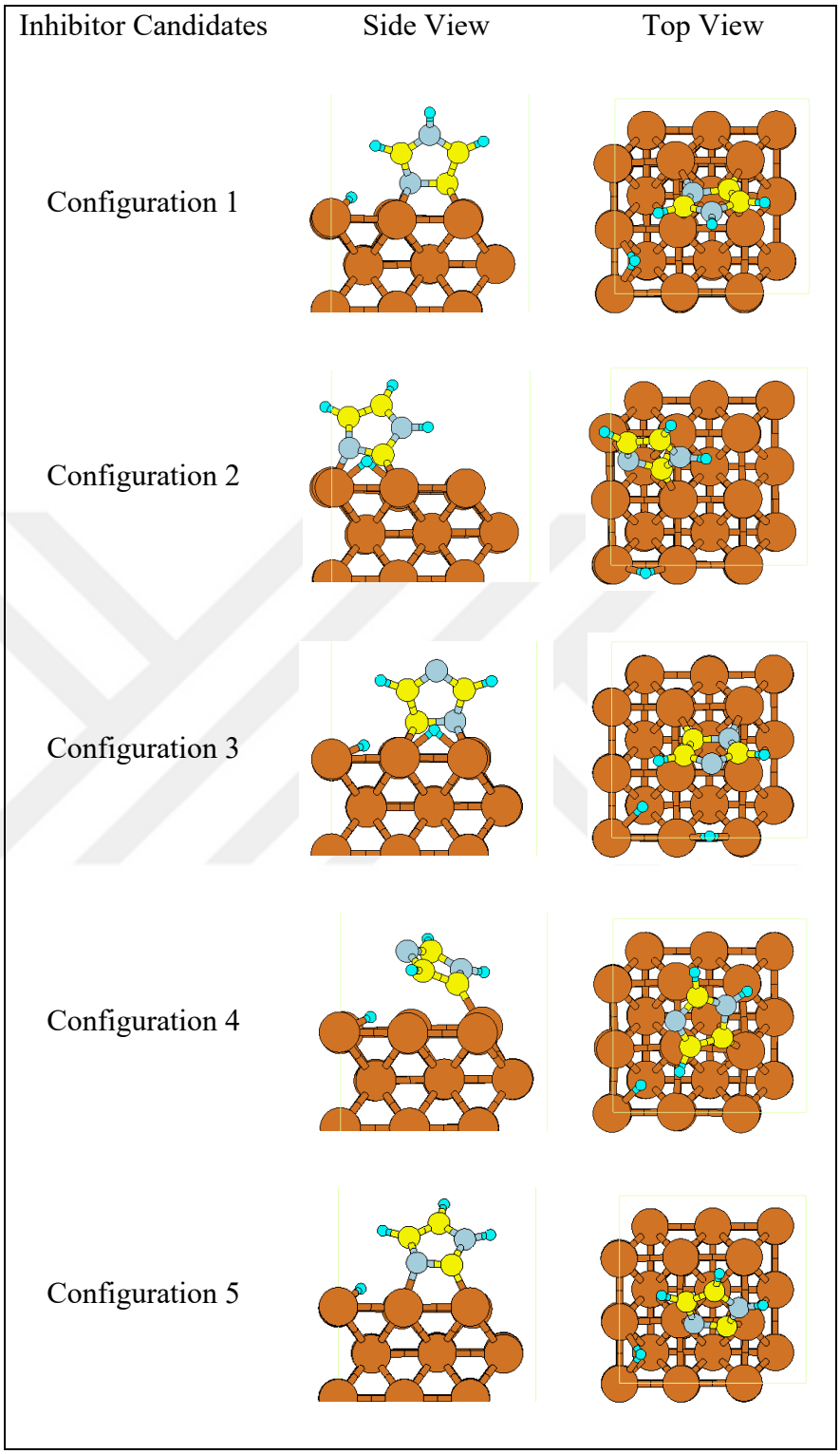

Figure 4.29. Optimized geometries of imidazole on p(3x3) Cu (100) surface (Cu: orange, H: cyan, C: yellow, N: light blue)

Thiophene

Table 4.28 gives the adsorption energies of thiophene on p(3x3) Cu (100) surface. Numbers indicate the different configurations of thiophene.

Table 4.28. Adsorption energies of thiophene at different configurations

Inhibitor Candidates	E_{ads} (kJ/mol)
Configuration 1	Surface distorted
Configuration 2	119
Configuration 3	123

Figure 4.30 represents optimized geometries of thiophene due to varying configurations on Cu (100) surface.

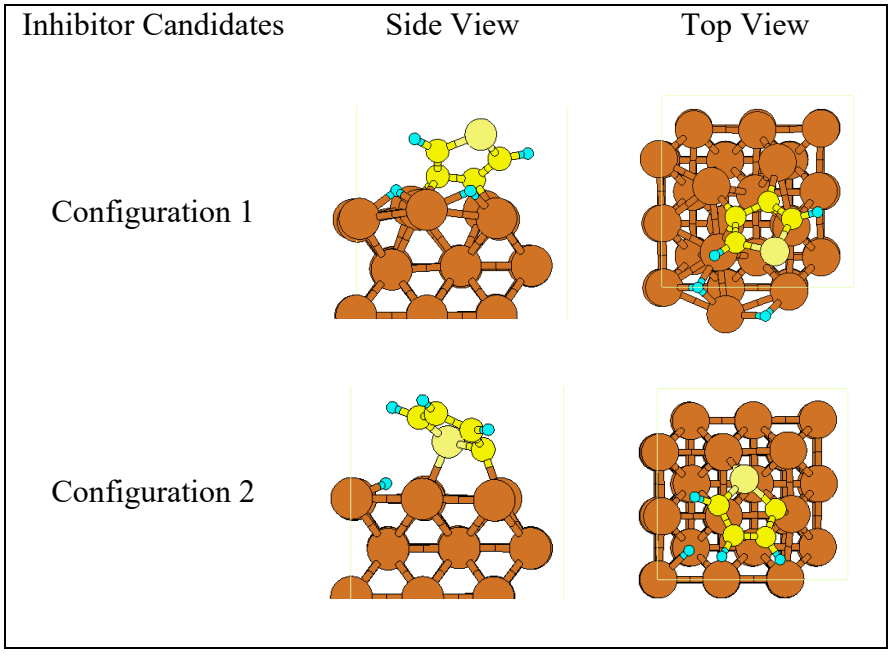

Figure 4.30. Optimized geometries of thiophen on p(3x3) Cu (100) surface (Cu: orange, H: cyan, C: yellow, S: (larger) light yellow)

Inhibitor Candidates	Side View	Top View
Configuration 3	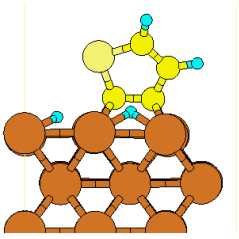	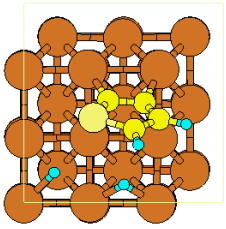

Figure 4.30. Optimized geometries of thiophen on p(3x3) Cu (100) surface (Cu: orange, H: cyan, C: yellow, S: (larger) light yellow) (Continued)

Pyridine

Table 4.29 gives the adsorption energies of pyridine on p(3x3) Cu (100) surface. Numbers indicate the different configurations of pyridine.

Table 4.29. Adsorption energies of pyridine at different conformation

Inhibitor Candidates	E_{ads} (kJ/mol)
Configuration 1	159
Configuration 2	172
Configuration 3	392
Configuration 4	490

Figure 4.31 represents optimized geometries of thiophen due to varying configurations on Cu (100) surface.

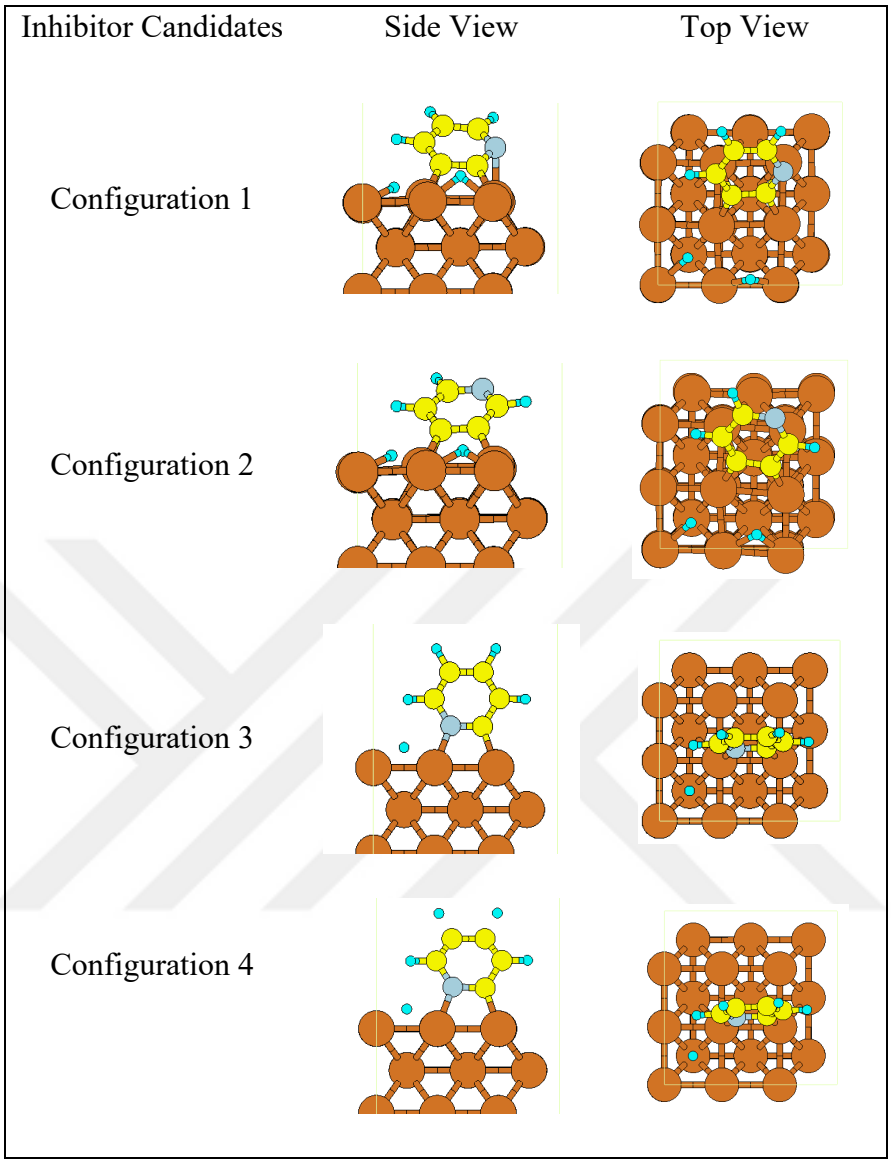

Figure 4.31. Optimized geometries of pyridine on p(3x3) Cu (100) surface (Cu: orange, H: cyan, C: yellow, N: light blue)

Aniline Derivatives

Table 4.30 gives the adsorption energies of p-anisidine on Cu (100) surface, p(3x3) slab. Numbers indicate the different conformations of p-anisidine.

Table 4.30. Adsorption energies of p-anisidine at different conformation

Inhibitor Candidates	E_{ads} (kJ/mol)
Configuration 1	136
Configuration 2	451

Figure 4.32. represents optimized geometries of p-anisidine due to varying conformations on Cu (100) surface.

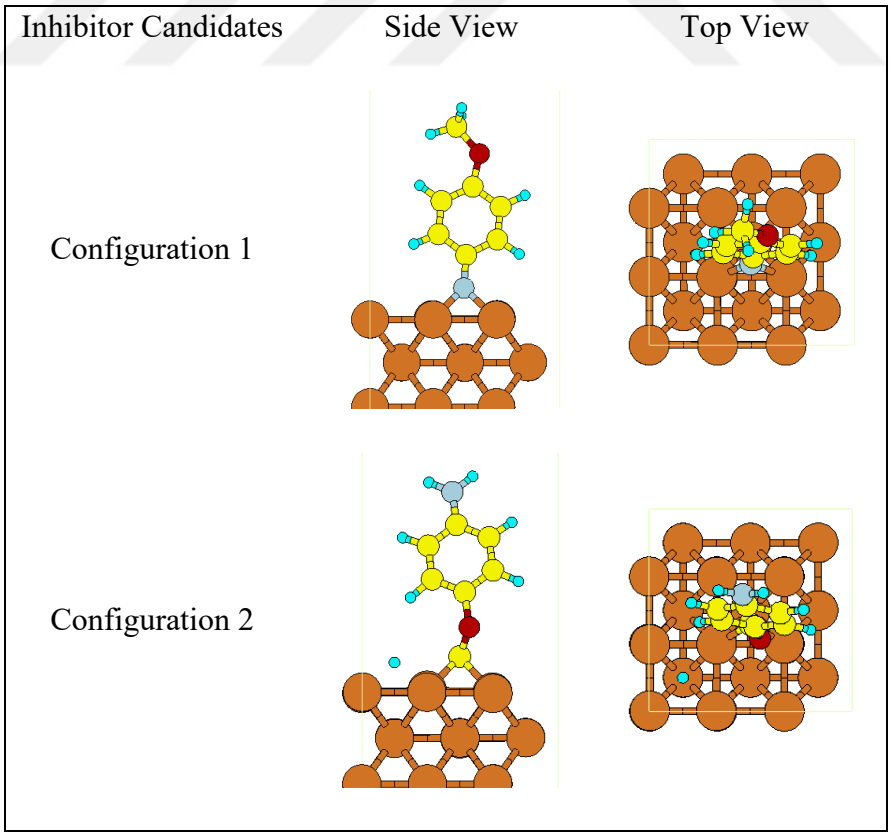

Figure 4.32. Optimized geometries of p-anisidine on p(3x3) Cu (100) surfaec (Cu: orange, H: cyan, C: yellow, N: light blue, O: red)

Table 4.31 gives the adsorption energies of p-toluidine on Cu (100) surface, p(3x3) slab. Numbers indicate the different conformations of p-toluidine.

Table 4.31. Adsorption energies of p-toluidine at different conformation

Inhibitor Candidates	E_{ads} (kJ/mol)
Configuration 1	126
Configuration 2	249

Figure 4.33 represents optimized geometries of p-toluidine due to varying conformations on Cu (100) surface.

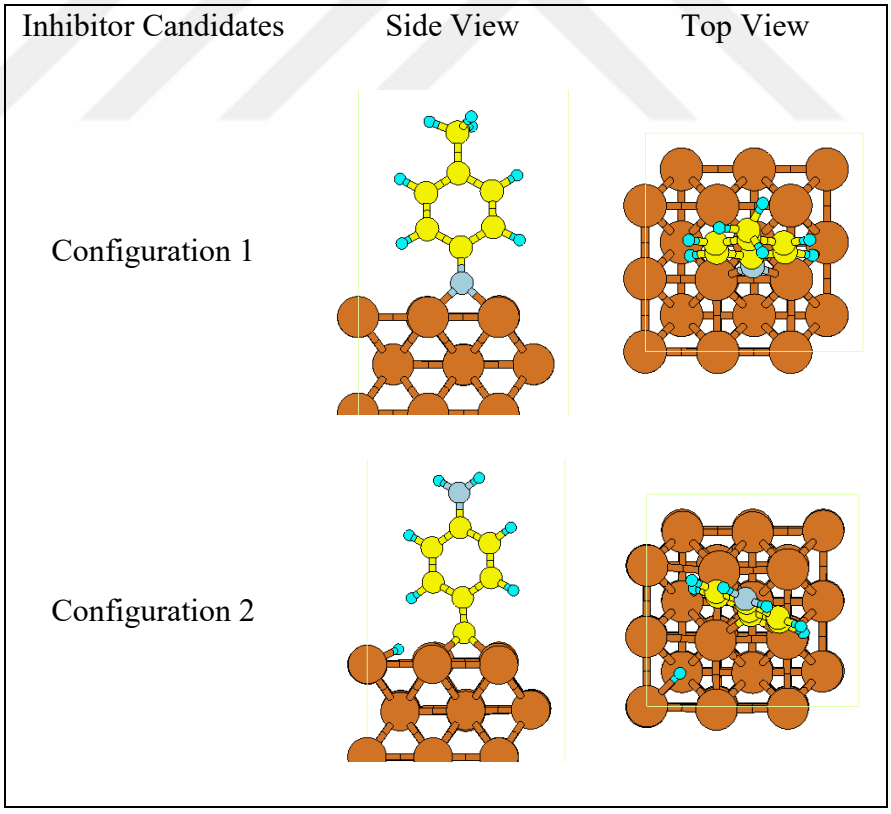

Figure 4.33. Optimized geometries of p-toluidine on p(3x3) Cu (100) surface (Cu: orange, H: cyan, C: yellow, N: light blue)

Surface Ions

Along with the selected inhibitors (or candidates) the ions that would already exist in the aqueous and/or marine environments were also tested for their inhibition effects. Table 4.32 gives the adsorption energies of atomic oxygen, atomic hydrogen, carbon monoxide, methoxy and hydroxide on Cu (100) surface, p(3x3) slab.

Table 4.32. Adsorption energies of surface ions at different configuration

Inhibitor Candidates	E_{ads} (kJ/mol)
Hydroxide (OH)	-331 -370 [119]
Atomic Oxygen (O)	-236 -512 [120]
Carbon monoxide (CO)	-84 -53[121]
Atomic Hydrogen (H)	-13 -223 [122]
Methoxy (OCH_3)	5

The adsorption positions for these ions are as given in several article. A good agreement was observed for O, CO, H and OH as in published values [119–122].

Figure 4.34 represents optimized geometries of atomic oxygen, atomic hydrogen, carbon monoxide, methoxy and hydroxide on Cu (100) surface.

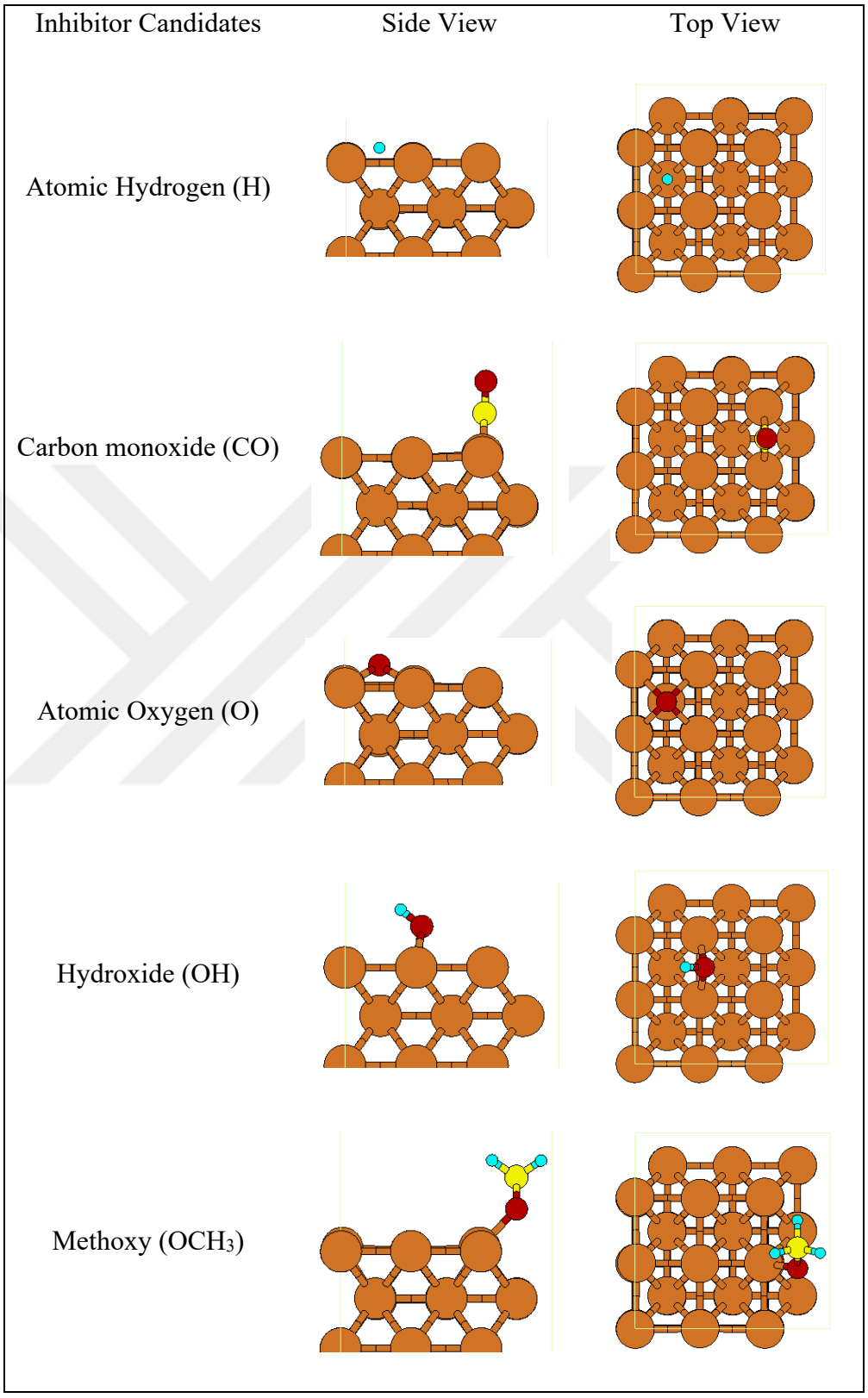

Figure 4.34. Optimized geometries of hydrogen (H), carbon monoxide (CO), oxygen (O), hydroxide (OH) and methoxy (OCH_3) on p(3x3) Cu (100) surface (Cu: orange, H: cyan, O: red, C: yellow)

Inorganic Inhibitor Candidates

Table 4.33 gives the adsorption energies of Ammonia (NH_3) and Chromic Acid (H_2CrO_4) on p(3x3) Cu (100) surface.

Table 4.33. Adsorption energies of ammonia and chromic acid

Inhibitor Candidates	E_{ads} (kJ/mol)
Chromic Acid (H_2CrO_4)	-20
Ammonia (NH_3)	2

Figure 4.35 represents optimized geometries of Ammonia (NH_3) and Chromic Acid (H_2CrO_4) on Cu (100) surface.

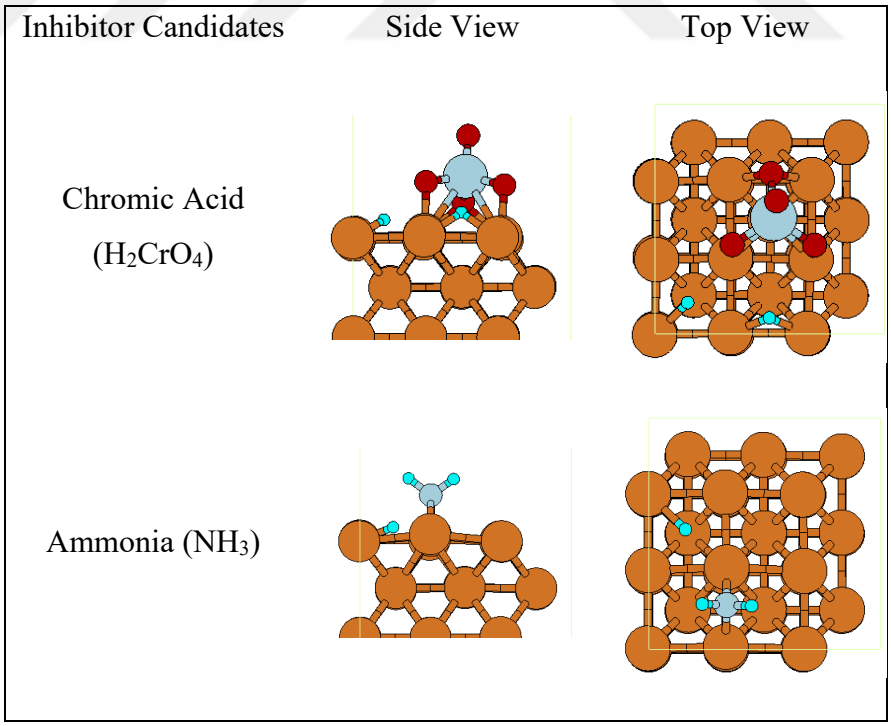

Figure 4.35. Optimized geometries of ammonia (HN_3) and chromic acid (H_2CrO_4) on p(3x3) Cu (100) surface (Cu: orange, H: cyan, N: light blue, Cr: (larger) light blue, O: red)

4.5.3. Chlorine and Inhibitor Co-adsorption

In order to study the effect of the inhibitors on the Cl corrosion (i.e. adsorption) co-adsorption of chlorine on an inhibitor-adsorbed surface was studied. Here again, geometry optimizations were performed by placing chlorine in high symmetry adsorption positions (top, bridge, 4-fold) in the presence of selected inhibitor molecules or ion atoms on the Cu (100) surface. As mentioned above, Cu (100) surface was selected for its higher activity (i.e. stronger Cl adsorption) although it does not have the highest stability. The expected result for a successful inhibition effect would be a significant decrease in the adsorption energy of chlorine in the presence of inhibitor.

4.5.3.1.Adsorption Energy and Geometry

Cl on Cu (100) in the Presence of Azole Derivatives

Table 4.34 gives Cl adsorption energies on p(3x3) Cu (100) surface, in presence of pyrazole molecule.

Table 4.34. Cl adsorption energies on Cu (100) surface in presence of pyrazole molecule

	E_{ads} (kJ/mol)
Cl in 4-fold	-131
Cl in 2-fold	-128
Cl in 1-fold	-154

Figure 4.36 shows the optimized geometry of the Cl in the presence of pre-adsorbed pyrazole on Cu (100) surface.

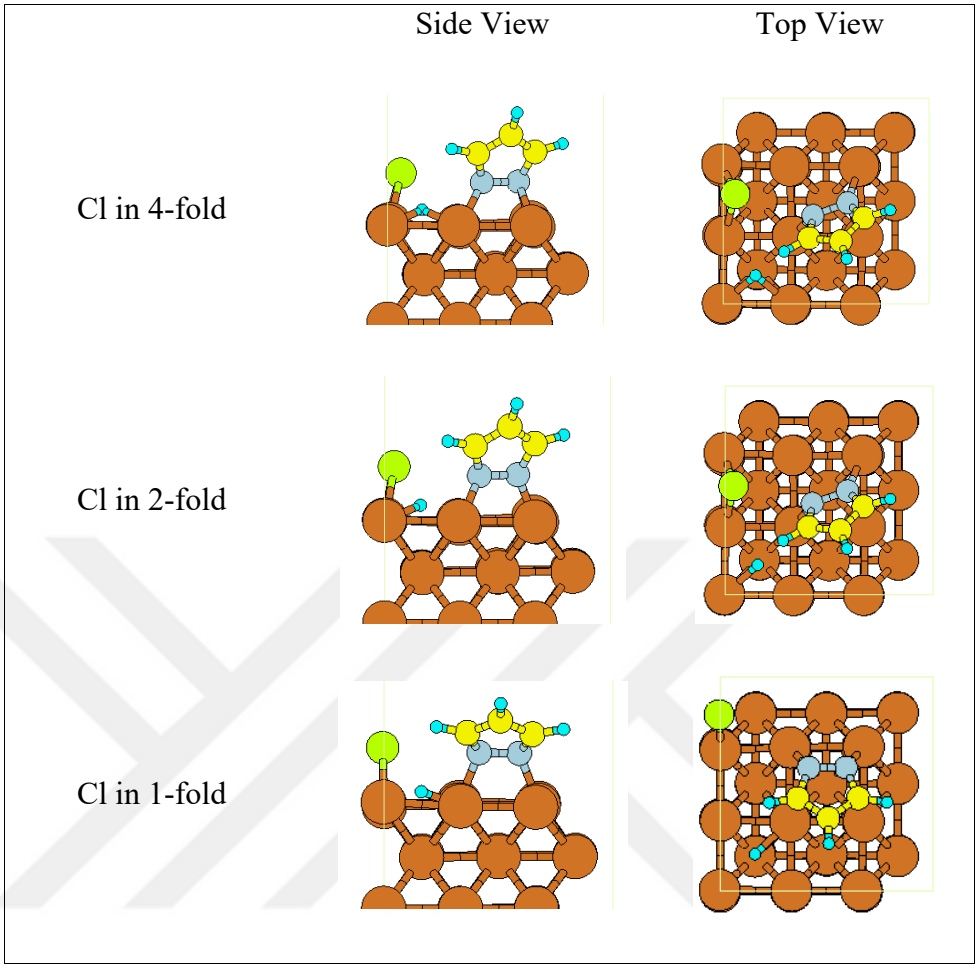

Figure 4.36. Optimized geometries of chlorine (Cl) and pyrazole co-adsorption on p(3x3) Cu (100) surface (Cu: orange, Cl: green, H: cyan, C: yellow, N: light blue)

Table 4.35 gives Cl adsorption energies on p(3x3) Cu (100) surface, in the presence of imidazole molecule.

Table 4.35. Cl adsorption energies on Cu (100) surface in presence of imidazole molecule

	E_{ads} (kJ/mol)
Cl in 4-fold	-137
Cl in 2-fold	-125
Cl in 1-fold	-153

Figure 4.37 shows the optimized geometry of the Cl in the presence of pre-adsorbed imidazole on Cu (100) surface.

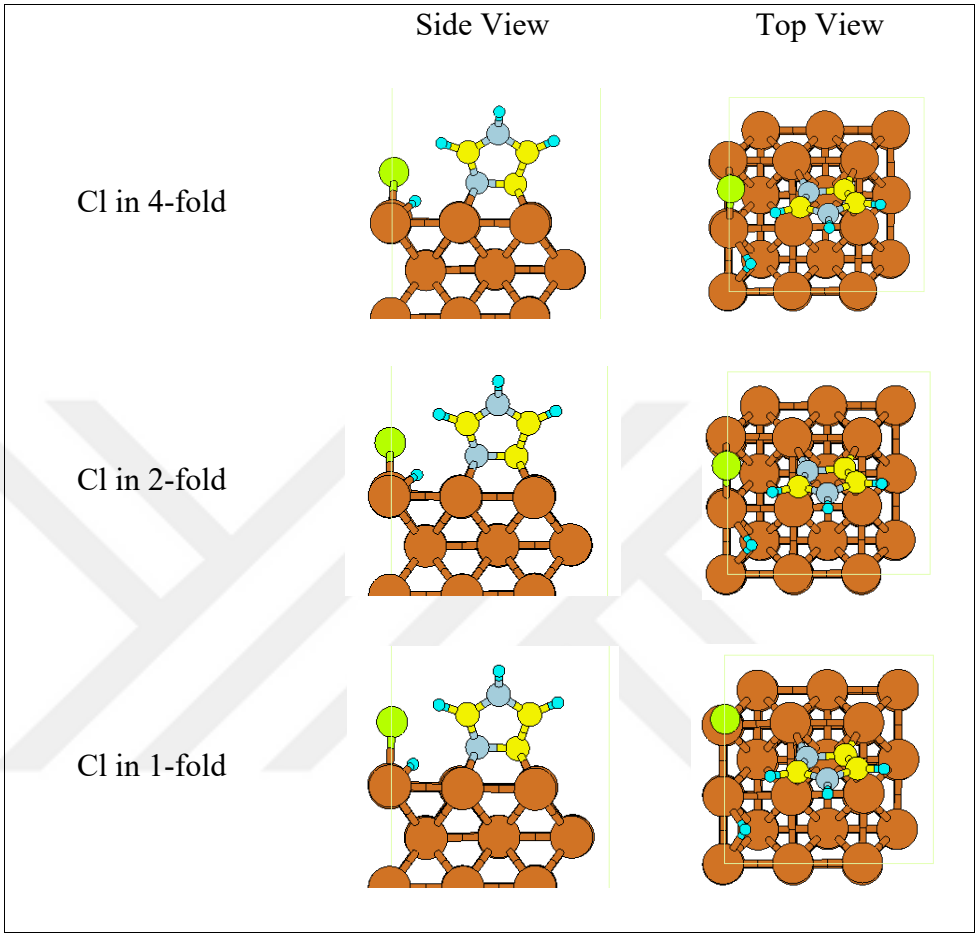

Figure 4.37. Optimized geometries of chlorine (Cl) and imidazole co-adsorption on p(3x3) Cu (100) surface (Cu: orange, Cl: green, H: cyan, C: yellow, N: light blue)

Cl on Cu (100) in the Presence of Surface Ion

Table 4.36 gives Cl adsorption energies on Cu (100) surface, p(3x3) slab, in presence of H atom.

Table 4.36. Cl adsorption energies on Cu (100) surface in presence of H atom

	E_{ads} (kJ/mol)
Cl in 4-fold	-182
Cl in 2-fold	-187
Cl in 1-fold	-147

Figure 4.38 shows the optimized geometry of the Cl in the presence of pre-adsorbed atomic hydrogen (H) on Cu (100) surface.

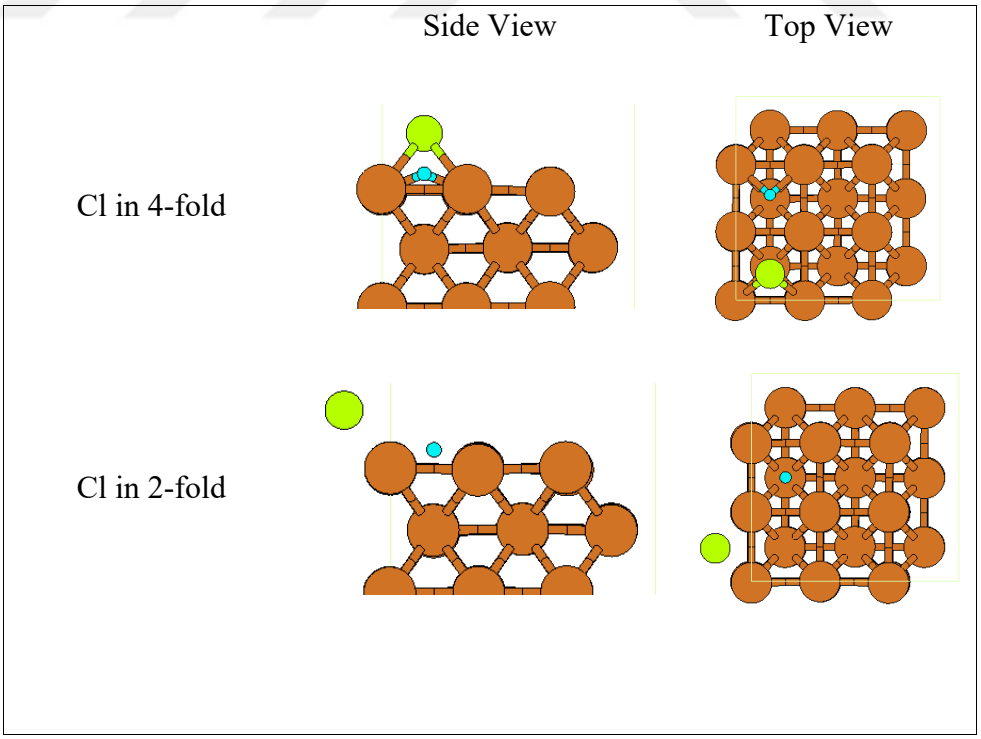

Figure 4.38. Optimized geometries of chlorine (Cl) and hydrogen (H) co-adsorption on p(3x3) Cu (100) surface (Cu: orange, Cl: green, H: cyan)

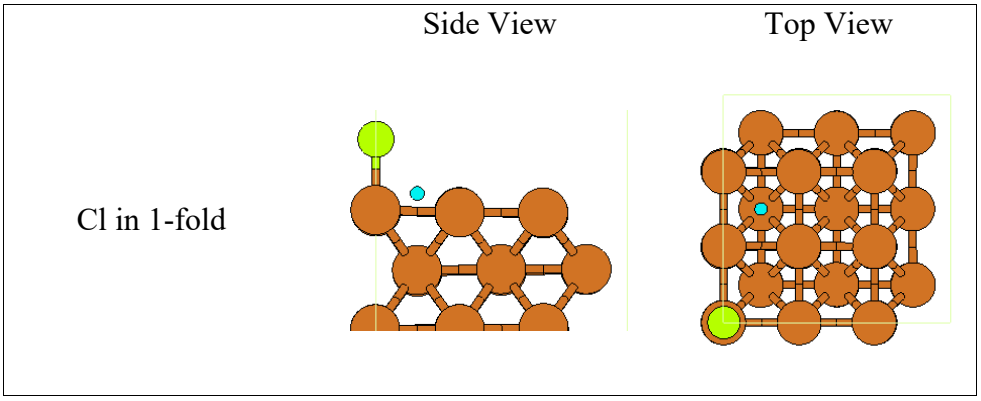

Figure 4.38. Optimized geometries of chlorine (Cl) and hydrogen (H) co-adsorption on p(3x3) Cu (100) surface (Cu: orange, Cl: green, H: cyan) (Continued)

Table 4.37 gives Cl adsorption energies on p(3x3) Cu (100) surface, in presence of O atom.

Table 4.37. Cl adsorption energies on Cu (100) surface in presence of O atom

	E_{ads} (kJ/mol)
Cl in 4-fold	-181
Cl in 2-fold	-184
Cl in 1-fold	-146

Figure 4.39 shows the optimized geometry of the Cl in the presence of pre-adsorbed atomic oxygen on Cu (100) surface.

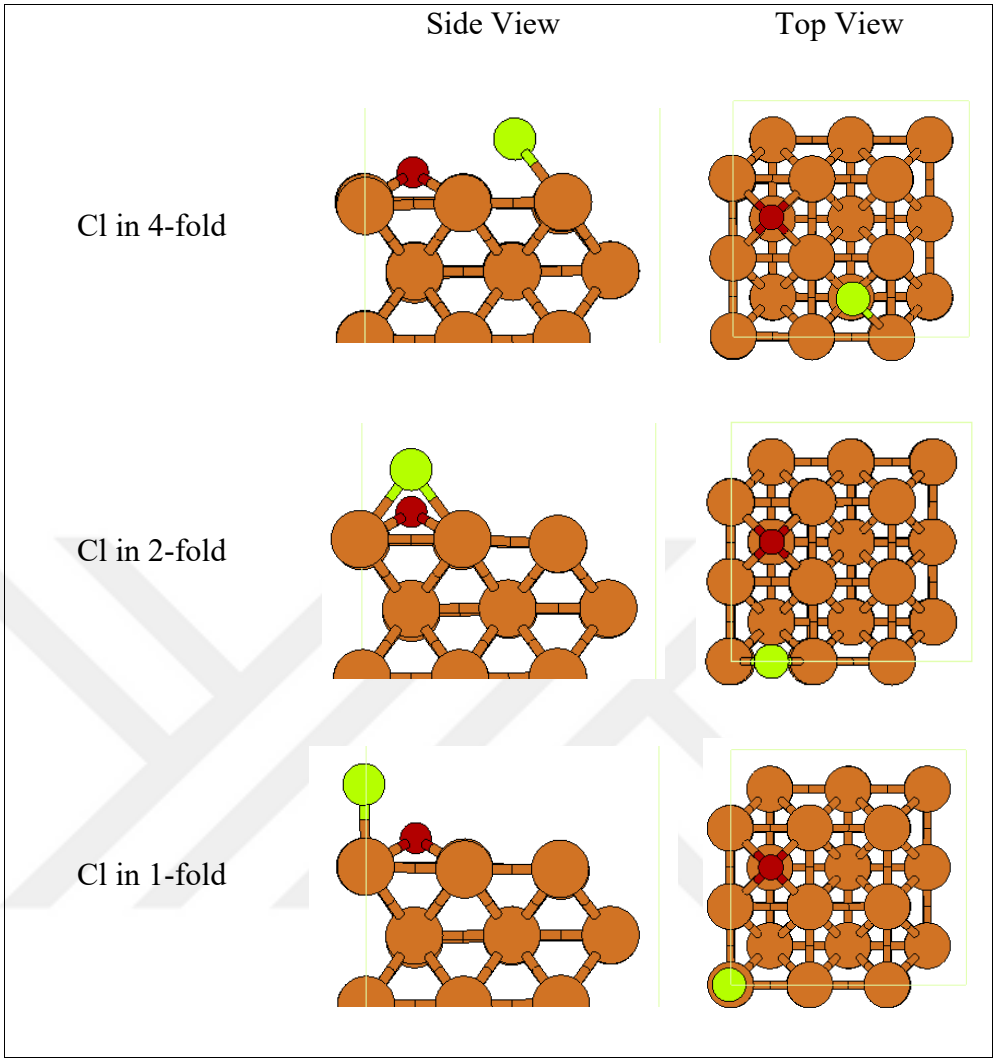

Figure 4.39. Optimized geometries of chlorine (Cl) and oxygen (O) co-adsorption p(3x3) Cu (100) surface (Cu: orange, Cl: green, O: red)

Table 4.38 gives Cl adsorption energies on p(3x3) Cu (100) surface, in presence of OH molecule.

Table 4.38. Cl adsorption energies on Cu (100) surface in presence of OH molecule

	E_{ads} (kJ/mol)
Cl in 4-fold	-192
Cl in 2-fold	-180
Cl in 1-fold	-179

Figure 4.40 shows the optimized geometry of the Cl in the presence of pre-adsorbed OH on Cu (100) surface.

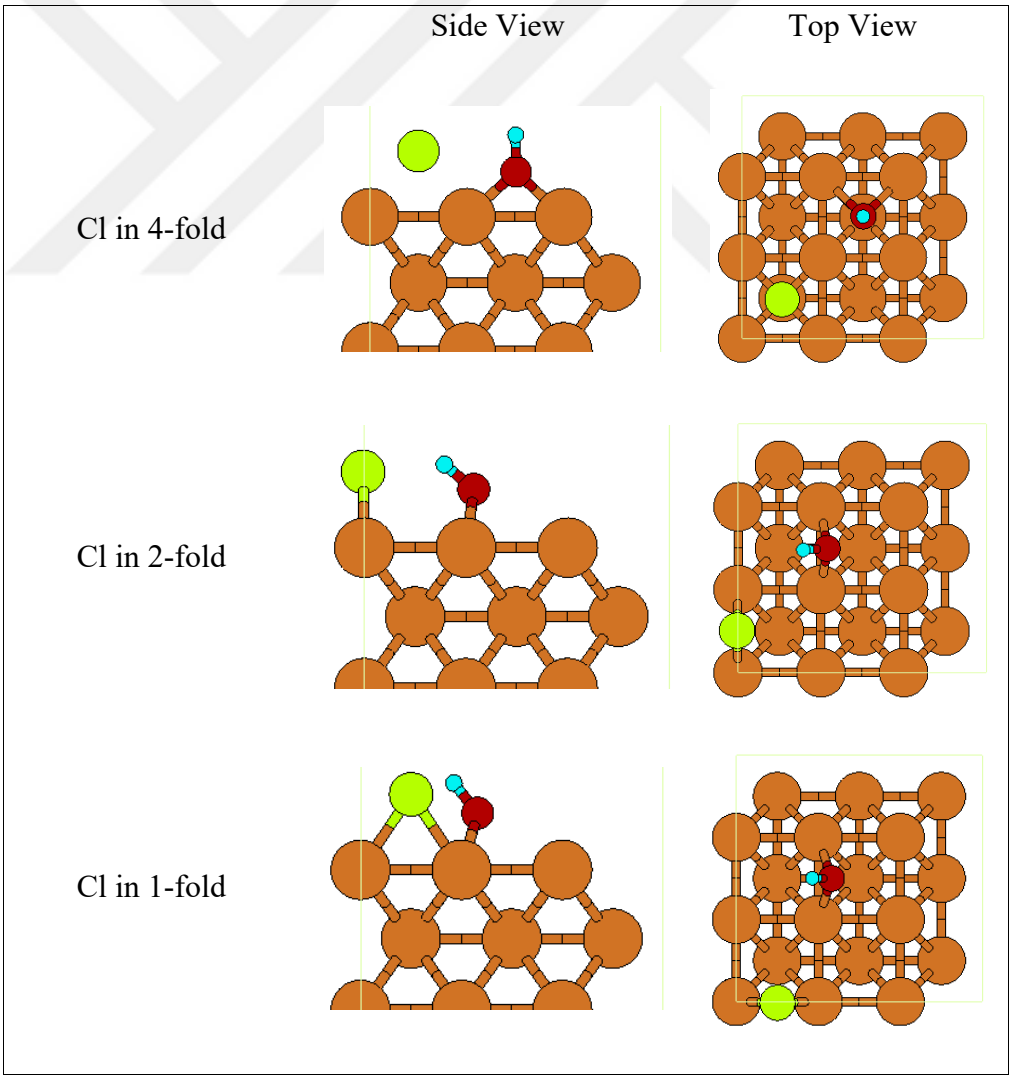

Figure 4.40. Optimized geometries of chlorine (Cl) and hydroxide (OH) co-adsorption on Cu (100) surface (Cu: orange, Cl: green, H: cyan, O: red)

Table 4.39 gives Cl adsorption energy on p(3x3) Cu (100) surface, in presence of CO molecule.

Table 4.39. Cl adsorption energies on Cu (100) surface in presence of CO molecule

	E_{ads} (kJ/mol)
Cl in 4-fold	-187
Cl in 2-fold	-180
Cl in 1-fold	-145

Figure 4.41 shows the optimized geometry of the Cl in the presence of pre-adsorbed CO on Cu (100) surface.

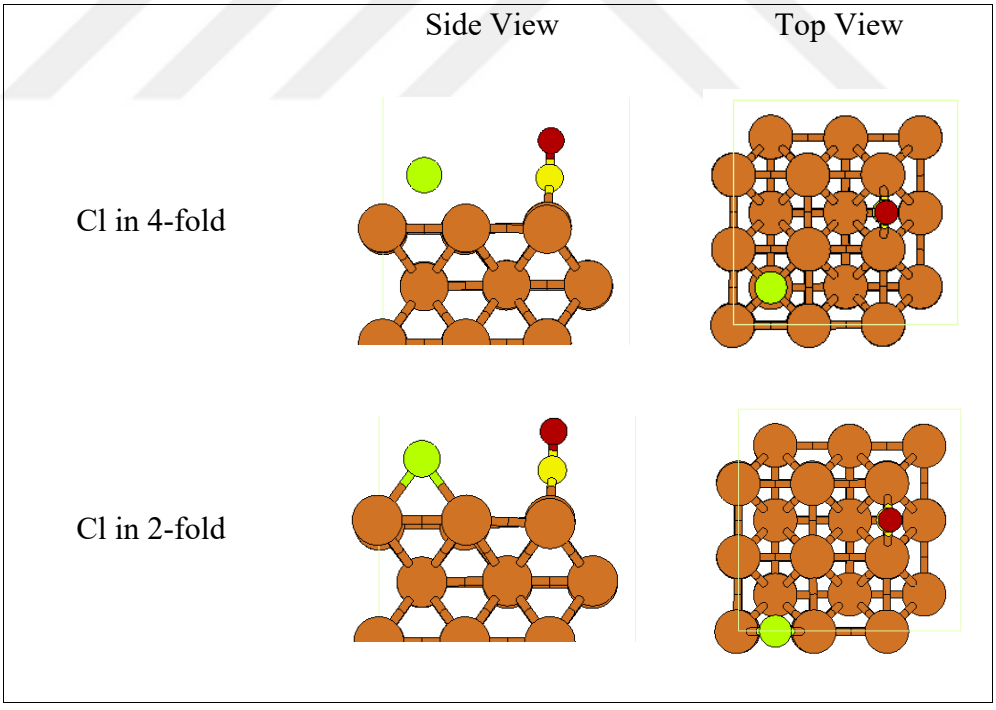

Figure 4.41. Optimized geometries of chlorine (Cl) and carbon monoxide (CO) co-adsorption on p(3x3) Cu (100) surface (Cu: orange, Cl: green, C: yellow, O: red)

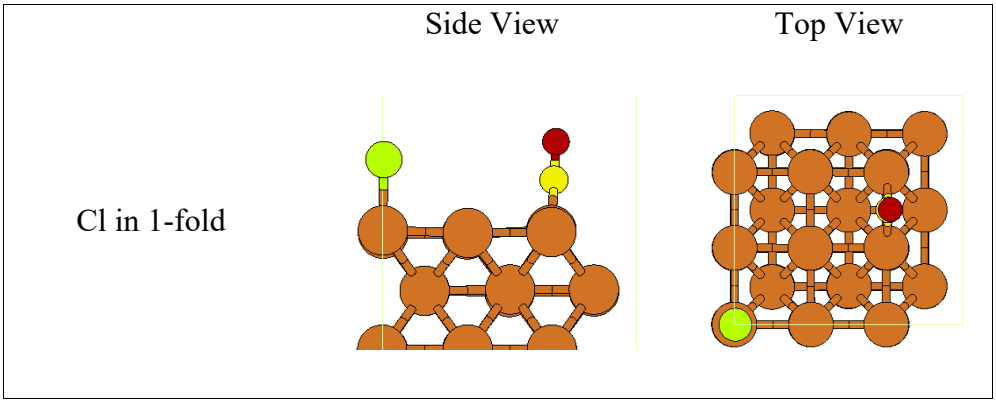

Figure 4.41. Optimized geometries of chlorine (Cl) and carbon monoxide (CO) co-adsorption on p(3x3) Cu (100) surface (Cu: orange, Cl: green, C: yellow, O: red) (Continued)

Table 4.40 gives Cl adsorption energies on p(3x3) Cu (100) surface, in presence of OCH_3 molecule.

Table 4.40. Cl adsorption energies on Cu (100) surface in presence of OCH_3 molecule

	E_{ads} (kJ/mol)
Cl in 4-fold	-186
Cl in 2-fold	-184
Cl in 1-fold	-188

Figure 4.42 shows the optimized geometry of the Cl in the presence of pre-adsorbed OCH_3 on Cu (100) surface.

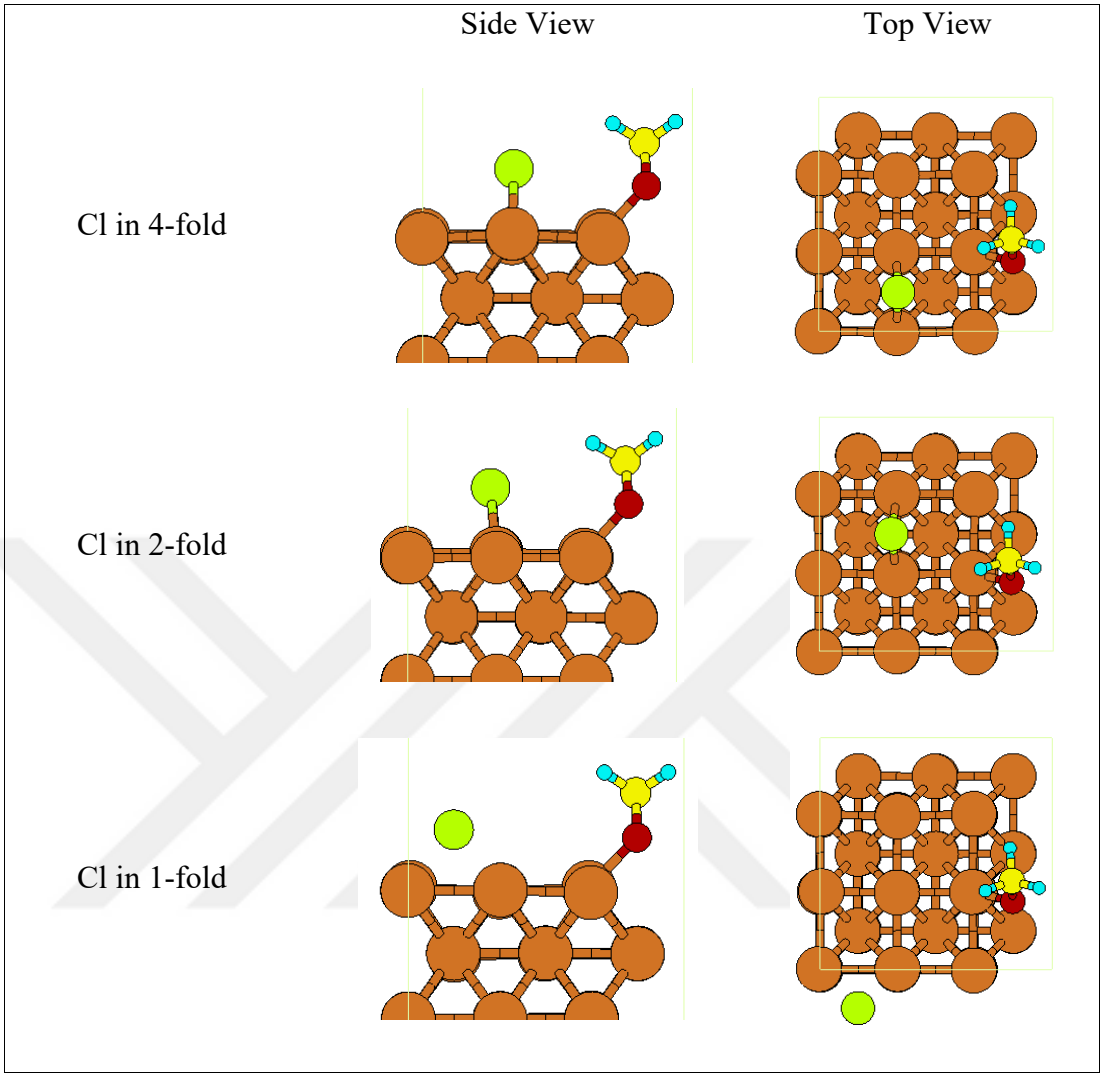

Figure 4.42. Optimized geometries of chlorine (Cl) and methoxy (OCH_3) co-adsorption on p(3x3) Cu (100) surface (Cu: orange, Cl: green, H: cyan, C: yellow, O: red)

Cl on Cu (100) in the Presence of Inorganic Inhibitors

Table 4.41 gives Cl adsorption energies on p(3x3) Cu (100) surface, in presence of NH_3 molecule.

Table 4.41. Cl adsorption energies on Cu (100) surface in presence of NH_3 molecule

	E_{ads} (kJ/mol)
Cl in 4-fold	-178
Cl in 2-fold	-195
Cl in 1-fold	-195

Figure 4.43 shows the optimized geometry of the Cl in the presence of pre-adsorbed NH_3 on Cu (100) surface.

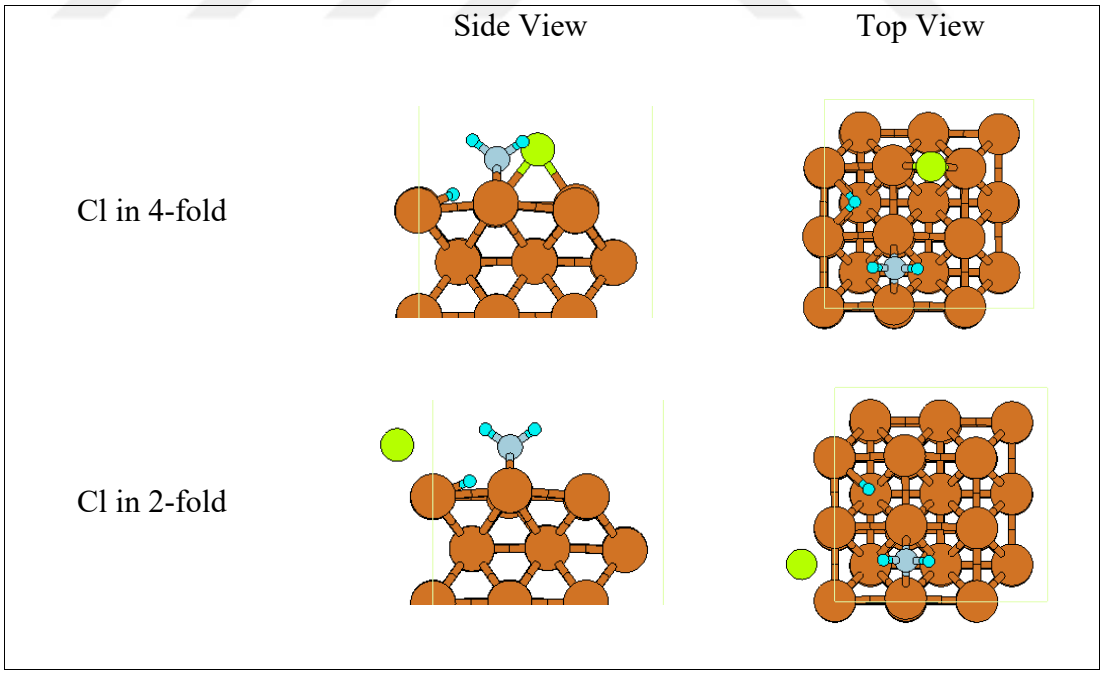

Figure 4.43. Optimized geometries of chlorine (Cl) and ammonia (NH_3) co-adsorption on p(3x3) Cu (100) surface (Cu: orange, Cl: green, H: cyan, N: light blue)

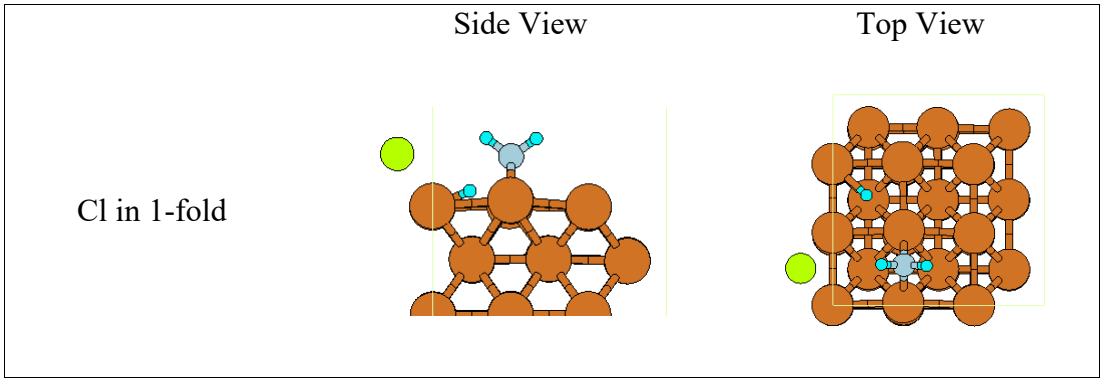

Figure 4.43. Optimized geometries of chlorine (Cl) and ammonia (NH_3) co-adsorption on p(3x3) Cu (100) surface (Cu: orange, Cl: green, H: cyan, N: light blue) (Continued)

Table 4.42 gives Cl adsorption energies on p(3x3) Cu (100) surface, in presence of H_2CrO_4 molecule.

Table 4.42. Cl adsorption energies on Cu (100) surface in presence of H_2CrO_4 molecule

	E_{ads} (kJ/mol)
Cl in 4-fold	-134
Cl in 2-fold	-134
Cl in 1-fold	-161

Figure 4.44 shows the optimized geometry of the Cl in the presence of pre-adsorbed H_2CrO_4 on Cu (100) surface.

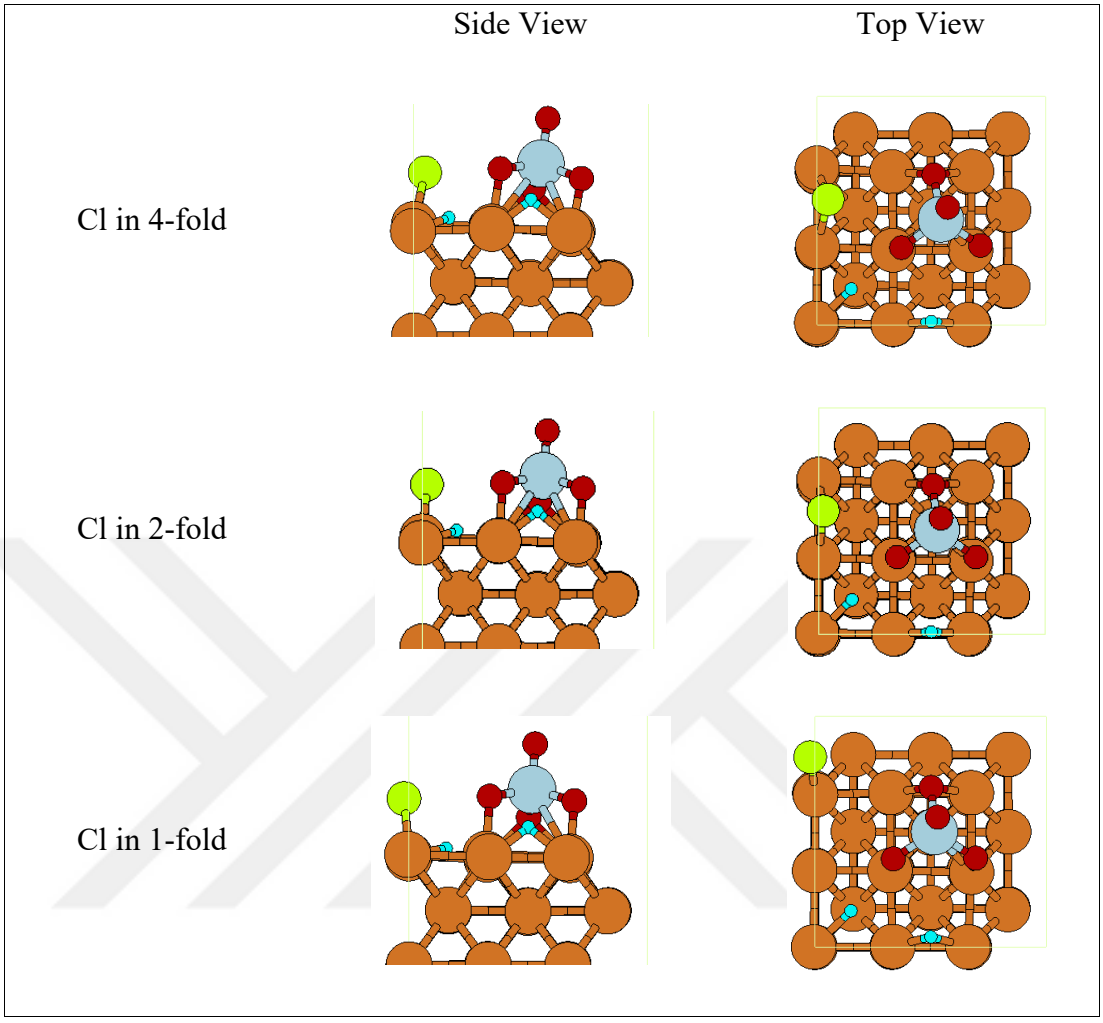

Figure 4.44. Optimized geometries of chlorine (Cl) and chromic acid (H_2CrO_4) co-adsorption on p(3x3) Cu (100) surface (Cu: orange, Cl: green, H: cyan, C: yellow, Cr: (larger) light blue, O: red)

4.6. DISCUSSION

4.6.1. Chlorine Adsorption Energies on Clean Copper Surfaces

When the strong electrophilic character of Cl is combined with copper, which is a good electron donor, corrosion is inevitable. When the Cl adsorption energies on different copper surfaces were compared, it was seen that changes in adsorption energies with increasing coverage showed similar behavior on Cu (100) and Cu (111) surfaces, while that of the Cu (110) surface was quite different. Cu (110) surface shows exothermic Cl adsorption for all the studied coverages up to and including 1 ML. This might be due to the over estimation of the PBE exchange correlation [123]. This observation is indeed not far from expectation, i.e. the surface energies (i.e. surface stabilities) are in the order of Cu (111) > Cu (100) > Cu (110) [39] the relative activities of these surfaces are Cu (110) > Cu (100) > Cu (111).

For the other surfaces the adsorption energies calculated at 1ML were positive (i.e endothermic) showing that chlorine is not stable at these high coverages (or saturation coverage was exceeded). Similarly, adsorption energies of Cu (111) at 0.75 ML were all endothermic, while those of the remaining surfaces were exothermic.

Figure 4.45 shows the adsorption energies of Cl on Cu (111) at varying surface coverage values and adsorption positions. As already mentioned, it can be seen that adsorption energy becomes positive between 0.50 and 0.75 ML, showing that the saturation coverage lies in this range. Adsorption energies were calculated between +66 kJ/mol to -195 kJ/mol. In agreement with the previous findings studied by Andryushechkin et al. [47], adsorption energies of 3-fold fcc and 3-fold hcp sites are found to be almost equal independent of the coverage. Adsorption on these positions is preferred over bridge and top positions which also agrees with former studies [60]. Strength of chlorine adsorption on Cu (111) surface follows the order 3-fold fcc ≈ 3-fold hcp > bridge > top as it was mentioned before [2]. It should be noted that most of the computations with bridge as their initial (starting) geometries converged to 3-fold fcc positions. Converging into different geometries (than that of starting geometries) was commonly observed for Cu (111) surface. The most possible reason for this is the negative lateral interactions because of the short distances between the adsorbates at the initial geometry. These repulsive forces cause a desire to move into a relatively more stable adsorption position.

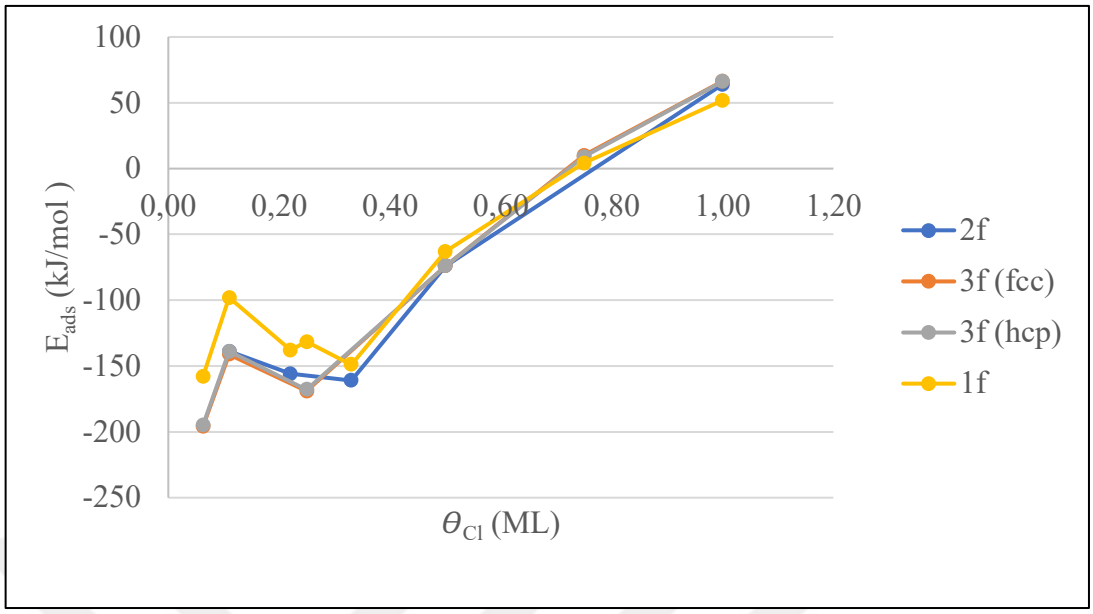

Figure 4.45. Adsorption energy of Cl at varying coverage and adsorption position on Cu (111) surface

When the Cl adsorption energies obtained in this work are compared to those of literature [2], it was seen that adsorption energies of the 3-fold fcc position at 1 ML, 0.25 ML and 0.0625 ML coverage are similar and the values calculated for 1 ML are endothermic. Adsorption energies are found to decrease as the coverage increases for all the positions, except for 0.11 ML. Although the expected value of the adsorption energies at 0.11 ML was in the range of -150 kJ/mol to -200 kJ/mol, much lower adsorption energies were calculated. This is indeed opposite to the findings reported in the literature. However, a linear like relation between E_{ads} and the θ_{Cl} could be obtained if the adsorption energy for 0.11 ML would be closer to the literature value of -182 kJ/mol [2].

Measured bond distances between the 3-fold fcc chlorine and copper is in between 2.172 Å to 2.691 Å. Longest bond distance belongs to 1 ML. These values are also in agreement with the previous findings [2].

Figure 4.46 shows the adsorption energies of Cl on Cu (110) surface at varying surface coverage values and adsorption positions. Adsorption energies were calculated in between -19 kJ/mol to -193 kJ/mol on Cu (110) surface for different coverage values. All the calculated adsorption energies over Cu (110) are negative in agreement with the previous calculations [65]. Adsorption computations with a 4-fold position at the initial geometry on

the Cu (110) surface generally failed to preserve its initial geometry and resulted in either short or long bridge positions. Accordingly, short bridge and long bridge positions are found to be the most stable adsorption positions over the Cu (110) surface, which was in line with the former results [65]. Among these two positions, chlorine showed high energy retention on short bridge position and the average Cl-Cu bond distance of short bridge is shorter compared to the long bridge position.

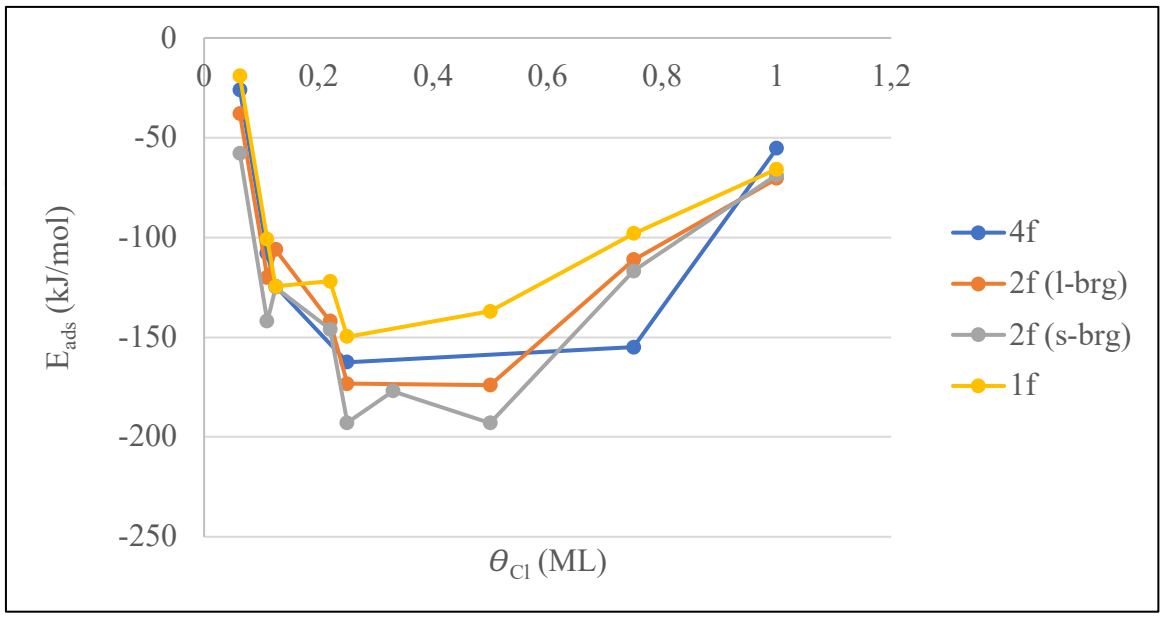

Figure 4.46. Adsorption energy of Cl at varying coverage and adsorption positions on Cu (110) surface

In general, a linear dependency is expected between the adsorption energy and surface coverage [115]. But on Cu (110), it was shown that adsorption energies first decrease (i.e. more exothermic) and then increase (i.e. less exothermic) as shown in Figure 4.46. The source of this anomaly appears to be the less exothermic adsorption energies at low coverages. In other words, one would expect higher adsorption energies at low coverages because of the higher chance of charge transfer (i.e. higher number of free-unshared ions). To clarify the reason of this, some computations were repeated but the result did not change. This anomaly was not investigated further.

Figure 4.47 shows that adsorption energies of Cl on Cu (100) surface at varying coverages and adsorption positions. This trend is more like that of the Cu (111) surface, i.e. linear like behavior, the curve-like trend of the Cu (110) case being absent.

The adsorption energies decreased with increasing coverage at Cu (100) surface except for 0.11 ML. Adsorption energies ranged in between +19 kJ/mol to -204 kJ/mol. The most stable adsorption position is 4-fold which is parallel to the previous reports [118]. The adsorption energies of chlorine on the top position were lower compared to the other adsorption positions. The chlorines, whose initial geometries were in the top position, moved to the bridge or 4-fold position in the final geometry. Overall, an adsorption strength in the order of 4-fold > bridge > top is observed.

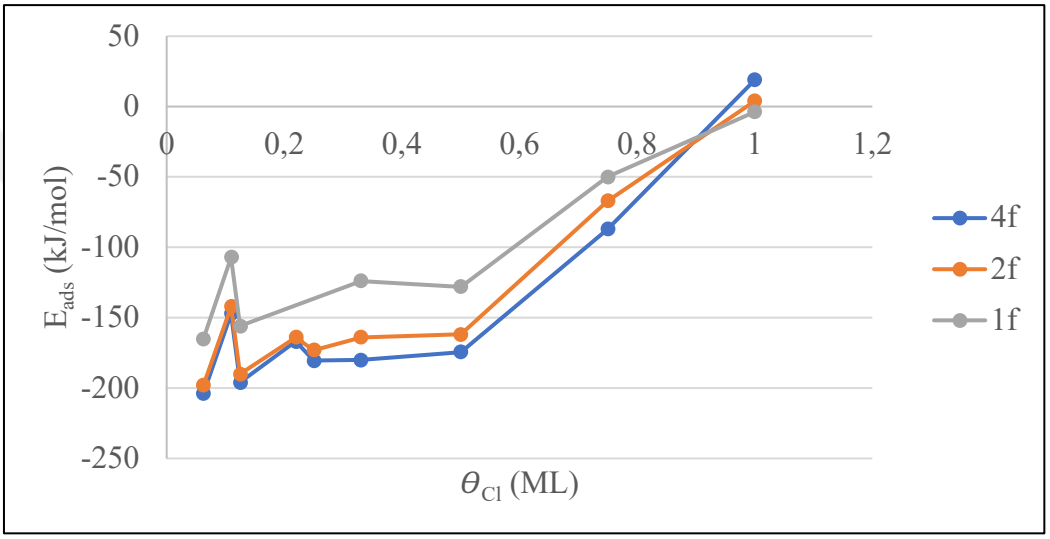

Figure 4.47. Adsorption energy of Cl at varying coverage and adsorption position on Cu (100) surface

It was observed that adsorption energies increase with increasing Cl-Cu bond distance, the highest bond distance belonging to 4-fold position. The average Cl-Cu nearest distance increase in the order 4-fold > bridge > top positions.

4.6.2. Vibrational Analysis

Figure 4.48, Figure 4.49 and Figure 4.50 show that the frequency is also coverage dependent. Figure 4.48 shows an increase in the computed frequencies with coverage for the Cu (111) surface. Although they are less clear, similar trends can be observed in Cu (110) and Cu (100) surfaces as well. For all three surfaces, a sharp drop is observed for 1 ML coverage. Since 1 ML coverage was studied using p(1x1) slabs for all surfaces, the adsorbed Cl might

be subject to strong lateral effects, which would explain the changes in frequencies. Another possible reason is that the adsorption becomes endothermic at 1 ML that shows the weakened Cl-Cu bonds, which would certainly effect the computed frequency. Gas phase chlorine frequency shift was observed at vibrational frequencies.

The stretching frequencies range in between 126 cm^{-1} to 471 cm^{-1} for Cl on Cu (111) surface. While an increase was observed between 0.33 ML and 0.75 ML, there was a dramatic decrease between 0.75 ML and 1 ML. Figure 4.48 shows the stretching frequencies of Cl on Cu (111) at varying surface coverage and adsorption positions.

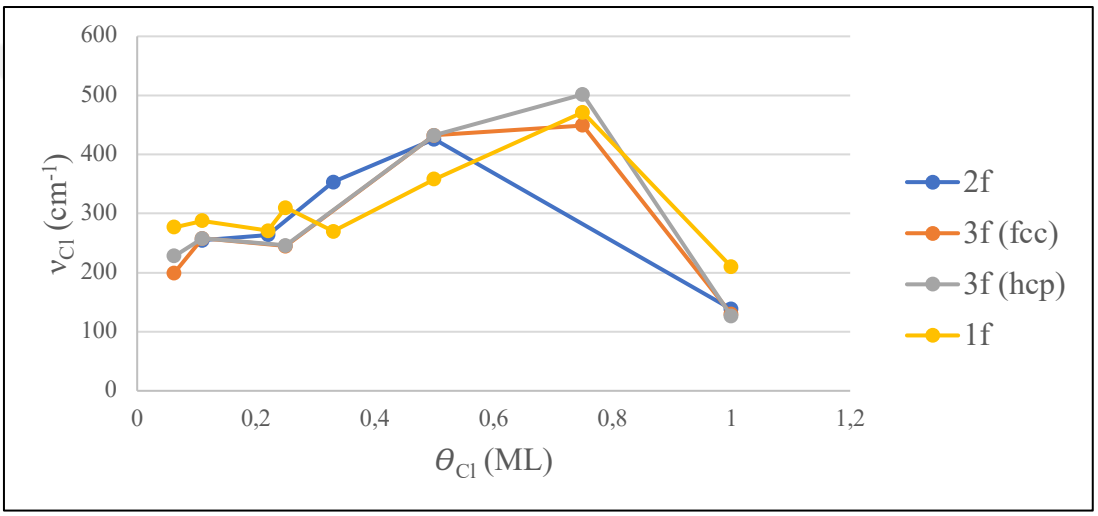

Figure 4.48. Cl stretching frequencies at varying coverage and adsorption positions on Cu (111) surface

The stretching frequencies varied in between 165 cm^{-1} to 422 cm^{-1} for Cl on the Cu (110) surface. Similar to Cu (111), the Cl frequency on the Cu (110) surface also decreases between 0.75 ML and 1 ML.

Figure 4.49 shows the stretching frequencies of Cl on Cu (110), at varying coverage and adsorption positions.

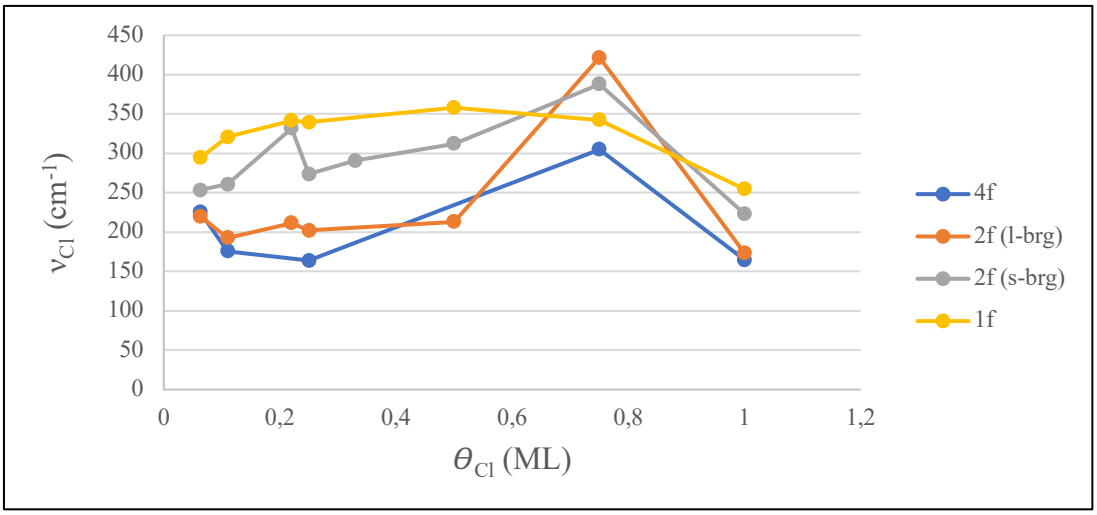

Figure 4.49. Cl stretching frequencies at varying coverage and adsorption positions on Cu (110) surface

The stretching frequencies varied between 72 cm^{-1} to 379 cm^{-1} for Cl on Cu (100) surface. , A similar behavior to those of Cu (111) and Cu (110) surfaces are seen in the Cu (100) plot.

Figure 4.50 shows the stretching frequencies of Cl on Cu (100), at varying coverage and adsorption positions.

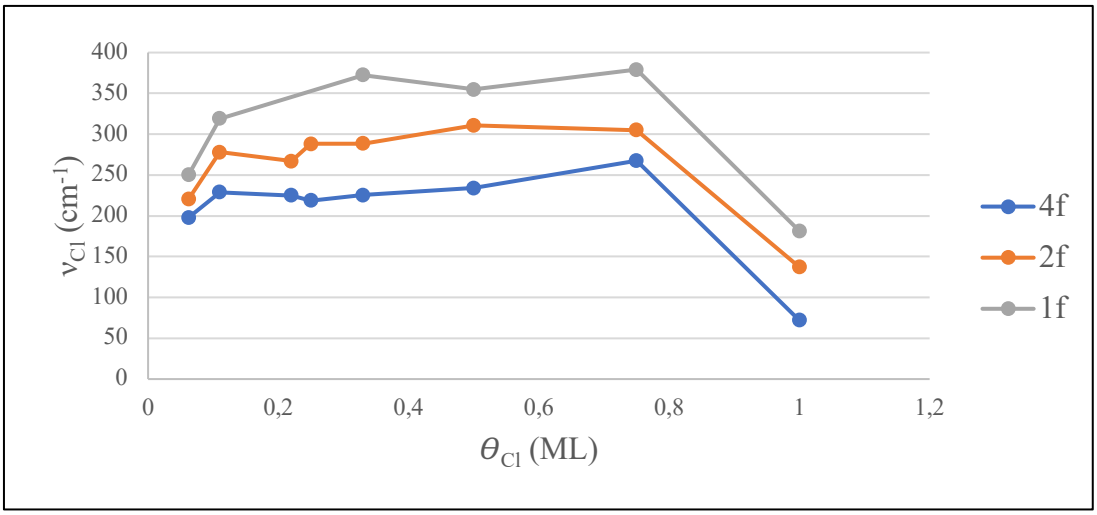

Figure 4.50. Cl stretching frequencies at varying coverage and adsorption positions on Cu (100) surface

4.6.3. Work Function

When a gas is adsorbed on a metal surface, the change in work function depends on the metal surface and the chemical nature of the adsorbents. Electron transfer can occur between atoms adsorbed and the metal surface. In the case where metal surface is the electron donor, the change in the work function is negative, and in the case where the adsorbate is the electron donor the work function change is positive. In other words, by measuring the change in the work function (i.e. experimentally) it is possible to deduce the direction of the charge transfer.

The work function values were calculated, by using Equation 3.15., for each adsorption position and coverage on Cu (100), Cu (110) and Cu (111) surfaces. The calculated work function changes can be seen in Figure 4.51, Figure 4.52 and Figure 4.53.

First, work function values were calculated for clean copper surfaces. These were obtained as 4.56 eV for Cu (100), 4.31 eV for Cu (110) and 4.85 eV for Cu (111) which are in agreement with the reported values of 4.73 eV, 4.56 eV and 4.90 eV, respectively for for Cu (100), Cu (110) and Cu (111) [124]. Figure 4.51 shows the work function change for Cl adsorption on Cu (111) surface at varying coverage and adsorption positions.

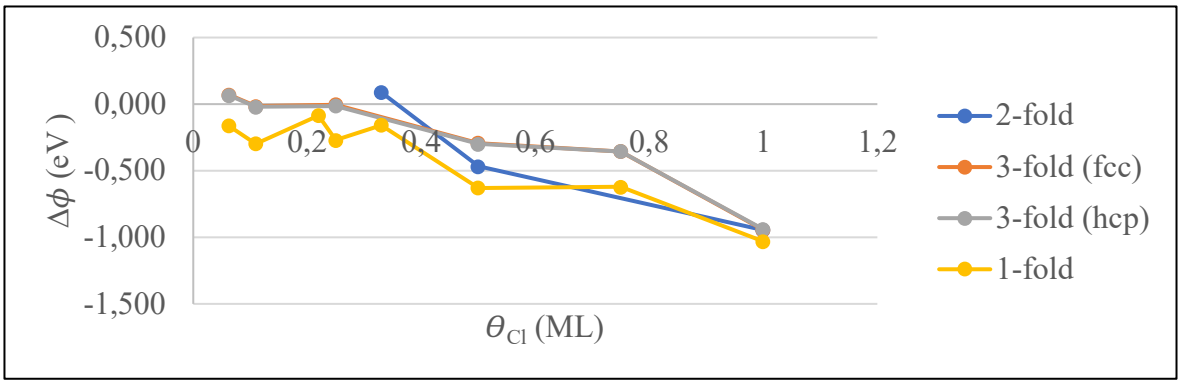

Figure 4.51. Work function changes for Cl adsorption on Cu (111) surface at varying coverage and adsorption positions

Figure 4.52 shows the work function change for Cl adsorption on the Cu (110) surface at varying coverage and adsorption positions.

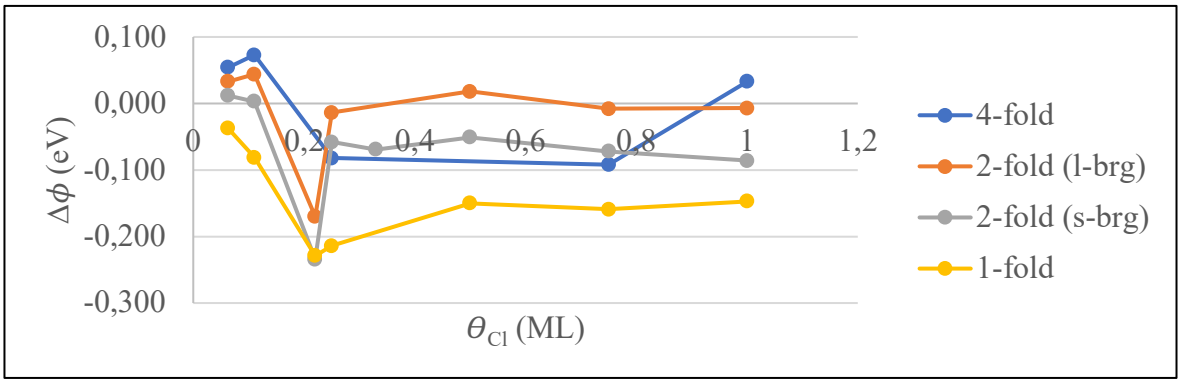

Figure 4.52. Work function changes for Cl adsorption on Cu (110) surface at varying coverage and adsorption positions

Figure 4.53 shows the work function change for Cl on the Cu (100) surface at varying coverage and adsorption positions.

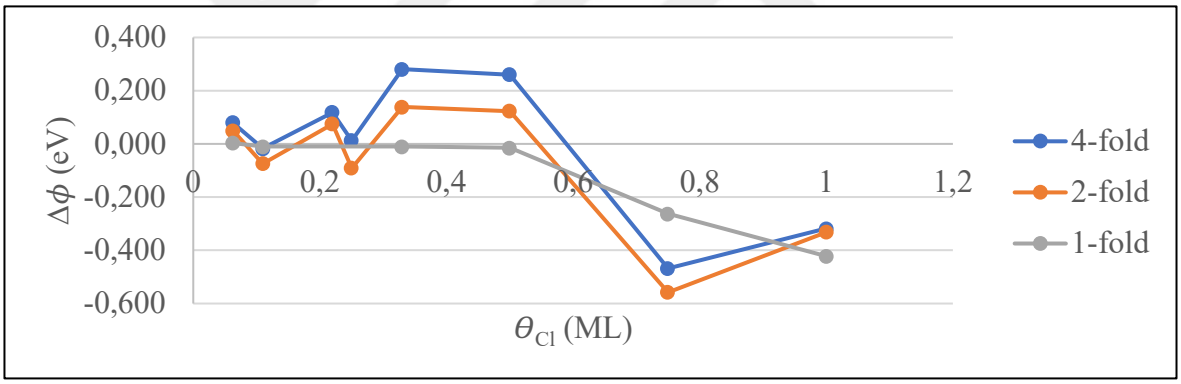

Figure 4.53. Work function changes for Cl adsorption on Cu (100) surface at varying coverage and adsorption positions

4.6.4. Inhibitor Adsorption on clean Cu (100) surface

This section presents the discussion about the inhibitor adsorption on clean p(3x3) Cu (100) surface. The selection of p(3x3) Cu (100) surface is based on the fact that, p(3x3) slabs is large enough to contain the larger inhibitor molecules and the Cu (100) surface has a higher activity compared to more stable Cu (111) surface. The results for azole derivatives, thiophene, pyridine, aniline derivatives, surface ions and inorganic inhibitor molecules are interpreted below, respectively.

Azole Derivatives

Azole derivatives are considered to be effective inhibitors for copper [125] and previous reports proposed that as the number of nitrogen atoms in the azole ring increases, the surface adsorption energy decreases [126]. Therefore, in this study, molecules such as imidazole and pyrazole (2 N-containing molecules) are studied instead of triazole, tetrazole or pentazole (3, 4, 5 N-containing molecules, respectively). Adsorption energies and optimized geometries of pyrazole and imidazole are given in Tables 4.26 and 4.27; in Figures 4.28 and 4.29. The configurations with the highest adsorption energies (34 kJ/mol and -6 kJ/mol) were named as 'Configuration number 1' and tested for their inhibition effects.

Thiophene

In addition to nitrogen, carbon and oxygen, heterocyclic compounds containing sulfur are also preferred as inhibitors. For this reason, as well as being a relatively small S-containing molecule, thiophene was studied as an inhibitor candidate.

Three different configurations of thiophene were studied. Configuration 1 distorts the surface quite a bit as can be seen in Figure 4.37. The adsorption energies of the second and third configurations are endothermic meaning that there is no tendency of the molecule to adsorb on the copper surface, which is supported by Malone et al. [127]. Therefore, in the next step, chlorine adsorption in the presence of thiophene was not studied.

Pyridine

In the review article published by Gece [73] and in the experimental study by Sassi et. al [128], pyridine was investigated as an effective corrosion inhibitor in chloride-containing environment due to its heterocyclic configuration. Contrary to the published results, no stable adsorption configuration of pyridine could be obtained in here. Therefore, its effect on chlorine adsorption in the next step was not studied.

Aniline Derivatives

Aniline derivatives are generally preferred as inhibitors for mild steel surfaces. It was included in this study to examine whether it works on the copper surfaces or not. Two different anisidine derivatives (p-anisidine and p-toluidine) are studied. However, they do

not tend to be adsorbed on the copper surface. For this reason, chlorine adsorption in the presence of these molecules on the surface has not been studied.

Surface Ions

Atomic and molecular adsorption of surface ions on copper surface have been the subject of several studies [115,129–131] but studies involving the adsorption of those atoms/molecules with chlorine are a few in number [118]. The positions of the ions and atoms have been selected regarding the previously-published positions resulting in the highest adsorption energies [120–122,132,133]. 4-fold is the most stable attachment position for H and O on the Cu (100) surface while 2-fold position was the most stable one for CO and OH on Cu (100) surface. Thus, ions and molecules were bonded in 4-fold and 2-fold positions in the initial geometries. A good agreement with the previously reported results was observed for O, CO, H and OH in terms of adsorption energy [119–122], all values being exothermic except for the methoxy.

Inorganic Molecules

In order to investigate the inhibition effect of inorganic inhibitors, chromic acid and ammonia were studied on a clean Cu (100) surface. Chromic acid can be an inhibitor candidate due to its ability to passivate metals by forming an oxide film on the surface. However, it is also known to accelerate the cathodic reaction. Ammonia, on the other hand, can interact with copper to form Cu-HN_3 complexes. Although the possibility of NH_3 corroding the copper surface is more than Cu-Cl complexes, it can prevent the formation of Cu-Cl complexes at a low rate in neutral and slightly alkaline solutions. While both chromic acid and ammonia can corrode copper at high concentrations, low concentrations are examined in terms of Cu-Cl adsorption reduction. The adsorption energy of deprotonated chromic acid on clean Cu (100) surface were calculated as -20 kJ/mol while adsorption energy of ammonia was calculated as +2 kJ/mol.

4.6.5. Chlorine and Inhibitor Co-adsorption

By keeping the optimum geometries of the inhibitors on the clean copper surface constant, the adsorption energies of the chlorine at different positions are calculated in the presence of the inhibitor on the surface. Table 4.43 presents the adsorption energy of chlorine in the

absence and presence of the azole derivatives, surface ions and inorganic inhibitor molecules on the surface.

Cl on Cu (100) in the Presence of Azole Derivatives

Chlorine adsorption was studied in the presence of pyrazole and imidazole on the surface (configuration 1) and it is observed that the adsorption energies decreased slightly in the 4-fold and 2-fold positions while it increased in the 1-fold position as shown in Table 4.43. A 4-fold attachment (initial geometry) did not occur in both pyrazole and imidazole and the geometry were retained in the 2-fold position.

Although imidazole or pyrazole do not appear to be a suitable inhibitor for other metal surfaces due to their low surface activity, high solubility in water, and apparently insufficient reactivity of heteroatoms; their complexes with copper can delay corrosion. The copper-imidazole or copper-pyrazole complex is expected to slow down the cathodic reaction in copper corrosion. In aggressive environments, such as in the presence of Cl^- ions in the environment, inhibitor molecules may exhibit different behavior. This study aimed to reduce corrosion attack (i.e. weaker Cl adsorption) by providing surface adsorption with imidazole and pyrazole. But some of the inhibitors have tendencies to protect the surface by forming a protective film layer. As it is clear from the calculations, it seems necessary to provide a film formation on the surface to reduce corrosion by using pyrazole and imidazole [85].

Although the film formation seems to be effective, it has many disadvantages as well. For example, the film coating of the inside of the heat exchanger pipe reduces the effectiveness and increases the cost in terms of material and labor. If it was possible to reduce the corrosion significantly by adsorption using imidazole or pyrazole, the molecules could be injected into the pipe with water, ensuring adhesion to the metal surface and preventing corrosion in chlorine-containing environments.

Cl on Cu (100) in the Presence of Surface Ions

Our calculations show that the presence of surface ions/molecules increases the strength of chlorine adsorption on the Cu (100) surface meaning that H, O, OH, CO and OCH_3 allow chlorine to adhere to the copper surface much better and do not act as inhibitors but promoters.

Cl on Cu (100) in the Presence of Inorganic Inhibitors

Chlorine adsorption on the surface with ammonia had higher adsorption energy compared to the results without ammonia, contrary to the expectations. On the other hand, chromic acid reduced the adsorption energies by about 15 kJ/mol at the 4-fold and bridge positions but it is not suitable for industrial use at all due to its toxicity.

Table 4.43. Comparison of the inhibition effect of the aforementioned inhibitors on p(3x3) Cu (100) surface

	(4-fold) kJ/mol	(2-fold) kJ/mol	(1-fold) kJ/mol
No inhibitor	-147	-142	-107
Pyrazole	-131	-128	-154
Imidazole	-137	-125	-153
H	-182	-187	-147
O	-181	-184	-146
OH	-192	-180	-179
CO	-187	-180	-145
OCH_3	-186	-184	-188

Table 4.43. Comparison of the inhibition effect of the aforementioned inhibitors on p(3x3) Cu (100) surface (Continued)

	(4-fold) kJ/mol	(2-fold) kJ/mol	(1-fold) kJ/mol
No inhibitor	-147	-142	-107
NH_3	-178	-195	-195
H_2CrO_4	-134	-134	-161

Our calculations also revealed that Cl always behaved as an electron acceptor in the presence of inhibitor molecules which strengthens the adsorption of Cl. The solution to this challenge may be to use an inhibitor with higher electron affinity (for example, fluorine) but since fluorine has a greater adsorption energy than chlorine (due to its higher electrophilic character) such an arrangement will produce fluorine corrosion.

5. CONCLUSIONS

In this study, the adsorption of Cl on Cu (100), Cu (110) and Cu (111) at varying coverage and adsorption positions were studied in detail through comprehensive DFT computations. Furthermore, inhibitor adsorption on the p(3x3) Cu (100) surface and the inhibition effect of these inhibitors were studied. All the conclusions reached at the end of the study are presented below:

- For the Cu (111) surface, the most stable Cl adsorption position was observed to be 3-fold fcc and 3-fold hcp. The least stable Cl adsorption occurred for 1-fold (on-top) position.
- For the Cu (110) surface, the most stable Cl adsorption position was observed as 2-fold short bridge while the least stable adsorption position was 1-fold (on-top) site.
- For the Cl adsorption on Cu (100) surface, the 4-fold position was the most stable whereas 1-fold (on-top) was the least stable position.
- A linear-like dependency was observed between the adsorption energies and surface coverage for the Cu (111) and Cu (100) surfaces.
- The saturation coverage lies between 0.50 ML and 0.75 ML for Cu (111) and Cu (100) surfaces. Adsorption becomes endothermic after that coverage. All calculated values were negative for Cu (110) surface.
- Vibrations and work functions were found to be coverage dependent. The maximum vibration values are observed at 0.75 ML coverage on Cu (100), Cu (110) and Cu (111) surfaces. The maximum work function values are calculated as 0.281 eV, 0.044 eV, 0.088 eV, respectively for Cu (100), Cu (110) and Cu (111); while the minimum work function values are -0.558 eV, -0.229 eV and-1.031 eV, respectively.
- Our results showed that Cl is always the electron acceptor in the presence of inhibitor molecules, making Cl adsorption stronger in the presence of inhibitors. The solution to this problem may be using an agent with higher electronegativity (for example Fluorine) as the inhibitor molecule. However, such an arrangement would cause fluorine corrosion, the fluorine adsorption energy being higher than that of the chlorine.

6. FUTURE WORK

As the continuum of this work, the following studies can be carried out.

- Temperature and entropy effects can be studied using ab-initio thermodynamics, and stability or phase diagrams can be constructed.
- Chlorine adsorption can be studied on an oxide layer on the copper surface to observe the inhibition effect.
- Different halogen-metal surfaces can be studied to create a more detailed data base.

REFERENCES

1. Tan B, Zhang S, Qiang Y, Li W, Li H, Feng L, et al. Experimental and theoretical studies on the inhibition properties of three diphenyl disulfide derivatives on copper corrosion in acid medium. J Mol Liq [Internet]. 2020;298(xxxx):111975. Available from: https://doi.org/10.1016/j.molliq.2019.111975
2. Peljhan S, Kokalj A. Adsorption of chlorine on Cu(111): A density-functional theory study. J Phys Chem C. 2009;113(32):14363–76.
3. Benefits of Copper: health, environment, sustainability and recyclability [Internet]. [cited 2020 Nov 6]. Available from: https://copperalliance.org.uk/benefits-copper/
4. THE IMPORTANCE OF RECYCLING. 2017 [cited 2021 Nov 10]; Available from: http://pubs.acs.org/doi/abs/10.1021/es400069b
5. Copper - Element information, properties and uses | Periodic Table [Internet]. [cited 2020 Nov 6]. Available from: https://www.rsc.org/periodic-table/element/29/copper
6. Buckyballs turn on copper's magnetism | Science News [Internet]. [cited 2021 Nov 23]. Available from: https://www.sciencenews.org/article/buckyballs-turn-coppers-magnetism
7. Copper Facts - 30 interesting facts about copper, brasses and bronzes [Internet]. [cited 2020 Nov 6]. Available from: https://copperalliance.org.uk/about-copper/copper-facts/
8. McCafferty E. Introduction to Corrosion Science. Springer Science & Business Media; 2010.
9. Cwalina B. Biodeterioration of concrete, brick and other mineral-based building materials [Internet]. Understanding Biocorrosion: Fundamentals and Applications.

Woodhead Publishing Limited; 2014. 281–312 p. Available from: http://dx.doi.org/10.1533/9781782421252.3.281

10. Hansson CM. The impact of corrosion on society. Metall Mater Trans A Phys Metall Mater Sci. 2011;42(10):2952–62.

11. Núñez L, Reguera E, Corvo F, González E, Vazquez C. Corrosion of copper in seawater and its aerosols in a tropical island. Corros Sci. 2005;47(2):461–84.

12. Yabuki A, Murakami M. Critical ion concentration for pitting and general corrosion of copper. Corrosion. 2007;63(3):249–57.

13. Burstein GT, Liu C, Souto RM, Vines SP. Origins of pitting corrosion. Corros Eng Sci Technol. 2004;39(1):25–30.

14. Alonso Frank M. Functionalization of Steels and other Metallic Materials with Hydrophobic Layers - Influence on Wetting and Corrosion Resistance. 2017;(January 2017):326–33. Available from: http://dx.doi.org/10.1016/j.apsusc.2017.01.199

15. Metal Corrosion - Industrial Metallurgists [Internet]. [cited 2020 Nov 27]. Available from: https://www.imetllc.com/training-article/metal-corrosion/

16. A Review of Current Knowledge CAUSES OF COPPER CORROSION IN PLUMBING SYSTEMS FR/R0007 [Internet]. 2017 [cited 2020 Nov 26]. Available from: www.fwr.org

17. Di Benedetti M, Loreto G, Matta F, Nanni A. Acoustic Emission Monitoring of Reinforced Concrete under Accelerated Corrosion. J Mater Civ Eng. 2013;25(8):1022–9.

18. Prifiharni S, Nuraini L, Priyotomo G, Sundjono, Gunawan H, Purawiardi I. Corrosion performance of steel and galvanized steel in Karangsong and Limbangan sea water

environment. AIP Conf Proc. 2018;1964:0–6.

19. Farro NW, Veleva L, Aguilar P. Copper Marine Corrosion: I. Corrosion Rates in Atmospheric and Seawater Environments of Peruvian Port. Open Corros J. 2009;2(1):130–8.

20. Metikoš-Huković M, Babić R. Some aspects in designing passive alloys with an enhanced corrosion resistance. Corros Sci. 2009;51(1):70–5.

21. Khaled KF. Guanidine derivative as a new corrosion inhibitor for copper in 3% NaCl solution. Mater Chem Phys. 2008;112(1):104–11.

22. Zhang DQ, Cai QR, He XM, Gao LX, Zhou GD. Inhibition effect of some amino acids on copper corrosion in HCl solution. Mater Chem Phys. 2008;112(2):353–8.

23. Marcus P. Surface science approach of corrosion phenomena. Electrochim Acta. 1998;43(1–2):109–18.

24. Yeow CW, Hibbert DB. Galvanostatic Pulse Plating of Copper and Copper (I) Halides from Acid Copper (II) Halide Solutions. J Electrochem Soc. 1983;130(4):786–90.

25. Wang C, Chen S, Zhao S. Inhibition Effect of AC-Treated, Mixed Self-Assembled Film of Phenylthiourea and 1-Dodecanethiol on Copper Corrosion. J Electrochem Soc. 2004;151(1):B11.

26. Sherif EM, Park S-M. Inhibition of Copper Corrosion in 3.0% NaCl Solution by N-Phenyl-1,4-phenylenediamine. J Electrochem Soc. 2005;152(10):B428.

27. Bellakhal N, Dachraoui M. Study of the benzotriazole efficiency as a corrosion inhibitor for copper in humid air plasma. Mater Chem Phys. 2004;85(2–3):366–9.

28. King F, Ahonen L, Taxén C, Vuorinen U, Werme L. Copper Corrosion under Expected Conditions in a Deep Geological Repository. Vols. 2002–01, Posiva Report.

2001. 171 p.

29. Christodoulou C, Glass G, Webb J, Austin S, Goodier C. Assessing the long term benefits of Impressed Current Cathodic Protection. Corros Sci [Internet]. 2010;52(8):2671–9. Available from: http://dx.doi.org/10.1016/j.corsci.2010.04.018

30. De Damborenea J, Conde A, Arenas MA. Corrosion inhibition with rare earth metal compounds in aqueous solutions [Internet]. Vol. 1907, Rare Earth-Based Corrosion Inhibitors. Woodhead Publishing Limited; 2014. 84–116 p. Available from: http://dx.doi.org/10.1533/9780857093585.84

31. Gurudatt DM, Mohana KN, Tandon HC. Adsorption and corrosion inhibition characteristics of some organic molecules containing methoxy phenyl moiety on mild steel in hydrochloric acid solution. Mater Discov. 2015;2:24–43.

32. Callister, William D.;Rethwisch DG. Materials Science and Engineering : SI Version. 9th ed. Sayre D, editor. Wiley. 2014.

33. Galio AF, Dariva CG. Corrosion inhibitors: Principles, mechanisms and applications. In: Corrosion Inhibitors: Principles, Mechanisms and Applications [Internet]. Nova Science Publishers, Inc.; [cited 2020 Nov 18]. p. 365–79. Available from: http://dx.doi.org/10.5772/57255

34. Ramezanzadeh M, Bahlakeh G, Ramezanzadeh B. Elucidating detailed experimental and fundamental understandings concerning the green organic-inorganic corrosion inhibiting molecules onto steel in chloride solution. J Mol Liq [Internet]. 2019;290:111212. Available from: https://doi.org/10.1016/j.molliq.2019.111212

35. Al-Azawi KF, Al-Baghdadi SB, Mohamed AZ, Al-Amiery AA, Abed TK, Mohammed SA, et al. Synthesis, inhibition effects and quantum chemical studies of a novel coumarin derivative on the corrosion of mild steel in a hydrochloric acid

solution. Chem Cent J. 2016;10(1):3–11.

36. Obayes HR, Alwan GH, Alobaidy AHMJ, Al-Amiery AA, Kadhum AAH, Mohamad AB. Quantum chemical assessment of benzimidazole derivatives as corrosion inhibitors. Chem Cent J. 2014;8(1):2–9.

37. Oura K, Lifshits VG, Saranin AA, Zotov AV, Katayama M. Surface Science An Introduction. 1st ed. Surface Science. Berlin: Springer Berlin Heidelberg; 2003.

38. Kiejna A. Work function of metals [Internet]. Encyclopedia of Interfacial Chemistry: Surface Science and Electrochemistry. Elsevier Inc.; 2018. 319–326 p. Available from: http://dx.doi.org/10.1016/B978-0-12-409547-2.11420-9

39. Vitos L, Ruban A V., Skriver HL, Kollár J. The surface energy of metals. Surf Sci. 1998;411(1–2):186–202.

40. Goddard PJ, Lambert RM. Adsorption-desorption properties and surface structural chemistry of chlorine on Cu(111) and Ag(111). Surf Sci. 1977;67(1):180–94.

41. Crapper MD, Jones RG, Riley CE, Sweene PJJ, Mc Conville CF, Woodruff DP. Complete adsorption site information for cl on cu(Lll) using x-ray absorption fine structure and photoelectron diffraction. Epl. 1986;2(11):857–61.

42. Woodruff DP, Seymour DL, McConville CF, Riley CE, Crapper MD, Prince NP, et al. Simple x-ray standing-wave technique and its application to the investigation of the Cu(111) (3 3) R30°-Cl structure. Phys Rev Lett. 1987;58(14):1460–2.

43. Kadodwala MF, Davis AA, Scragg G, Cowie BCC, Kerkar M, Woodruff DP, et al. Structural determination of the Cu(111) -(√3 × √3) R30°- Cl Br surface using the normal incidence X-ray standing wave method. Surf Sci. 1995;324(2–3):122–32.

44. Way WK, Pike AC, Rosencrance SW, Braun RM, Winograd, N. Coverage-dependent

Bond Length of Chlorine. Surf Interface Anal. 1996;24(June 1995):137–41.

45. Motai K, Hashizume T, Lu H, Jeon D, Sakurai T, Pickering HW. STM of the Cu(111)1 × 1 surface and its exposure to chlorine and sulfur. Appl Surf Sci. 1993;67(1–4):246–51.

46. Walter WK, Manolopoulos DE, Jones RG. Chlorine adsorption and diffusion on Cu(111). Surf Sci. 1996;348(1–2):115–32.

47. Andryushechkin B V., Zheltov V V., Cherkez V V., Zhidomirov GM, Klimov AN, Kierren B, et al. Chlorine adsorption on Cu(111) revisited: LT-STM and DFT study. Surf Sci [Internet]. 2015;639:7–12. Available from: http://dx.doi.org/10.1016/j.susc.2015.03.030

48. Vosta J, Eliásek J. Study on corrosion inhibition from aspect of quantum chemistry. Corros Sci. 1971;11(4):223–9.

49. Khaled KF. Studies of iron corrosion inhibition using chemical, electrochemical and computer simulation techniques. Electrochim Acta. 2010;55(22):6523–32.

50. Ser CT, Žuvela P, Wong MW. Prediction of corrosion inhibition efficiency of pyridines and quinolines on an iron surface using machine learning-powered quantitative structure-property relationships. Appl Surf Sci. 2020;512(October 2019).

51. Shokry H, Mabrouk EM. Computational and electrochemical investigation for corrosion inhibition of nickel in molar sulfuric acid by dihydrazide derivatives. Part II. Arab J Chem [Internet]. 2017;10:S3402–11. Available from: http://dx.doi.org/10.1016/j.arabjc.2014.01.023

52. Basharnavaz H, Habibi-Yangjeh A, Kamali SH. A first-principles study on the interaction of CO molecules with VIII transition metals-embedded graphitic carbon

nitride as an excellent candidate for CO sensor. Phys Lett Sect A Gen At Solid State Phys [Internet]. 2019;383(21):2472–80. Available from: https://doi.org/10.1016/j.physleta.2019.05.013

53. Saraireh SA, Altarawneh M. Thermodynamic stability and structures of iron chloride surfaces: A first-principles investigation. J Chem Phys. 2014;141(5).

54. Finšgar M, Lesar A, Kokalj A, Milošev I. A comparative electrochemical and quantum chemical calculation study of BTAH and BTAOH as copper corrosion inhibitors in near neutral chloride solution. Electrochim Acta. 2008;53(28):8287–97.

55. Kokalj A, Peljhan S. Density functional theory study of ATA, BTAH, and BTAOH as copper corrosion inhibitors: Adsorption onto Cu(111) from gas phase. Langmuir. 2010;26(18):14582–93.

56. Kovačević N, Milošev I, Kokalj A. The roles of mercapto, benzene, and methyl groups in the corrosion inhibition of imidazoles on copper: II. Inhibitor-copper bonding. Corros Sci. 2015;98:457–70.

57. Wang W, Li Z, Sun Q, Du A, Li Y, Wang J, et al. Insights into the nature of the coupling interactions between uracil corrosion inhibitors and copper: A DFT and molecular dynamics study. Corros Sci [Internet]. 2012;61:101–10. Available from: http://dx.doi.org/10.1016/j.corsci.2012.04.025

58. Kovačević N, Kokalj A. Chemistry of the interaction between azole type corrosion inhibitor molecules and metal surfaces. Mater Chem Phys. 2012;137(1):331–9.

59. Kovačević N, Kokalj A. The relation between adsorption bonding and corrosion inhibition of azole molecules on copper. Corros Sci [Internet]. 2013;73(March):7–17. Available from: http://dx.doi.org/10.1016/j.corsci.2013.03.016

60. Doll K, Harrison NM. Chlorine adsorption on the Cu(111) surface. Chem Phys Lett. 2000;317(3–5):282–9.

61. Migani A, Sousa C, Illas F. Chemisorption of atomic chlorine on metal surfaces and the interpretation of the induced work function changes. Surf Sci. 2005;574(2–3):297–305.

62. Migani A, Illas F. A systematic study of the structure and bonding of halogens on low-index transition metal surfaces. J Phys Chem B. 2006;110(24):11894–906.

63. Roman T, Groß A. Periodic density-functional calculations on work-function change induced by adsorption of halogens on Cu(111). Phys Rev Lett. 2013;110(15):1–4.

64. Pavlova T V., Andryushechkin B V., Zhidomirov GM. First-Principle Study of Adsorption and Desorption of Chlorine on Cu(111) Surface: Does Chlorine or Copper Chloride Desorb? J Phys Chem C. 2016;120(5):2829–36.

65. Suleiman IA, Radny MW, Gladys MJ, Smith P V., MacKie JC, Kennedy EM, et al. Chlorination of the Cu(110) surface and copper nanoparticles: A density functional theory study. J Phys Chem C. 2011;115(27):13412–9.

66. Muster TH, Trinchi A, Markley TA, Lau D, Martin P, Bradbury A, et al. A review of high throughput and combinatorial electrochemistry. Electrochim Acta [Internet]. 2011;56(27):9679–99. Available from: http://dx.doi.org/10.1016/j.electacta.2011.09.003

67. White PA, Smith GB, Harvey TG, Corrigan PA, Glenn MA, Lau D, et al. A new high-throughput method for corrosion testing. Corros Sci [Internet]. 2012;58:327–31. Available from: http://dx.doi.org/10.1016/j.corsci.2012.01.016

68. Chambers BD, Taylor SR, Kendig MW. Rapid discovery of corrosion inhibitors and

synergistic combinations using high-throughput screening methods. Corrosion. 2005;61(5):480–9.

69. Lamaka S V., Vaghefinazari B, Mei D, Petrauskas RP, Höche D, Zheludkevich ML. Comprehensive screening of Mg corrosion inhibitors. Corros Sci [Internet]. 2017;128:224–40. Available from: http://dx.doi.org/10.1016/j.corsci.2017.07.011

70. Winkler DA, Breedon M, Hughes AE, Burden FR, Barnard AS, Harvey TG, et al. Towards chromate-free corrosion inhibitors: Structure-property models for organic alternatives. Green Chem. 2014;16(6):3349–57.

71. Würger T, Feiler C, Musil F, Feldbauer GBV, Höche D, Lamaka S V., et al. Data science based mg corrosion engineering. Front Mater. 2019;6(April):1–9.

72. Cole IS, Hughes AE. Designing molecular protection: New paradigm for developing corrosion resistant materials uniting high throughput studies, multiscale modelling and self-repair. Corros Eng Sci Technol. 2014;49(2):109–15.

73. Gece G. The use of quantum chemical methods in corrosion inhibitor studies. Corros Sci [Internet]. 2008;50(11):2981–92. Available from: http://dx.doi.org/10.1016/j.corsci.2008.08.043

74. Ke H, Taylor CD. Density functional theory: An essential partner in the integrated computational materials engineering approach to corrosion. Corrosion. 2019;75(7):708–26.

75. Peljhan S, Kokalj A. DFT study of gas-phase adsorption of benzotriazole on Cu(111), Cu(100), Cu(110), and low coordinated defects thereon. Phys Chem Chem Phys. 2011;13(45):20408–17.

76. Kokalj A, Gustinčič D, Poberžnik M, Lozinšek M. New insights into adsorption

bonding of imidazole: A viable C2–H bond cleavage on copper surfaces. Appl Surf Sci [Internet]. 2019;479:463–8. Available from: https://doi.org/10.1016/j.apsusc.2018.12.246

77. Winkler DA, Breedon M, White P, Hughes AE, Sapper ED, Cole I. Using high throughput experimental data and in silico models to discover alternatives to toxic chromate corrosion inhibitors. Corros Sci [Internet]. 2016;106:229–35. Available from: http://dx.doi.org/10.1016/j.corsci.2016.02.008

78. Feiler C, Mei D, Vaghefinazari B, Würger T, Meißner RH, Luthringer-Feyerabend BJC, et al. In silico screening of modulators of magnesium dissolution. Corros Sci. 2020;163.

79. Galvão TLP, Novell-Leruth G, Kuznetsova A, Tedim J, Gomes JRB. Elucidating Structure-Property Relationships in Aluminum Alloy Corrosion Inhibitors by Machine Learning. J Phys Chem C. 2020;124(10):5624–35.

80. Li L, Zhang X, Gong S, Zhao H, Bai Y, Li Q, et al. The discussion of descriptors for the QSAR model and molecular dynamics simulation of benzimidazole derivatives as corrosion inhibitors. Corros Sci. 2015;99:76–88.

81. Keshavarz MH, Esmaeilpour K, Golikand AN, Shirazi Z. Simple Approach to Predict Corrosion Inhibition Efficiency of Imidazole and Benzimidazole Derivatives as well as Linear Organic Compounds Containing Several Polar Functional Groups. Zeitschrift fur Anorg und Allg Chemie. 2016;642(16):906–13.

82. Al-Fakih AM, Algamal ZY, Lee MH, Abdallah HH, Maarof H, Aziz M. Quantitative structure–activity relationship model for prediction study of corrosion inhibition efficiency using two-stage sparse multiple linear regression. J Chemom. 2016;30(7):361–8.

83. Winkler DA. Predicting the performance of organic corrosion inhibitors. Metals (Basel). 2017;7(12):1–8.

84. Antonijevic MM, Petrovic MB. Copper corrosion inhibitors. A review. Int J Electrochem Sci. 2008;3(1):1–28.

85. Antonijević MM, Milić SM, Petrović MB. Films formed on copper surface in chloride media in the presence of azoles. Corros Sci. 2009;51(6):1228–37.

86. Kuznetsov YI, Kazansky LP. Physicochemical aspects of metal protection by azoles as corrosion inhibitors. Russ Chem Rev. 2008;77(3):219–32.

87. Petrović Mihajlović MB, Antonijević MM. Copper corrosion inhibitors. Period 2008-2014. A review. Int J Electrochem Sci. 2015;10(2):1027–53.

88. Finšgar M, Milošev I. Corrosion study of copper in the presence of benzotriazole and its hydroxy derivative. Mater Corros. 2011;62(10):956–66.

89. Grillo F, Tee DW, Francis SM, Früchtl H, Richardson N V. Initial stages of benzotriazole adsorption on the Cu(111) surface. Nanoscale. 2013;5(12):5269–73.

90. Awad MK, Mustafa MR, Elnga MMA. Computational simulation of the molecular structure of some triazoles as inhibitors for the corrosion of metal surface. J Mol Struct THEOCHEM [Internet]. 2010;959(1–3):66–74. Available from: http://dx.doi.org/10.1016/j.theochem.2010.08.008

91. Obot IB, Gasem ZM, Umoren SA. Understanding the mechanism of 2-mercaptobenzimidazole adsorption on Fe (110), Cu (111) and Al (111) surfaces: DFT and molecular dynamics simulations approaches. Int J Electrochem Sci. 2014;9(5):2367–78.

92. Kokalj A. Is the analysis of molecular electronic structure of corrosion inhibitors

sufficient to predict the trend of their inhibition performance. Electrochim Acta [Internet]. 2010;56(2):745–55. Available from: http://dx.doi.org/10.1016/j.electacta.2010.09.065

93. Laird BB, Ross RB, Ziegler T. Density-Functional Methods in Chemistry : An Overview Density-functional theory (DFT), in its various forms , has become an important research tool for chemists , physicists and materials scientists . Its development in recent years has proceeded along . 1996;1–17.

94. Sholl DS, Steckel JA. Density Functional Theory : A Practical Introduction. Electrocatalysis: Computational, Experimental, and Industrial Aspects. Wiley; 2009. 1–256 p.

95. Morin, J; Pelletier JM. DENSITY FUNCTIONAL THEORY: Principles, Applications and Analysis. Morin, J; Pelletier JM, editor. USA: Nova Science; 2013. 1–322 p.

96. Fermi E. Eine statistische Methode zur Bestimmung einiger Eigenschaften des Atoms und ihre Anwendung auf die Theorie des periodischen Systems der Elemente. Zeitschrift für Phys. 1928;48(1–2):73–9.

97. Thomas LH. The calculation of atomic fields. Math Proc Cambridge Philos Soc. 1927;23(5):542–8.

98. Wesolowski TA. Part III : Kohn-Sham DFT Kohn-Sham Equation. 2016;

99. Lundqvist S, March NH, editors. Theory of the Inhomogeneous Electron. Springer US; 1983.

100. Roy AK. Theoretical and Computational Developments in Modern Density Functional Theory [Internet]. Roy AK, editor. Nova Publishers. USA; 2012. 1–598 p.

Available from: https://ejournal.poltektegal.ac.id/index.php/siklus/article/view/298%0Ahttp://repositorio.unan.edu.ni/2986/1/5624.pdf%0Ahttp://dx.doi.org/10.1016/j.jana.2015.10.005%0Ahttp://www.biomedcentral.com/1471-2458/12/58%0Ahttp://ovidsp.ovid.com/ovidweb.cgi?T=JS&P

101. Kohn W, Sham LJ. Self-Consistent Equations Including Exchange and Correlation Effects. Phys Rev [Internet]. 1965 Nov 15;140(4A):A1133–8. Available from: https://link.aps.org/doi/10.1103/PhysRev.140.A1133

102. Perdew JP, Burke K, Ernzerhof M. Generalized gradient approximation made simple. Phys Rev Lett. 1996;77(18):3865–8.

103. Becke AD. A new mixing of Hartree-Fock and local density-functional theories. J Chem Phys. 1993;98(2):1372–7.

104. Giannozzi P, Baroni S, Bonini N, Calandra M, Car R, Cavazzoni C, et al. QUANTUM ESPRESSO: A modular and open-source software project for quantum simulations of materials. J Phys Condens Matter. 2009;21(39).

105. Kokalj A. XCrySDen-a new program for displaying crystalline structures and electron densities. J Mol Graph Model. 1999;17(3–4):176–9.

106. Reveles JU, Köster AM. Geometry optimization in density functional methods. J Comput Chem. 2004;25(9):1109–16.

107. Ul-Haq Z. Introduction to Geometry Optimization.

108. pw.x: input description [Internet]. [cited 2021 Dec 7]. Available from: https://www.quantum-espresso.org/Doc/INPUT_PW.html

109. Broglia RA, Colò G, Onida G, Roman HE. Solid State Physics of Finite Systems

[Internet]. Berlin, Heidelberg: Springer Berlin Heidelberg; 2004. (Advanced Texts in Physics). Available from: http://link.springer.com/10.1007/978-3-662-09938-4

110. Czarnacki M, Hałas S. Isotope fractionation in aqua-gas systems: Cl 2-HCl-Cl -, Br 2-HBr-Br - and H 2S-S 2-. Isotopes Environ Health Stud. 2012;48(1):55–64.

111. Arnaldson A, Tang W, Chill W, Anselm R, Henkelman G. Code: Bader Charge Analysis [Internet]. 2020 [cited 2021 Nov 16]. Available from: http://theory.cm.utexas.edu/henkelman/code/bader/

112. Solyom J. Fundamentals of the Physics of Solids. 1st ed. Media. Springer; 2007. 706 p.

113. Chen S, Duan YH, Huang B, Hu WC. Structural properties, phase stability, elastic properties and electronic structures of Cu-Ti intermetallics. Philos Mag. 2015;95(32):3535–53.

114. WILLIAM D. CALLISTER J, DAVID G. RETHWISCH. Fundamentals Materials science and Engineering : An Integrated Approach [Internet]. 5th ed. Fundamentals of Materials Science and Engineering AN INTEGRATED APPROACH. Wiley; 2015. 1–964 p. Available from: 9781119230403

115. ÖZBEK MO. Theoretical Investigation Of Coverage Effects Of CO Adsorption On Cu(100) Surface. Sak Univ J Sci [Internet]. 2021 Jan 18;25(1):200–11. Available from: https://dergipark.org.tr/en/doi/10.16984/saufenbilder.795798

116. ZHENG J-C, WANG H-Q, WEE ATS, HUAN CHA. RELAXATION OF Cu (100), (110) AND (111) SURFACES USING AB INITIO PSEUDOPOTENTIALS . Surf Rev Lett. 2001;08(05):541–7.

117. Ning T, Yu Q, Ye Y. Multilayer relaxation at the surface of fcc metals: Cu, Ag, Au,

Ni, Pd, Pt, Al. Surf Sci. 1988;206(1–2).

118. Suleiman IA, Radny MW, Gladys MJ, Smith P V., MacKie JC, Kennedy EM, et al. Interaction of chlorine and oxygen with the Cu(100) surface. J Phys Chem C. 2010;114(44):19048–54.

119. Gómez E del V., Amaya-Roncancio S, Avalle LB, Gimenez MC. DFT Study of adsorption and diffusion of H2O and related species on Cu(100) surfaces. Surf Sci. 2021;714(August).

120. Alatalo M, Jaatinen S, Salo P, Laasonen K. Oxygen adsorption on Cu(100): First-principles pseudopotential calculations. Phys Rev B - Condens Matter Mater Phys. 2004;70(24):1–6.

121. Gameel KM, Sharafeldin IM, Abourayya AU, Biby AH, Allam NK. Unveiling CO adsorption on Cu surfaces: New insights from molecular orbital principles. Phys Chem Chem Phys. 2018;20(40):25892–900.

122. Ferrin P, Kandoi S, Nilekar AU, Mavrikakis M. Hydrogen adsorption, absorption and diffusion on and in transition metal surfaces: A DFT study. Surf Sci [Internet]. 2012;606(7–8):679–89. Available from: http://dx.doi.org/10.1016/j.susc.2011.12.017

123. Gajdoš M, Hafner J. CO adsorption on Cu(1 1 1) and Cu(0 0 1) surfaces: Improving site preference in DFT calculations. Surf Sci. 2005;590(2–3):117–26.

124. Derry GN, Kern ME, Worth EH. Recommended values of clean metal surface work functions. J Vac Sci Technol A Vacuum, Surfaces, Film [Internet]. 2015;33(6):060801. Available from: http://dx.doi.org/10.1116/1.4934685

125. Fateh A, Aliofkhazraei M, Rezvanian AR. Review of corrosive environments for

copper and its corrosion inhibitors. Arab J Chem [Internet]. 2020;13(1):481–544. Available from: http://dx.doi.org/10.1016/j.arabjc.2017.05.021

126. Kovačević N, Kokalj A. DFT study of interaction of azoles with Cu(111) and Al(111) surfaces: Role of azole nitrogen atoms and dipole-dipole interactions. J Phys Chem C. 2011;115(49):24189–97.

127. Malone W, Yildirim H, Matos J, Kara A. A van der Waals Inclusive Density Functional Theory Study of the Nature of Bonding for Thiophene Adsorption on Ni(100) and Cu(100) Surfaces. J Phys Chem C. 2017;121(11):6090–103.

128. Sassi W, Msaadi R, Hihn JY, Zrelli R. Effect of pyridine as advanced polymeric inhibitor for pure copper: adsorption and corrosion mechanisms. Polym Bull [Internet]. 2021;78(8):4261–80. Available from: https://doi.org/10.1007/s00289-020-03311-3

129. Liem SY, Clarke JHR, Kresse G. CMS 17 (2000) Dissociation pathways of oxygen on copper (…110)† surface.pdf. 2000;17:133–40.

130. Diao ZY, Han LL, Wang ZX, Dong CC. The adsorption and dissociation of O2 on Cu low-index surfaces. J Phys Chem B. 2005;109(12):5739–45.

131. Xu L, Lin J, Bai Y, Mavrikakis M. Atomic and Molecular Adsorption on Cu(111). Top Catal [Internet]. 2018;61(9–11):736–50. Available from: http://dx.doi.org/10.1007/s11244-018-0943-0

132. Wang ZX, Tian FH. The adsorption of O atom on Cu (100), (110), and (111) low-index and step defect surfaces. J Phys Chem B. 2003;107(25):6153–61.

133. Pang XY, Xue LQ, Wang GC. Adsorption of atoms on Cu surfaces: A density functional theory study. Langmuir. 2007;23(9):4910–7.

APPENDIX A: EXAMPLE OF INPUT-OUTPUT FILES

Table A.1. pw.x input file (p(2x2) Cu (100) 0.25 ML)

```
&CONTROL
calculation             = 'relax' ,
!restart_mode           = 'restart' ,
outdir                  = './temp' ,
pseudo_dir              = './' ,
prefix                  = 'cu100cl',
tefield                 = .TRUE.,
dipfield                = .TRUE.,
/
&SYSTEM
edir                    = 3,
ibrav                   = 0,
nat                     = 21,
ntyp                    = 2,
ecutwfc                 = 45 ,
ecutrho                 = 250 ,
occupations             = 'smearing' ,
degauss                 = 0.02 ,
smearing                = 'gaussian' ,
/
&ELECTRONS
adaptive_thr = .true. ,
!               mixing_mode = 'plain' ,
!           diagonalization = 'david' ,
!         diago_david_ndim = 8 ,
/
&IONS
!              ion_dynamics = 'bfgs' ,
!             ion_positions = 'from_input' ,
/
K_POINTS automatic
4 4 1   0 0 0
CELL_PARAMETERS angstrom
5.1519999504        0.0000000000        0.0000000000
0.0000000000        5.1519999504        0.0000000000
0.0000000000        0.0000000000       22.2859992981
ATOMIC_SPECIES
Cu      63.54600        Cu.pbe-dn-kjpaw_psl.1.0.0.UPF
Cl      35.44600        Cl.pbe-n-kjpaw_psl.1.0.0.UPF
ATOMIC_POSITIONS angstrom
Cu      0.000000000   0.000000000   0.000000000    0   0   0
Cu      0.000000000   2.603284326   0.000000000    0   0   0
Cu      2.603284326   0.000000000   0.000000000    0   0   0
```

Table A.1. pw.x input file (p(2x2) Cu (100) 0.25 ML) (Continued)

```
Cu      2.603284326  2.603284326  0.000000000  0  0  0
Cu      1.301642163  1.301642163  1.840800000  0  0  0
Cu      1.301642163  3.904926488  1.840800000  0  0  0
Cu      3.904926488  1.301642163  1.840800000  0  0  0
Cu      3.904926488  3.904926488  1.840800000  0  0  0
Cu      0.000000000  0.000000000  3.649944343  0  0  0
Cu      0.000000000  2.603284326  3.649948664  0  0  0
Cu      2.603284326  0.000000000  3.649948664  0  0  0
Cu      2.603284326  2.603284326  3.649949976  0  0  0
Cu      1.302141748  1.302290925  5.416497226
Cu      1.302060376  3.878247122  5.475310002
Cu      3.878038723  1.302242507  5.475040996
Cu      3.878045924  3.878262485  5.541926808
Cu      0.001254393  0.001393338  7.261003136
Cu      0.001330600  2.603065246  7.260975870
Cu      2.602578390  0.001498560  7.261030014
Cu      2.602534406  2.602992904  7.261014884
Cl      1.300458593  1.301320389  8.922277462
```

Table A.2. ph.x input file (p(2x2) Cu (100) 0.25 ML)

```
Cu_Cl
&INPUTPH
!recover        = .true. ,

outdir          = './temp' ,
fildyn          = 'dyn.mat' ,
trans           = .true.,
!lraman         = .true. ,
!epsil          = .true.,
asr             = .true. ,
amass(1)        = 63.54600,
amass(2)        = 35.44600,
tr2_ph          = 1.0d-12 ,
alpha_mix(1)  = 0.7,
alpha_mix(2)  = 0.4,
alpha_mix(3)  = 0.1,

nat_todo        = 1,
prefix          = 'cu100cl' ,
 /
0.0 0.0 0.0
21
```

Table A.3. Post-process dynmat input file (p(2x2) Cu (100) 0.25 ML)

```
&input
fildyn = 'dyn.mat',
asr     = 'zero-dim',
!asr    = 'simple',
!asr    = 'crystal',
!q(3)  = 1,
/
```

Table A.4. Post-process potential input file (p(2x2) Cu (100) 0.25 ML)

```
&inputPP
prefix          = 'cu100cl',
outdir          = './temp',
plot_num        = 11
filplot         = 'potential.pot'
/

&plot
iflag           = 3,
output_format = 5,
/
```

Table A.5. Post-process average input file (p(2x2) Cu (100) 0.25 ML)

```
1
potential.pot
1.D0
2880
3
3.3
```

Table A.6. Post-process charge input file (p(2x2) Cu (100) 0.25 ML)

```
&inputpp
   prefix  = 'cu100cl'
   outdir = './temp'
   filplot = 'cube.dat'
! valace electron 17, core + val 21, LDOS 10
   plot_num= 21
/
&plot
   nfile = 1
   iflag = 3
!   output_format = 0, fileout = 'file.ldos'
!   output_format = 5, fileout = 'file.chg'
    output_format = 6, fileout = 'file.cube'
/
```

Table A.7. Bader charge ACF.dat output file (p(2x2) Cu (100) 0.25 ML)

#	X	Y	Z	CHARGE	MIN DIST	ATOMIC VOL
1	9.735869	9.735869	42.114435	720.420133	2.143000	343.479669
2	9.735869	4.919494	42.114435	32.381535	2.115338	346.488369
3	4.919494	9.735869	42.114435	32.381536	2.115338	346.584470
4	4.919494	4.919494	42.114435	28.514383	2.144240	346.510546
5	2.459747	2.459747	3.478608	27.387720	2.125883	82.439852
6	2.459747	7.379242	3.478608	27.989496	2.096224	81.597120
7	7.379242	2.459747	3.478608	27.989496	2.096224	81.597120
8	7.379242	7.379242	3.478608	36.727324	2.076506	80.702642
9	9.735869	9.735869	6.897395	28.489369	2.085927	80.983552
10	9.735869	4.919494	6.897403	27.673223	2.110486	81.434488
11	4.919494	9.735869	6.897403	27.673459	2.110486	81.441880
12	4.919494	4.919494	6.897406	27.427891	2.076413	81.841069
13	2.460545	2.460822	10.230344	27.297066	2.086022	81.515804
14	2.460534	7.328635	10.339837	27.463083	2.081112	80.813528
15	7.328287	2.460870	10.339860	27.462831	2.081155	80.806135
16	7.328135	7.328505	10.467464	27.300511	2.013030	79.638139
17	0.006926	0.007475	13.707742	29.997298	1.855163	121.981707
18	0.007146	4.914147	13.707770	28.162371	1.821647	121.168545
19	4.913590	0.007756	13.707790	28.180447	1.821057	121.567733
20	4.913422	4.913921	13.707857	27.576325	1.819490	118.869514
21	2.457877	2.459386	16.882063	16.255426	2.247846	1150.424771

VACUUM CHARGE: 0.0000
VACUUM VOLUME: 0.0000
NUMBER OF ELECTRONS: 1284.7509

Table A.8. Bader charge BCF.dat output file (p(2x2) Cu (100) 0.25 ML)

#	X	Y	Z	CHARGE	ATOM	DISTANCE
1	0.0000	0.0000	0.0000	720.4197	1	0.0001
2	7.3992	7.3992	3.5095	36.7273	8	0.0419
3	0.0000	0.0000	6.8241	28.4894	9	0.0733
4	0.0000	0.0000	13.6482	29.9973	17	0.0604
5	2.5313	2.5313	16.9627	16.2545	21	0.1307
6	7.3992	2.5313	3.5095	27.9895	7	0.0805
7	7.3992	2.5313	10.3336	27.4628	15	0.1002
8	2.5313	2.5313	10.1386	27.2971	13	0.1356
9	0.0000	4.8679	0.0000	32.3811	2	0.0516
10	0.0000	4.8679	6.8241	27.6732	10	0.0896
11	0.0000	4.8679	13.6482	28.1624	18	0.0758
12	7.3992	7.3992	10.5286	27.3005	16	0.1175
13	2.5313	7.3992	10.3336	27.4631	14	0.1002
14	2.5313	7.3992	3.5095	27.9895	6	0.0805
15	2.5313	2.5313	3.5095	27.3877	5	0.1058
16	4.8679	0.0000	0.0000	32.3811	3	0.0516
17	4.8679	4.8679	0.0000	28.5140	4	0.0729
18	4.8679	0.0000	6.8241	27.6735	11	0.0896
19	4.8679	0.0000	13.6482	28.1804	19	0.0755
20	4.8679	4.8679	6.8241	27.4279	12	0.1034
21	4.8679	4.8679	13.6482	27.5763	20	0.0880

Table A.9. Post-process projwfc input file (p(2x2) Cu (100) 0.25 ML)

```
&PROJWFC
prefix             = 'cu100cl',
outdir             = './temp' ,
degauss            = 0.02 ,
lwrite_overlaps    = .true.,
filpdos            = 'pdos.dat',
plotboxes          = .true.
/
```

APPENDIX B: SURFACE RELAXIATION

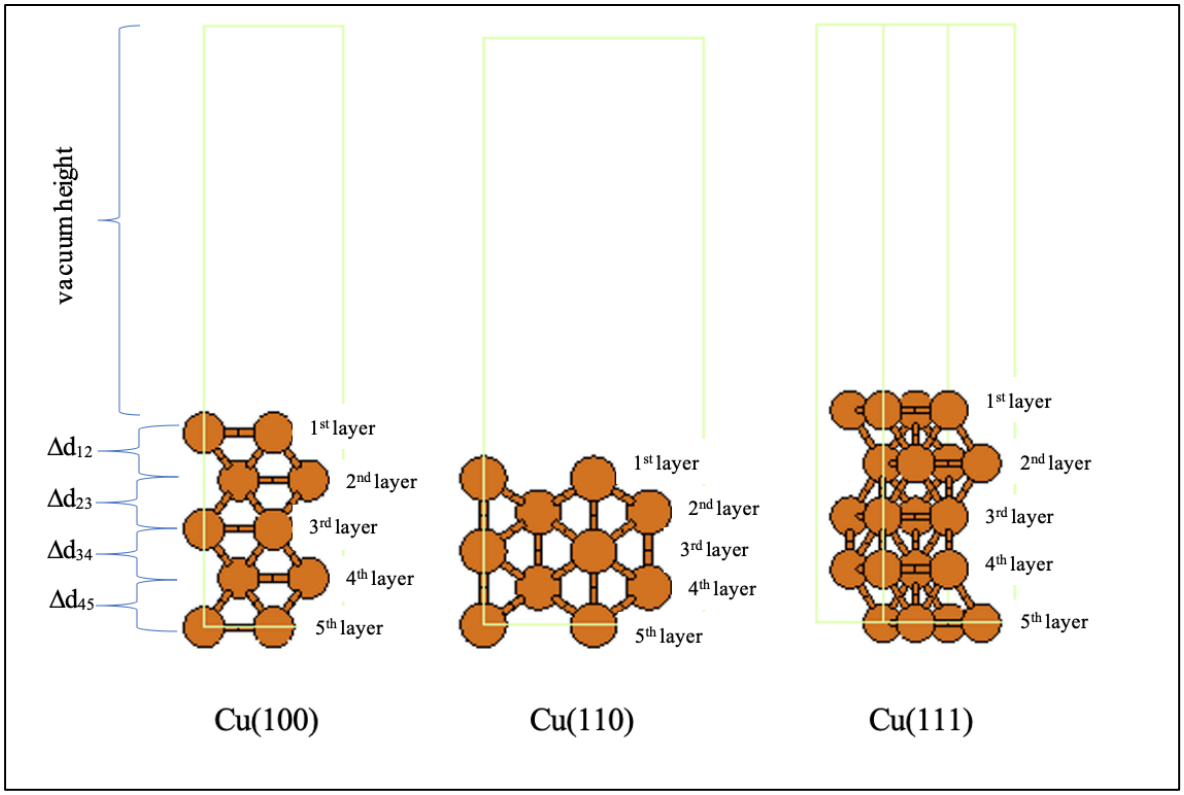

Figure B.1. Schematic representation of layers and distance between layers on studied metallic surfaces (Cu: orange)

APPENDIX C: BADER CHARGES

Table C.1. Bader charges of Cl at varying coverage and adsorption positions on Cu (111) surface

Coverage	Initial Geometry	σ_{Cl}	σ_{Cl}	σ_{Cl}
1 ML	2-fold	0.722	-	-
	3-fold (fcc)	0.858	-	-
	3-fold (hcp)	0.864	-	-
	1-fold	-15.850	-	-
0.75 ML	2-fold	NaN	NaN	NaN
	3-fold (fcc)	0.693	0.688	0.695
	3-fold (hcp)	0.679	0.684	0.674
	1-fold	-13.210	-13.247	-13.218
0.50 ML	2-fold	0.234	0.235	-
	3-fold (fcc)	0.339	-0.086	-
	3-fold (hcp)	-0.022	-0.120	-
	1-fold	0.078	0.075	-
0.33 ML	2-fold	0.755	0.755	0.586
	3-fold (fcc)	NaN	NaN	NaN
	3-fold (hcp)	NaN	NaN	NaN
	1-fold	0.017	0.202	0.002
0.25 ML	2-fold	NaN	-	-
	3-fold (fcc)	0.407	-	-
	3-fold (hcp)	-0.037	-	-
	1-fold	-4.367	-	-
0.22 ML	2-fold	NaN	NaN	-
	3-fold (fcc)	NaN	NaN	-
	3-fold (hcp)	NaN	NaN	-
	1-fold	-1.035	-1.048	-
0.11 ML	2-fold	NaN	-	-
	3-fold (fcc)	0.680	-	-
	3-fold (hcp)	0.602	-	-
	1-fold	-17.125	-	-
0.0625 ML	2-fold	NaN	-	-
	3-fold (fcc)	0.181	-	-
	3-fold (hcp)	0.120	-	-
	1-fold	-0.602	-	-

Table C.2. Bader charges of Cl at varying coverage and adsorption positions on Cu (110) surface

Coverage	Initial Geometry	σ_{Cl}	σ_{Cl}	σ_{Cl}
1 ML	4-fold	0.020	-	-
	2-fold (l-brg)	-15.966	-	-
	2-fold (s-brg)	-0.401	-	-
	1-fold	-5.070	-	-
0.75 ML	4-fold	0.803	0.075	0.783
	2-fold (l-brg)	-9.035	-0.235	-0.336
	2-fold (s-brg)	0.119	0.298	0.269
	1-fold	-4.496	-6.606	-5.291
0.50 ML	4-fold	NaN	NaN	-
	2-fold (l-brg)	-0.810	-0.133	-
	2-fold (s-brg)	0.048	-0.289	-
	1-fold	-0.287	-0.306	-
0.33 ML	4-fold	NaN	NaN	NaN
	2-fold (l-brg)	NaN	NaN	NaN
	2-fold (s-brg)	0.655	-8.957	0.395
	1-fold	NaN	NaN	NaN
0.25 ML	4-fold	-0.426	-	-
	2-fold (l-brg)	-21.630	-	-
	2-fold (s-brg)	0.609	-	-
	1-fold	-19.122	-	-
0.22 ML	4-fold	NaN	NaN	-
	2-fold (l-brg)-1	-0.263	-0.340	-
	2-fold (l-brg)-2	-0.268	-0.163	
	2-fold (s-brg)-1	0.443	0.447	-
	2-fold (s-brg)-2	0.449	0.449	
	1-fold	-4.657	-4.340	-
0.11 ML	4-fold	0.693	-	-
	2-fold (l-brg)	-1.327	-	-
	2-fold (s-brg)	0.330	-	-
	1-fold	-5.541	-	-
0.0625 ML	4-fold	0.505	-	-
	2-fold (l-brg)	-16.476	-	-
	2-fold (s-brg)	0.420	-	-
	1-fold	-1.487	-	-

Table C.3. Bader charges of Cl at varying coverage and adsorption positions on Cu (100) surface

Coverage	Initial Geometry	σ_{Cl}	σ_{Cl}	σ_{Cl}
1 ML	4-fold	-1.733	-	-
	2-fold	-3.297	-	-
	1-fold	0.060	-	-
0.75 ML	4-fold	0.570	0.922	0.948
	2-fold	-0.226	0.678	0.126
	1-fold	-6.001	-14.403	-6.001
0.50 ML	4-fold	0.488	0.571	-
	2-fold	0.484	0.404	-
	1-fold	-0.848	-0.014	-
0.33 ML	4-fold	-0.178	-0.293	-0.021
	2-fold	0.388	0.245	0.476
	1-fold	-3.754	-0.995	-0.988
0.25 ML	4-fold	0.745	-	-
	2-fold	-0.778	-	-
	1-fold	NaN	-	-
0.22 ML	4-fold-1	0.603	0.602	-
	4-fold-2	0.581	0.581	-
	2-fold	0.324	0.507	-
	1-fold	NaN	NaN	-
0.11 ML	4-fold	0.706	-	-
	2-fold	0.018	-	-
	1-fold	-2.201	-	-
0.0625 ML	4-fold	0.754	-	-
	2-fold	0.029	-	-
	1-fold	-2.772	-	-